UNIIVERSITY OF CALIFORNIA

Los Angeles

Sexually Differentiated Neuron Populations in the Ventromedial Hypothalamus Contribute to Sex-Specific Regulation of Energy Balance

A dissertation submitted in partial satisfaction of the

requirements for the degree Doctor of Philosophy

in Molecular, Cellular, and Integrative Physiology

by

Laura Gabriela Kammel

2019

ABSTRACT OF THE DISSERTATION

Sexually Differentiated Neuron Populations in the Ventromedial Hypothalamus Contribute to Sex-Specific Regulation of Energy Balance

by

Laura Gabriela Kammel

Doctor of Philosophy in Molecular, Cellular, and Integrative Physiology

University of California, Los Angeles, 2019

Professor Stephanie Correa Van Veen, Chair

Estrogen receptor α (*ERα*)-expressing neurons in the ventrolateral region of the ventromedial hypothalamus (VMHvl) mediate sex-specific aspects of energy balance. Elegant studies by Miguel López and colleagues showed that central delivery of estradiol (E2) promotes increased energy expenditure, increased core body temperature, and induces the expression of thermogenic markers consistent with increased BAT thermogenesis. Conversely, loss-of-function studies by our group and others have shown that ablation of *ERα* or *ERα*-containing neurons in the VMH of female mice leads to a positive energy balance, marked by reduced locomotor activity, decreased thermogenic function of BAT, and a food intake-independent weight gain. Finally, epidemiologic data shows that women transitioning to menopause exhibit decreased energy expenditure and decreased fat oxidation compared to age-matched

premenopausal women. Therefore, identifying the neuronal mediators of estrogenic regulation of energy balance in the VMH could begin to unravel the mechanisms that predispose post-menopausal women to obesity.

By way of single-cell RNA sequencing of murine VMH lineage neurons, we identified 6 distinct neuron clusters in the VMH. Using *in situ* hybridization, I found that 4 of these clusters, marked by differential expression of the neuropeptide (or neuropeptide-precursor)-encoding genes tachykinin 1 (*Tac1),* prodynorphin (*Pdyn*), and somatostatin (*Sst*), as well as the p53-induced gene reprimo (*Rprm*), identified distinct *ERα*$^{+}$ neuron populations in the VMHvl. Furthermore, I determined that *Tac1* and *Rprm* also identified female-biased, sexually differentiated neuron populations. Using *in vivo* stereotaxic targeting, I observed that siRNA-mediated knockdown of *Rprm* in the VMHvl leads to an increase in core body temperature in female but not male mice. Using thermographic image analysis I found that siRNA-mediated knockdown of *Rprm* in the VMHvl induces increased temperature of the interscapular BAT area indicative of enhanced thermogenesis. Finally, to determine the significance of *Rprm* neuron activity on energy balance independent of *Rprm* gene expression manipulation, I contributed to the development of a novel *Rprm*-Cre-FRT mouse model that will enable chemogenetic/optogenetic activation of *Rprm* neurons. Furthermore, this model will allow for long-term studies on the role of *Rprm* on body weight and energy expenditure regulation, as well as the interaction of *Rprm* with *ERα* signaling.

Together, my findings suggest that *Rprm* identifies a sexually differentiated VMH neuron population that contributes to the female-specific regulation of core body temperature and BAT thermogenesis attributed to E2 signaling in the VMH.

The dissertation of Laura Gabriela Kammel is approved.

Paul E. Micevych

Thomas J. O'Dell

Andrea L. Hevener

Stephanie Correa Van Veen, Committee Chair

University of California, Los Angeles

2019

This dissertation is dedicated to my family, my colleagues and mentors, and ultimately the animal subjects that made this research possible.

Table of Contents

Page

List of Figures

Page

Acknowledgements

I received stipend support from the UCLA Laboratories of Neuroendocrinology Training Grant (5T32HD007228), the NRSA Individual Predoctoral Fellowship (F31AG051381), the ULCA IBP Hyde Fellowship, and the UCLA Graduate Division Dissertation Year Fellowship. For Chapter 3, I received additional research support from the UCLA BRI Predoctoral Research Grant.

Chapter 1 is a version of Kammel LG, Correa SM. Selective sexual differentiation of neuron populations may contribute to sex-specific outputs of the ventromedial hypothalamus (*Accepted-Journal of Neuroendocrinology)*. For this chapter, I thank Megan Massa and Ed van Veen for comments and input. SMC received research support by the UCLA Division of Life Sciences, UCLA CTSI (L1TR001811), Iris Cantor UCLA Women's Health Center, and UCSD/UCLA Diabetes Research Center (P30 DK063491).

Chapter 2 is a version of Van Veen JE*, Kammel LG*, Bunda PC, Shum M, Reid MS, Park JW, Zhang Z, Massa MG, Arneson D, Hrncir H, Liesa M, Arnold AP, Yang X, Correa SM. Single cell profiling of the VMH reveals a sexually dimorphic regulatory node of energy expenditure (*In revision*), BioRxiv preprint: https://doi.org/10.1101/549725. *equal contribution. JEV, LGK, and SMC conceived of and designed the studies. JEV, LGK, PCB, MS, MSR, JWP, ZZ, MGM, HH, and SMC acquired and analyzed data. JEV, LGK, PCB, MS, DA, ML, APA, XY, and SMC contributed to data interpretation. JEV, LGK, and SMC wrote the manuscript with substantial input from MS, ZZ, MGM, DA, ML, APA, and XY. The research was supported by UCLA Division of Life Sciences funds to SMC, K01DK098320 to SMC,

UL1TR001811 and Iris Cantor-UCLA Women's Health Center/UCLA National Center of Excellence in Women's Health Pilot Awards to SMC and ZZ, UCSD/UCLA Diabetes Research Center P30 DK063491 Pilot and Feasibility awards to SMC and ML, DK104363 and NS103088 to XY, HD076125 and HL131182 to APA, UCLA Department of Medicine Chair commitment to ML, UCLA Dissertation Year Fellowships to DA, Canadian Diabetes Association Postdoctoral fellowship to MS, American Heart Association Postdoctoral Fellowship (18POST33960457) to ZZ, and NSF Graduate Research Fellowship to MGM. I thank Carolina De La Cruz for technical assistance.

Chapter 3 is a version of Van Veen JE, Kammel LG, Leon K, and Correa SM. Generation of a novel mouse model to study the regulation of thermogenesis by the ventromedial hypothalamus (*In preparation*). JEV, LGK, and SMC conceived of and designed the studies. JEV and KL acquired and analyzed data. JEV, LGK, KL, and SMC contributed to data interpretation. JEV, LGK, KL, and SMC wrote the manuscript.

Chapter 5 is a re-print of Kammel LG*, Wei W*, Jami SA, Voskuhl RR, O'Dell TJ. Enhanced GABAergic tonic inhibition reduces intrinsic excitability of hippocampal CA1 pyramidal cells in experimental autoimmune encephalomyelitis. Neuroscience. 2018 Nov 14. pii: S0306-4522(18)30727-9. doi: 10.1016/j.neuroscience.2018.11.003. *equal contribution. T.J.O directed research. I thank Noriko Itoh, Heaveen Ahdi, Valerie Vessels, and Darian Nitin Mangu for assistance with animal care. I also thank Drs. Ryan Guglietta and Walter Babiec for technical advice. L.G.K, W.W., S.A.J., R.R.V., and T.J.O. designed research; L.G.K., W.W., S.A.J., and T.J.O. performed research; L.G.K, W.W., S.A.J., and T.J.O. analyzed data; L.G.K., W.W., S.A.J., R.R.V., and T.J.O. wrote the paper. RRV received research support from the Conrad N. Hilton Foundation

(20150232), the California Community Foundation (BAPP-15-118094), and the Tom Sherak MS Hope Foundation. Permission for re-print was requested from publisher.

My deepest gratitude goes to my mentor Dr. Stephanie Correa, for showing me that the best science is borne out of joy, humanity, and fearlessness. Thank you for your unfailing support of my career, your passion for mentorship, and for always taking the time to celebrate successes. And most of all, thank you for culturing an environment where scientists of all personalities and backgrounds can thrive. I also want to thank Dr. Tom O'Dell, for treating me like a member of his lab (lab key included) from the very beginning. There are few individuals who truly embody the "open door policy" as you do, and to know that there would always be support available was incredibly important and motivating to me. Thank you for all our various discussions. I am grateful to Dr. Paul Micevych, Dr. Art Arnold, Catherine Weston, and the rest of the LNE community for the remarkable platform they have provided us trainees. To be a part of the LNE has truly been one of the best aspects of my graduate training, and I hope to carry on its mission in my future career. I thank Dr. Andrea Hevener for her enthusiasm and insights into metabolism that she brought to this project. I want to thank my lab mates and class cohort for their friendship and generosity, especially Dr. Roy Kim, Dr. Ting Zhang, and Correa Lab members Dr. Zhi Zhang, Dr. Ed van Veen, Megan Massa, Jae Park, and John DiVittorio. I want to thank my undergraduate students for their hard work and for helping me to become a better mentor. I want to thank my family and friends for their endless love and encouragement. And finally, I want to thank my dear fiancé Alex for being by my side through it all. The love and happiness you bring to my life are beyond words.

VITA

Education

2008-2012	**B.Sc. Neuroscience, with Honors** Brown University; Providence RI, USA

Research Experience

04/2017-present	**Graduate Student Researcher, Dept. of Integrative Biology and Physiology** University of California, Los Angeles; Los Angeles CA, USA Principal Investigator: Dr. Stephanie Correa
03/2013-03/2017	**Graduate Student Researcher, Dept. of Neurology** University of California, Los Angeles; Los Angeles CA, USA Principal Investigators: Dr. Tom O'Dell, Dr. Rhonda Voskuhl
09/2012-03/2013	**Graduate Rotation Student** University of California, Los Angeles; Los Angeles CA, USA Principal Investigators: Dr. Reggie Edgerton, Dr. Baljit Khakh
01/2011-05/2012	**Undergraduate Student Researcher, Dept. of Molecular Pharmacology, Physiology, and Biotechnology** Brown University; Providence RI, USA Principal Investigator: Dr. Elena Oancea
09/2009-01/2010	**Laboratory Intern, Water Microbiology Laboratory** Rhode Island Department of Health Laboratories, Providence RI, USA Principal Investigator: Dr. Kerry Patterson

Academic Honors and Fellowships

2019	Travel Award, Steroids and Nervous System Meeting; Turin, Italy
11/1/2018-10/31/2019	UCLA BRI Predoctoral Research Grant: $10,000 PI: Kammel, Laura
2018-2019	UCLA Hyde Fellowship: $33,000 PI: Kammel, Laura
10/1/2018-10/1/2019	UCLA Graduate Division Dissertation Fellow: $36,818 PI: Kammel, Laura
9/30/2016-9/29/2018	Individual NRSA (F31AG051381): $70,502 PI: Kammel, Laura Title: "*Estrogen receptor beta-targeted treatment to maintain cognitive function during menopause*"
2016-2018	UCLA GPB Fellowship Incentive Program: $6,000
2016	Best poster in Biological Sciences category: $75 prize, 2016 UCLA Research Conference on Aging
11/01/2015-9/29/2016	LNE Training Grant (5T32HD007228-35): $22,920 PI: Arnold, Arthur
1/6/2015-9/30/2015	Core Voucher Award for UCLA BTC (UL1TR 000124): $8,000 PI: Voskuhl, Rhonda, Co-I: Kammel, Laura
11/1/2014-10/31/2015	LNE Training Grant (5T32HD007228-34): $22,476 PI: Arnold, Arthur
10/1/2012-9/30/2013	MCIP Training Grant (5T32GM 65823-10): $32,046 PI: Tidball, James
2012-2013	Graduate Dean's Scholar Award: $14,500, UCLA
2012-2013	Sigma Xi, Scientific Research Society, Member
2011	UTRA Research Collaboration Award: $3,000, Brown University

Publications

Kammel LG, Correa SM. Selective sexual differentiation of neuron populations may contribute to sex-specific outputs of the ventromedial hypothalamus (*Accepted - Journal of Neuroendocrinology*).

Van Veen JE*, **Kammel LG***, Bunda PC, Shum M, Reid MS, Park JW, Zhang Z, Massa MG, Arneson D, Hrncir H, Liesa M, Arnold AP, Yang X, Correa SM. Single cell profiling of the VMH reveals a sexually dimorphic regulatory node of energy expenditure (*In revision*). BioRxiv preprint: https://doi.org/10.1101/549725 ***equal contribution**

Kammel LG*, Wei W*, Jami SA, Voskuhl RR, O'Dell TJ. Enhanced GABAergic tonic inhibition reduces intrinsic excitability of hippocampal CA1 pyramidal cells in experimental autoimmune encephalomyelitis. Neuroscience. 2018 Nov 14. pii: S0306-4522(18)30727-9. doi: 10.1016/j.neuroscience.2018.11.003. ***equal contribution**

Bellono NW, **Kammel LG**, Zimmerman AL, Oancea E. UV light phototransduction activates transient receptor potential A1 ion channels in human melanocytes. Proceedings of the National Academy of Sciences of the United States of America. 2013;110(6):2383-8. doi: 10.1073/pnas.1215555110. PubMed PMID: 23345429; PubMed Central PMCID: PMC3568351.

Oral Presentations and Selected Posters

Kammel LG, Van Veen JE, Bunda PC, Shum M, Zhang Z, Massa MG, Reid MS, Hrncir H, Arnold AP, Liesa M, Yang X, Correa SM. Sex Differences in the Transcriptional Architecture of the VMH Reveals Two Estrogen-Sensitive Neuron Clusters that Coordinately Regulate Energy Expenditure in Females. Turin, Italy; 10th International Steroids and Nervous System Meeting, 2019. Oral Presentation.

Kammel LG, Van Veen JE, Bunda PC, Shum M, Zhang Z, Massa MG, Reid MS, Hrncir H, Arnold AP, Liesa M, Yang X, Correa SM. Sex Differences in the Transcriptional Architecture of the VMH Reveals Two Estrogen-Sensitive Neuron Clusters that Coordinately Regulate Energy Expenditure in Females. Los Angeles, CA; 6th Annual Research Symposium, USC Diabetes and Research Institute, 2019. Oral Presentation.

Kammel LG, Van Veen JE, Bunda PC, Reid MS, Correa SM. Single-cell RNA Profiling Reveals Sex Differences and a Mediator of Estrogen Signaling in the Transcriptional Architecture of the Ventromedial Nucleus of the Hypothalamus. Los Angeles, CA: 2018 UCSD/UCLA Diabetes Research Center Retreat. 2018. Poster.

Kammel LG, Wei W, Voskuhl R, and O'Dell TJ. Increased GABAergic inhibition through α5-subunit containing $GABA_A$Rs contributes to impaired hippocampal synaptic plasticity in EAE. Neuroscience Meeting Planner. San Diego, CA: Society for Neuroscience, 2016. Poster.

Kammel LG, Itoh N, H Ahdi, O'Dell TJ, Voskuhl R. The neuronal beta estrogen receptor supports hippocampal-dependent cognitive function. Los Angeles, CA: 21th Annual UCLA Research Conference on Aging, 2016. Poster.

Chapter 1

Selective sexual differentiation of neuron populations may contribute to sex-specific outputs of the ventromedial hypothalamus

ABSTRACT

The ventromedial hypothalamus (VMH) regulates a wide array of sex-specific behaviors and physiological responses, from mating to metabolism. We propose that underlying these sex-specific functions is a hierarchical architecture of sex differences that arises from selective sexual differentiation of neuron populations in the VMH. Technologies that increase the resolution of molecular profiling or targeting of manipulations can help reveal these embedded sex differences. Here we examine where and when sex differences emerge within the VMH, how sex differences within VMH sub-regions or cell subpopulations drive sex-specific outputs, and how other areas of research could benefit from examining sex differences at the level of individual cells.

INTRODUCTION

Sex differences in the brain describe the variations in structure, molecular signature, or other parameters between analogous brain areas in males and females. Sexual differentiation of neuroanatomical features such as cell numbers, synaptic densities, and fiber projection patterns are characteristic to several hypothalamic nuclei, and underlie the masculinization of the medial preoptic area (mPOA) and the feminization of the anteroventral periventricular nucleus (AVPV) in rodents. Sexual differentiation also extends to nonneuronal cells, including astrocytes (McCarthy et al

2003) and microglia (Lenz & McCarthy 2015). Earlier studies have revealed several key paradigms regarding sex differences in the brain: (1) because sexual differentiation is influenced by a variety of hormonal and non-hormonal factors, brain areas are subject to mosaicism in terms of their degree of masculinization or feminization (McCarthy 2015), and (2) although they are remarkably diverse in quality, sex differences within these brain areas rarely present as binary sexual dimorphisms, but rather as quantitative differences (Yang & Shah 2014). Because each brain area contains diverse and heterogeneous clusters of cell types and cell subpopulations, sexually differentiated regions may also be mosaic. That is, cell populations within a sexually dimorphic brain area could differ in whether they are differentiated or neutral in regards to sex. Approaches that increase the resolution of molecular analyses could therefore aid in the detection of these sexually differentiated cell populations and reveal how they contribute to the functional heterogeneity of a particular brain area.

The ventromedial hypothalamus (VMH) is a sexually differentiated structure that mediates a wide range of physiological processes, from sexual receptivity and mating behaviors, to social behaviors and metabolic processes. Why sex differences are embedded in non-reproductive, homeostatic circuits within the VMH has been reviewed elsewhere (Krause & Ingraham 2017). Recently, new technologies such as single cell RNA sequencing (scRNA-seq), optogenetics, and chemogenetics have been used to study if sexual differentiation occurs at the level of neuronal populations or subpopulations within the VMH, and how these sex differences could contribute to the display of sex-typical responses (Correa et al 2015, Hashikawa et al 2017, Lee et al 2014, Remedios et al 2017, Van Veen Kammel et al 2019, Yang et al 2013). Selective

sexual differentiation of neurons within the VMH could explain why some, but not all, functions mediated by the VMH occur in a sex-biased manner and why some aspects of sex-biased functions can be elicited in the opposite sex under the right conditions. Specialization among sexually differentiated neurons, whereby distinct subpopulations mediate specific behaviors and processes attributed to the VMH, could also explain how the VMH mediates such a wide array of physiological processes. Together, the studies we review here support the hypothesis that sex differences emerge at multiple hierarchies within the VMH architecture, from morphology to the neurochemistry of specialized subpopulations to the recruitment of specialized neural circuitry, and that these sex differences allow for the display of sexually differentiated behaviors mediated by the VMH.

HIERACHIES OF SEX DIFFERENCES IN THE VMH

Heterogeneity of hormone responsive neurons in the VMH

Sex hormone effects during development, puberty, and adulthood are the most robust mechanisms that drive sexual differentiation in the brain. Therefore, sex differences within the VMH are most likely to manifest within populations of sex hormone-responsive neurons, and the VMH is rich in sex hormone receptor expression. Neurons co-expressing estrogen receptor α (ERα) and progesterone receptor (PR) localize to the ventrolateral region of the VMH (VMHvl) (McClellan et al 2006, Yang et al 2013) and these neurons are estimated to constitute 40-50% of VMHvl cells (Lee et al 2014, Yang et al 2013). Sexually differentiated expression of ERα arises during the neonatal period and persists into adulthood, with females expressing higher levels of

ERα in the VMHvl (Devidze et al 2005, Ikeda et al 2003). Neurons expressing the other ER subtype, estrogen receptor β (ERβ), are also localized to the VMHvl and largely overlap with $ERα^+$ neurons, although ERβ expression is much lower than that of ERα (Ikeda et al 2003). ERβ also is expressed at higher levels in females than males during the neonatal period, although this sex difference becomes marginal by adulthood (Ikeda et al 2003). Finally, androgen receptor (AR)-expressing neurons are localized throughout the VMH and are also expressed in neonates and adults, but do not show sexually differentiated expression (Juntti et al 2010, McAbee & DonCarlos 1998, Simerly et al 1990). However, AR neurons are thought to contribute to sex differences in the VMH through the regulation of aromatase expression and activity. Indeed, testosterone treatment increases aromatase activity more in males than females, while mutations that render males unresponsive to androgens contribute to decreased aromatase activity and demasculinization of the VMH (Dugger et al 2007, Roselli et al 1987).

Molecularly distinct subpopulations of sex hormone-sensitive neurons could allow for the diverse set of physiological processes attributed to the VMH. Recently, we used single cell RNA sequencing to characterize the transcriptomes of VMH neurons from male and female pups on a cell-by-cell basis (Van Veen Kammel et al 2019). We identified 6 distinct clusters of glutamatergic neurons that were found in both males and females. This supports previous work suggesting that males and females share qualitatively similar pools of molecularly defined neurons (Yang & Shah 2014). The top most differentially expressed gene within each of the clusters was tachykinin-1 (*Tac1*),

somatostatin (*Sst*), reprimo (*Rprm*), prodynorphin (*Pdyn*), hippocalcin-like protein 1 (*Hpcal1*), and galanin (*Gal*), respectively.

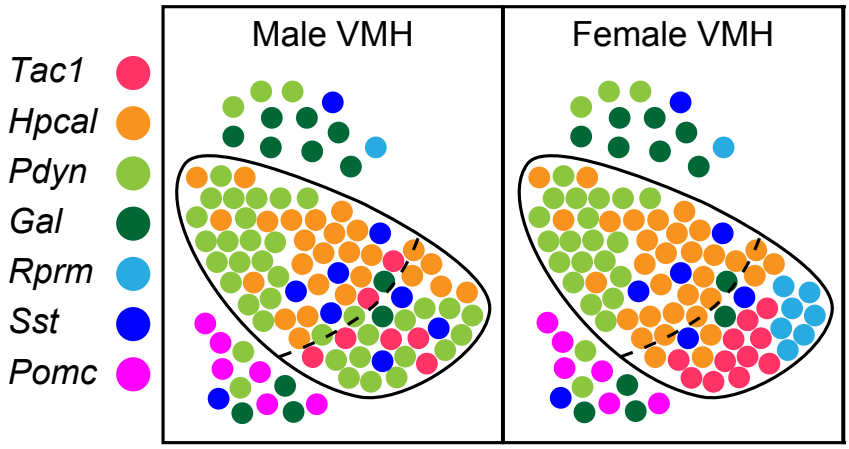

Figure 1.1 Diagram of neuronal populations found in the VMH with focus on sexually differentiated female VMHvl.

To determine if some of these genes identified subsets of estrogen-sensitive neurons, we co-localized ERα with each cluster marker. In females, the majority of ERα immunoreactivity was restricted to the two subpopulations identified by *Tac1* and *Rprm*, and this paralleled enriched expression of *Tac1* and *Rprm* in the VMHvl of females. *Pdyn* also co-localized with ERα immunoreactivity in the VMHvl, although the expression of *Pdyn* was significantly higher in males than females. Finally, only limited ERα immunoreactivity was detected in neuronal subpopulations expressing *Sst* and *Hpcal1*, with colocalization undetectable in the *Gal* subpopulation. These findings suggest that hormone responsive neurons are heterogeneous in their molecular signatures. We suggest the possibility that these subpopulations can be selectively sexually differentiated (Figure 1.1).

Non-hormonal mechanisms, such as the sex chromosome complement, can also contribute to neuronal sexual differentiation, either by supplementing or opposing hormonal sex differences(De Vries 2004). In particular, X chromosome genes regulate aspects of metabolism, including food intake and adiposity (Chen et al 2012). However, we did not find evidence that the sex chromosome complement was contributing to the sex differences in *Tac1*, *Rprm*, or *Pdyn* expression in the VMHvl (Van Veen Kammel et al 2019). Rather, gonadal sex was critical for determining the sex difference in *Tac1* and *Rprm* expression, suggesting that these patterns are established during development and maintained into adulthood (Van Veen Kammel et al 2019). Finally, testicular hormones were required for the sex difference in *Pdyn* expression in adulthood, as this difference was eliminated by castration (Van Veen Kammel et al 2019). Another group reported that half of the genes that showed sex differences in the VMHvl are regulated by adult sex hormones (Xu et al 2012). Therefore, while we cannot rule out the possibility that sex chromosome-linked genes may regulate other aspects of the molecular signature of VMH neurons. However, the combined effects of gonadal hormones during development and in adulthood are likely to account for the majority of the selective sex differences in the VMH.

Sex differences in cytoarchitecture

Sex and estrus cycle phase can differentiate cell morphology and cytoarchitecture within the VMH. The volume of the VMH is greater in males than females across all subregions, although due to a gain in VMH volume from diestrus to proestrus, this sex difference is smaller when comparing males to proestrus females

than to diestrus females (Madeira et al 2001). Males that are unresponsive to androgens show significantly smaller VMHvl volumes compared to wild-type males (Dugger et al 2007). VMH volume differences are primarily accounted for by the larger neuronal soma sizes and neuropil volume in males than females rather than reflecting relative differences in neuronal numbers between males and females within VMH subdivisions (Dugger et al 2007, Madeira et al 2001). Hormone-sensitive inputs may contribute to both early sexual differentiation and dynamic changes across the estrus cycle in cell populations without steroid receptor expression. Male VMH neurons receive greater numbers of spine synapses, a sex difference which is reversible with neonatal castration in males or testosterone treatment in females (Matsumoto & Arai 1986). Thus, the masculinization of VMH neuropil reflects greater innervation of the male VMH by various synaptic inputs, which include serotonergic and aromatase-positive fibers (Patisaul et al 2008, Wu et al 2009). In contrast, spine density is greater throughout the VMH in females compared to males regardless of estrus stage (Madeira et al 2001). Furthermore, spine density is differentially regulated by estradiol in males and females, with estradiol decreasing spine density in the male VMH but increasing spine density in the female VMH (reviewed in (Flanagan-Cato 2011)). Finally, within the VMHvl, spine density, dendritic branching density, and length of terminal segments also are greater in proestrus females than in diestrus females (Madeira et al 2001). Sex differences that manifest in all regions of the VMH are therefore likely to result from modulation of hormone sensitive afferents, while those that pertain to VMHvl neurons are likely to be mediated by direct actions of hormone receptors within these neurons (Madeira et al

2001). Therefore, selective sexual differentiation can occur in both a cell autonomous and non-cell autonomous manner within the VMH.

Sex differences in efferent projection patterns from hormone sensitive neurons the VMH could also contribute to the display of sexually differentiated behaviors, in particular because subpopulations of ERα$^+$ neurons along the anterior-posterior axis of the VMHvl differ in their projection targets. ERα$^+$ neurons in the posterior VMHvl project to more anterior brain areas such as the amygdala and hypothalamus, while ERα$^+$ neurons in the anterior VMHvl project more to posterior, premotor brain areas (Lo et al 2019). In one study, ERα$^+$ neurons localized to the lateral aspect of the VMHvl that project to the AVPV in females were reported to be largely absent in males (Yang et al 2013). However, another study reported no consistent differences between the sexes in the projection strength of ERα$^+$ neurons to numerous targets (Lo et al 2019). Therefore, the significance of sex differences in efferent projections from hormone sensitive VMH neurons remains unclear.

SEX DIFFERENCES IN VMH-MEDIATED PROCESSES

Sexual receptivity and male pattern mating

VMHvl neurons contribute to the circuitry underlying female sexual receptivity and male pattern mating behavior. In females, the VMH is the final integration site for the hypothalamic and limbic circuits that underlie the expression of lordosis (Micevych & Meisel 2017). Female rodents are sexually receptive at specific times in their estrus cycle, starting with the evening of proestrus and ending with the morning of estrus, in a manner that is dependent on estradiol and progesterone (Micevych & Meisel 2017).

Silencing ERα signaling in the VMHvl impairs the display of receptive behavior, and instead triggers vigorous rejection of the male (Musatov et al 2006). Unlike ERα, ERβ does not seem to play a major role in female sexual behavior, as ERβ null mice show normal reproductive behavior (Ogawa et al 1999).

Several receptors and neuromodulators expressed by ERα neurons in the VMHvl that are important for lordosis behavior are expressed in a sexually differentiated manner. *Cckar,* the cholecystokinin A receptor, is expressed by the majority of $ERα^+/PR^+$ neurons in the lateral VMHvl in females and is induced by estrogen signaling (Hashikawa et al 2017, Xu et al 2012). Females with a global deletion of *Cckar* show specific deficits in sexual receptivity, but show wild-type maternal behaviors and estrus cycles (Xu et al 2012). In contrast, *Cckar* is only very weakly expressed in males and males with global deletion of *Cckar* show wild-type male-typical mating behaviors (Xu et al 2012, Yang et al 2013). Other genes, including some restricted to specific VMH clusters, may also relate to lordosis behavior. Subsets of neurons in the VMH expressing the *Tac1*-encoded neuropeptide substance P project to the dorsal midbrain central grey, a region where substance P facilitates estrogen-induced lordosis behavior (Dornan et al 1990). Knockdown of preproenkephalin (*Penk*) in the VMHvl leads to decreased lordosis behavior without affecting locomotor behavior (Nicot et al 1997). Interestingly, although *Penk* is induced by estrogen signaling, single cell RNA-seq identified transcripts to be largely restricted to the *Gal* cluster, in line with other studies showing that only very few enkephalin-immunoreactive cells in the VMHvl co-express PR (Olster & Blaustein 1990, Van Veen Kammel et al 2019). Thus, genes expressed by

sex hormone sensitive cells, or induced by sex hormones, have been linked to female-specific receptive behaviors.

In contrast to females, VMHvl ERα^{+}/PR^{+} neurons play a less robust role in male mating behavior (Hashikawa et al 2016). Ablation of these neurons in the VMHvl of males leads to reduced mounting, intromission, and reduced intromission length (Yang et al 2013). However, activation of this population alone is not sufficient to increase mounting frequency towards females, although it does increase mounting duration (Lee et al 2014). In fact, unlike females where mating-related VMHvl neurons increase their activity during and throughout a male encounter, VMHvl neurons in males show only a transient increase in activity with a female encounter, and this is extinguished during progression of the behavior (Lin et al 2011). Inhibition of this population also is insufficient in affecting frequency, duration, or halt ongoing mounting of females (Lee et al 2014). Of note, residual neuronal activity in these experiments may have impeded complete behavioral manipulation, accounting for some of these discrepancies (Lee et al 2014). However, inactivation of ERα neurons in the mPOA was later shown sufficient for inhibit mounting, suggesting a more nuanced role for the VMHvl in male mounting behavior (Hashikawa et al 2016, Wei et al 2018).

Social behaviors (Social investigation and Aggression)

Subpopulations of neurons within the VMH have been implicated in mediating specific social behaviors, including defensive behavior, social investigation, and aggression. Activation of neurons in the dorsomedial and central regions of the VMH induces defensive behavior in both males and females (Wang et al 2015). Males also

have neurons within the VMHvl that are excited when initiating an aggressive behavior in response to a male intruder, and normally, these neurons are inhibited when encountering a female (Lin et al 2011). In males, activation of these VMHvl neurons induces rapid, time-bounded attack of intruder animals, including female mice (Lin et al 2011). *Esr1*$^{+}$*/PR*$^{+}$ neurons in the VMHvl are necessary and sufficient to induce and maintain this aggressive behavior towards intruders in males (Lee et al 2014, Yang et al 2013, Yang et al 2017). In addition, the social behavior elicited by this population is scalable, such that a larger population of activated cells preferentially induces aggressive behavior, while a weaker activation of cells (via a lower photostimulation intensity, lower virus volumes, shorter viral infection times, or lower CNO dose) preferentially induces mounting and social investigative behavior towards both sexes (Lee et al 2014, Yang et al 2017). Furthermore, aggression is elicited by activating this population in males even in the absence of testicular hormones (Yang et al 2017). In contrast, activation of this same population in females fails to elicit aggressive behavior at any stimulation intensity, although it does induce social investigation and occasional mounting (Lee et al 2014, Yang et al 2017). In another study, it was determined that stimulating *Esr1*$^{+}$ VMHvl neurons induces aggressive behaviors in females that are spontaneously more aggressive and that these “fighting” neurons are localized more medially within the VMHvl (Hashikawa et al 2017). Furthermore, these neurons are functionally distinct from VMHvl neurons mediating mating behaviors (Hashikawa et al 2017). Finally, activation of projections onto VMHvl neurons from the lateral septum selectively inhibits an ongoing attack behavior, without affecting mounting behavior (Wong et al 2016). VMHvl neurons also receive synaptic inputs from GABAergic

subparaventricular zone neurons, as well as neurons in the central VMH, part of a larger circuitry that induces circadian phase-dependent regulation on VMH-mediated aggressive behaviors (Todd et al 2018). Together, these studies suggest that social behaviors elicited by hormone sensitive neurons in the VMHvl are modulated by both intra-VMH and external circuitry.

Metabolism (Energy expenditure and glucose sensing)

Neurons within the VMH also have important roles in regulating aspects of metabolism, including energy expenditure and glucose sensing, and many of these show sex-specific characteristics. In females, loss of ERα signaling in the VMH impairs estrogen-dependent wheel running and ambulatory movement, metabolic rate, and brown adipose tissue (BAT) thermogenesis (Correa et al 2015, Musatov et al 2007, Xu et al 2011). Activation of ERα neurons in the VMHvl is sufficient to induce increased movement, metabolic rate, and thermogenesis in females (Van Veen Kammel et al 2019). Interestingly, female *Tac1* null mice show an impaired movement phenotype upon activation of VMHvl neurons, suggesting a role for *Tac1*$^{+}$/ERα^{+} neurons in mediating this behavior (Correa et al 2015). Recently, we found that knockdown of *Rprm* in the VMH of females leads to a baseline increase in core body temperature without an increase in movement, suggesting the *Rprm*$^{+}$/ERα^{+} neurons could also differentially contribute to sex-specific regulation of energy expenditure (Van Veen Kammel et al 2019) (Figure 1.2).

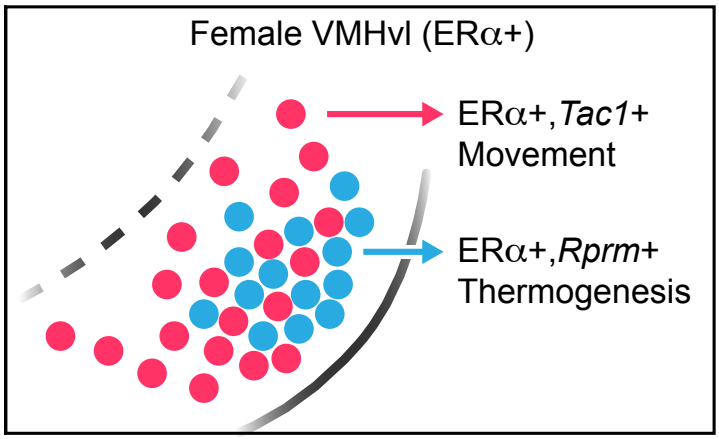

Figure 1.2 Tac1 and Rprm neurons populations mediate distinct aspects of E2-mediated regulation of energy balance.

Finally, the estrogen-induced gene, oxytocin receptor (*Otr*), also is co-expressed with ERα^{+}/PR^{+} neurons in the VMH, and upregulation of *Otr* in the VMH also is related to enhanced locomotor activity (Devidze et al 2005, Narita et al 2016). Interestingly, *Otr* expression in the VMH is higher in males than females (Bale & Dorsa 1995) and activating the VMH can increase locomotion in males (Narita et al 2016), but the role of *Otr* has not been tested in males.

Sex differences in glucose homeostasis are mediated in part by hormone-sensitive glucose sensing neurons in the VMHvl. Glucose-excited (GE) and glucose-inhibited (GI) neurons, as well as a subclass of GI neurons that respond transiently to glucose (AdGI), are differentially distributed throughout the VMH and work together to control glucose homeostasis (Santiago et al 2016, Song et al 2001). Within the VMHvl, the majority of glucose-sensing neurons are GE, which increase their activity with higher extracellular glucose levels (Cotero & Routh 2009, Khodai et al 2018, Santiago et al 2016). Glucose-sensing neurons within the VMHvl also show overlapping expression

with ERα^{+} neurons (Santiago et al 2016). Male GI neurons show increased excitability in response to low glucose compared to females, suggesting an inherent sex difference in glucose-elicited activity (Santiago et al 2016). Furthermore, both types of GI neurons, but only small populations of GE neurons, showed activity blunting in response to estradiol (Santiago et al 2016). These findings that females may have reduced abilities to detect low glucose, which are further blunted by cyclic increases in estradiol, provide a mechanism for the clinical observations that females have weaker counterregulatory responses to hypoglycemia than males (Cryer 2000, Santiago et al 2016). Recently, one type of GI neuron was identified by expression of the pituitary adenylate cyclase-activating peptide (PACAP), and activation of this subset of VMH neurons was sufficient to inhibit insulin secretion and increase plasma glucose (Khodai et al 2018).

Finally, it was found that development ablation of glucokinase (*Gck*), the major glucose-sensing enzyme, in VMH neurons leads to sexually differentiated changes in fat mass, glucagon secretion, and autonomic nervous activity, with females showing increased gonadal, inguinal, and total fat mass, decreased hypoglycemia-induced glucagon secretion, and reduced neuroglucopenia-induced parasympathetic and sympathetic nerve activity compared to males (Steinbusch et al 2016). These findings further suggest that VMH *Gck* is required for hypoglycemia counter-regulation in females but not males (Steinbusch et al 2016). Together, sex differences in the VMH contribute to the differential recruitment of molecular signaling pathways and downstream circuitry required for glucose homeostasis.

STUDYING SEX DIFFERENCES AT THE SINGLE CELL LEVEL

Classically, the presence or absence of the Y-linked *Sry* gene leads to differentiation of the gonads through the initiation of the testis or ovary differentiation pathways. Subsequent sex differences in gonadal hormones then lead to masculinization or feminization of other tissues. However, a large body of evidence has revealed cell autonomous sex differences in tissues all over the body (Arnold 2017). The advent of single cell profiling technology provides the exciting opportunity to dissect sex differences at the level of single cells or cell populations in any tissue, including specific regions of the brain.

Transcriptional profiling studies with single cell resolution often include samples from both male and female mice. However, few studies are designed to detect sex differences or distinguish between sex differences in gene expression or cell composition within a tissue. A recent study examined sex differences in the various cell lineages of the developing mouse gonad (Stevant et al 2019). Even during the differentiation of testes or ovaries, the cells of the gonad upregulate hundreds of genes equally in both sexes and the majority of sex differences are restricted to the lineage that expresses *Sry*. Thus, it is not surprising that single cell transcriptional profiling within the brain also finds limited sex differences in gene expression. In the medial amygdala, GABAergic neurons exhibit sex differences in gene expression, whereas gene expression in glutamatergic neurons is neutral with respect to sex (Chen et al 2019). Of the 40-60 genes that are differentially expressed in GABAergic neurons, at least two validated by histological analysis; however, it is unclear how many are due to sexual differentiation of this neuron population compared to activational effects of hormone signaling. We analyzed the VMH of 10-day-old male and female pups by

single cell RNA sequencing before activational effects of sex steroids. Many transcripts were enriched in males or females but these were expressed throughout the VMH and were not robust when analyzed by histology (Van Veen Kammel et al 2019). Instead, spatial analyses revealed robust sex differences in a few transcripts within the VMHvl sub-region. Importantly, manipulation of either *Tac1* or *Rprm* function seems to alter the function of the VMHvl (Correa et al 2015, Van Veen Kammel et al 2019), suggesting that wholesale differences in molecular signature are not required for sex differences in cell, neuron, or circuit function.

From these studies, it seems that sex differences in gene expression are restricted to certain cell populations and may involve a limited number of key transcripts. Therefore, sex differences in a few genes may lead to sex-specific functions without sex differences in the overall molecular signature of cells. However, the ability to detect the key differences that underlie sex differences in physiology will largely depend on the sensitivity of our methods to interrogate gene expression within sub-regions or individual cell populations. We argue that single cell resolution studies coupled with validation and functional manipulations will be crucial in our efforts to pinpoint the biological underpinnings of sex differences in physiology and behavior.

CONCLUDING REMARKS

The VMH mediates various sex-specific and hormone-sensitive changes in physiology or behavior. It appears that the cells that mediate these sex-specific functions are specialized, sexually differentiated, and intermingled with cells that are neutral with respect to sex. Thus, we propose that the concept of mosaicism in the

degree of sexual differentiation (McCarthy 2015) applies to distinct cell types within regions classically considered to be “sexually dimorphic”. Further, we suggest that the heterogeneity in the degree of masculinization or feminization is a result of selective sexual differentiation of specific cell types within the VMHvl region or other nodes in the circuit that can alter the function of VMH cell types. Single cell resolution studies have revealed surprising cellular heterogeneity in a wide variety of tissues. We propose that sexual differentiation builds on this cellular heterogeneity and leads to sex differences in some but not all cell populations within a tissue or brain region. Unicellular analysis tools will therefore help us dissect the molecular underpinnings of sex-specific neural circuits and define the key molecular mediators of these responses.

REFERENCES

Arnold AP. 2017. A general theory of sexual differentiation. *J Neurosci Res* 95: 291-300

Bale TL, Dorsa DM. 1995. Sex differences in and effects of estrogen on oxytocin receptor messenger ribonucleic acid expression in the ventromedial hypothalamus. *Endocrinology* 136: 27-32

Chen PB, Hu RK, Wu YE, Pan L, Huang S, et al. 2019. Sexually Dimorphic Control of Parenting Behavior by the Medial Amygdala. *Cell* 176: 1206-21 e18

Chen X, McClusky R, Chen J, Beaven SW, Tontonoz P, et al. 2012. The number of x chromosomes causes sex differences in adiposity in mice. *PLoS Genet* 8: e1002709

Correa SM, Newstrom DW, Warne JP, Flandin P, Cheung CC, et al. 2015. An estrogen-responsive module in the ventromedial hypothalamus selectively drives sex-specific activity in females. *Cell Rep* 10: 62-74

Cotero VE, Routh VH. 2009. Insulin blunts the response of glucose-excited neurons in the ventrolateral-ventromedial hypothalamic nucleus to decreased glucose. *Am J Physiol Endocrinol Metab* 296: E1101-9

Cryer PE. 2000. Are gender differences in the responses to hypoglycemia relevant to iatrogenic hypoglycemia in type 1 diabetes? *J Clin Endocrinol Metab* 85: 2145-7

De Vries GJ. 2004. Minireview: Sex differences in adult and developing brains: compensation, compensation, compensation. *Endocrinology* 145: 1063-8

Devidze N, Mong JA, Jasnow AM, Kow LM, Pfaff DW. 2005. Sex and estrogenic effects on coexpression of mRNAs in single ventromedial hypothalamic neurons.

Proceedings of the National Academy of Sciences of the United States of America 102: 14446-51

Dornan WA, Akesson TR, Micevych PE. 1990. A substance P projection from the VMH to the dorsal midbrain central gray: implication for lordosis. *Brain Res Bull* 25: 791-6

Dugger BN, Morris JA, Jordan CL, Breedlove SM. 2007. Androgen receptors are required for full masculinization of the ventromedial hypothalamus (VMH) in rats. *Horm Behav* 51: 195-201

Ferran JL, Puelles L, Rubenstein JL. 2015. Molecular codes defining rostrocaudal domains in the embryonic mouse hypothalamus. *Front Neuroanat* 9: 46

Flanagan-Cato LM. 2011. Sex differences in the neural circuit that mediates female sexual receptivity. *Front Neuroendocrinol* 32: 124-36

Hashikawa K, Hashikawa Y, Falkner A, Lin D. 2016. The neural circuits of mating and fighting in male mice. *Curr Opin Neurobiol* 38: 27-37

Hashikawa K, Hashikawa Y, Tremblay R, Zhang J, Feng JE, et al. 2017. Esr1(+) cells in the ventromedial hypothalamus control female aggression. *Nature neuroscience* 20: 1580-90

Ikeda Y, Nagai A, Ikeda MA, Hayashi S. 2003. Sexually dimorphic and estrogen-dependent expression of estrogen receptor beta in the ventromedial hypothalamus during rat postnatal development. *Endocrinology* 144: 5098-104

Juntti SA, Tollkuhn J, Wu MV, Fraser EJ, Soderborg T, et al. 2010. The androgen receptor governs the execution, but not programming, of male sexual and territorial behaviors. *Neuron* 66: 260-72

Khodai T, Nunn N, Worth AA, Feetham CH, Belle MDC, et al. 2018. PACAP Neurons in the Ventromedial Hypothalamic Nucleus Are Glucose Inhibited and Their Selective Activation Induces Hyperglycaemia. *Front Endocrinol (Lausanne)* 9: 632

Kim JH, Lee SR, Li LH, Park HJ, Park JH, et al. 2011. High cleavage efficiency of a 2A peptide derived from porcine teschovirus-1 in human cell lines, zebrafish and mice. *PloS one* 6: e18556

Krause WC, Ingraham HA. 2017. Origins and Functions of the Ventrolateral VMH: A Complex Neuronal Cluster Orchestrating Sex Differences in Metabolism and Behavior. *Adv Exp Med Biol* 1043: 199-213

Lee H, Kim DW, Remedios R, Anthony TE, Chang A, et al. 2014. Scalable control of mounting and attack by Esr1+ neurons in the ventromedial hypothalamus. *Nature* 509: 627-32

Lenz KM, McCarthy MM. 2015. A starring role for microglia in brain sex differences. *Neuroscientist* 21: 306-21

Lin D, Boyle MP, Dollar P, Lee H, Lein ES, et al. 2011. Functional identification of an aggression locus in the mouse hypothalamus. *Nature* 470: 221-6

Lo L, Yao S, Kim DW, Cetin A, Harris J, et al. 2019. Connectional architecture of a mouse hypothalamic circuit node controlling social behavior. *Proceedings of the National Academy of Sciences of the United States of America*

Madeira MD, Ferreira-Silva L, Paula-Barbosa MM. 2001. Influence of sex and estrus cycle on the sexual dimorphisms of the hypothalamic ventromedial nucleus: stereological evaluation and Golgi study. *J Comp Neurol* 432: 329-45

Matsumoto A, Arai Y. 1986. Development of sexual dimorphism in synaptic organization in the ventromedial nucleus of the hypothalamus in rats. *Neuroscience letters* 68: 165-8

McAbee MD, DonCarlos LL. 1998. Ontogeny of region-specific sex differences in androgen receptor messenger ribonucleic acid expression in the rat forebrain. *Endocrinology* 139: 1738-45

McCarthy MM. 2015. Sex Differences in the Brain. *The Scientist*, Oct 1, 2015:

McCarthy MM, Todd BJ, Amateau SK. 2003. Estradiol modulation of astrocytes and the establishment of sex differences in the brain. *Ann N Y Acad Sci* 1007: 283-97

McClellan KM, Parker KL, Tobet S. 2006. Development of the ventromedial nucleus of the hypothalamus. *Front Neuroendocrinol* 27: 193-209

Micevych PE, Meisel RL. 2017. Integrating Neural Circuits Controlling Female Sexual Behavior. *Front Syst Neurosci* 11: 42se models using long ssDNA donors. *Nat Protoc* 13: 195-215

Musatov S, Chen W, Pfaff DW, Kaplitt MG, Ogawa S. 2006. RNAi-mediated silencing of estrogen receptor {alpha} in the ventromedial nucleus of hypothalamus abolishes female sexual behaviors. *Proceedings of the National Academy of Sciences of the United States of America* 103: 10456-60

Musatov S, Chen W, Pfaff DW, Mobbs CV, Yang XJ, et al. 2007. Silencing of estrogen receptor alpha in the ventromedial nucleus of hypothalamus leads to metabolic syndrome. *Proceedings of the National Academy of Sciences of the United States of America* 104: 2501-6

Narita K, Murata T, Matsuoka S. 2016. The ventromedial hypothalamus oxytocin induces locomotor behavior regulated by estrogen. *Physiol Behav* 164: 107-12

Nicot A, Ogawa S, Berman Y, Carr KD, Pfaff DW. 1997. Effects of an intrahypothalamic injection of antisense oligonucleotides for preproenkephalin mRNA in female rats: evidence for opioid involvement in lordosis reflex. *Brain research* 777: 60-8

Ogawa S, Chan J, Chester AE, Gustafsson JA, Korach KS, Pfaff DW. 1999. Survival of reproductive behaviors in estrogen receptor beta gene-deficient (betaERKO) male and female mice. *Proceedings of the National Academy of Sciences of the United States of America* 96: 12887-92

Olster DH, Blaustein JD. 1990. Immunocytochemical colocalization of progestin receptors and beta-endorphin or enkephalin in the hypothalamus of female guinea pigs. *J Neurobiol* 21: 768-80

Patisaul HB, Fortino AE, Polston EK. 2008. Sex differences in serotonergic but not gamma-aminobutyric acidergic (GABA) projections to the rat ventromedial nucleus of the hypothalamus. *Endocrinology* 149: 397-408

Remedios R, Kennedy A, Zelikowsky M, Grewe BF, Schnitzer MJ, Anderson DJ. 2017. Social behaviour shapes hypothalamic neural ensemble representations of conspecific sex. *Nature* 550: 388-92

Roselli CE, Salisbury RL, Resko JA. 1987. Genetic evidence for androgen-dependent and independent control of aromatase activity in the rat brain. *Endocrinology* 121: 2205-10

Santiago AM, Clegg DJ, Routh VH. 2016. Estrogens modulate ventrolateral ventromedial hypothalamic glucose-inhibited neurons. *Mol Metab* 5: 823-33

Simerly RB, Chang C, Muramatsu M, Swanson LW. 1990. Distribution of androgen and estrogen receptor mRNA-containing cells in the rat brain: an in situ hybridization study. *J Comp Neurol* 294: 76-95

Song Z, Levin BE, McArdle JJ, Bakhos N, Routh VH. 2001. Convergence of pre- and postsynaptic influences on glucosensing neurons in the ventromedial hypothalamic nucleus. *Diabetes* 50: 2673-81

Steinbusch LK, Picard A, Bonnet MS, Basco D, Labouebe G, Thorens B. 2016. Sex-Specific Control of Fat Mass and Counterregulation by Hypothalamic Glucokinase. *Diabetes* 65: 2920-31

Stevant I, Kuhne F, Greenfield A, Chaboissier MC, Dermitzakis ET, Nef S. 2019. Dissecting Cell Lineage Specification and Sex Fate Determination in Gonadal Somatic Cells Using Single-Cell Transcriptomics. *Cell Rep* 26: 3272-83 e3

Todd WD, Fenselau H, Wang JL, Zhang R, Machado NL, et al. 2018. A hypothalamic circuit for the circadian control of aggression. *Nature neuroscience* 21: 717-24

Van Veen JE, Kammel LG, Bunda PC, Shum M, Reid MS, et al. 2019. Single cell profiling of the VMH reveals a sexually dimorphic regulatory node of energy expenditure. *bioRxiv* 549725

Wang L, Chen IZ, Lin D. 2015. Collateral pathways from the ventromedial hypothalamus mediate defensive behaviors. *Neuron* 85: 1344-58

Wei YC, Wang SR, Jiao ZL, Zhang W, Lin JK, et al. 2018. Medial preoptic area in mice is capable of mediating sexually dimorphic behaviors regardless of gender. *Nature communications* 9: 279

Wong LC, Wang L, D'Amour JA, Yumita T, Chen G, et al. 2016. Effective Modulation of Male Aggression through Lateral Septum to Medial Hypothalamus Projection. *Curr Biol* 26: 593-604

Wu MV, Manoli DS, Fraser EJ, Coats JK, Tollkuhn J, et al. 2009. Estrogen masculinizes neural pathways and sex-specific behaviors. *Cell* 139: 61-72

Xu X, Coats JK, Yang CF, Wang A, Ahmed OM, et al. 2012. Modular genetic control of sexually dimorphic behaviors. *Cell* 148: 596-607

Xu Y, Nedungadi TP, Zhu L, Sobhani N, Irani BG, et al. 2011. Distinct hypothalamic neurons mediate estrogenic effects on energy homeostasis and reproduction. *Cell Metab* 14: 453-65

Yang CF, Chiang MC, Gray DC, Prabhakaran M, Alvarado M, et al. 2013. Sexually dimorphic neurons in the ventromedial hypothalamus govern mating in both sexes and aggression in males. *Cell* 153: 896-909

Yang CF, Shah NM. 2014. Representing sex in the brain, one module at a time. *Neuron* 82: 261-78

Yang T, Yang CF, Chizari MD, Maheswaranathan N, Burke KJ, Jr., et al. 2017. Social Control of Hypothalamus-Mediated Male Aggression. *Neuron* 95: 955-70 e4

Chapter 2

Single cell profiling of the VMH reveals a sexually dimorphic regulatory node of energy expenditure

Abstract

Estrogen signaling in the ventromedial hypothalamus (VMH) promotes weight loss by increasing thermogenesis and physical activity, but the precise neuronal populations regulating these aspects of energy expenditure remain unclear. Here we define the molecular and functional heterogeneity of the VMH using single cell RNA sequencing, *in situ* hybridization, chemogenetic activation, and targeted gene knockdown. We describe six molecularly distinct neuron clusters in the VMH. In females, estrogen receptor α (ERα) is restricted to neurons expressing tachykinin-1 (*Tac1*) or reprimo (*Rprm*). Further, *Tac1* and *Rprm* expression is enriched in females, a sex difference that is established by permanent effects of gonadal hormones early in life. Finally, while *Tac1* ablation selectively impairs movement, here we show that silencing *Rprm* selectively dysregulates temperature without affecting physical activity. Together this work provides a novel architectural framework whereby distinct and sexually differentiated neuron populations within the VMH mediate sex-specific aspects of metabolic homeostasis.

Main

Women transitioning to menopause exhibit decreased energy expenditure and decreased fat oxidation compared to age-matched premenopausal women[1]. Similar to humans, rodents exhibit estrogen-induced changes in energy expenditure; female rats exhibit cyclic patterns of wheel running throughout the estrous cycle[2,3] and female mice exhibit similar cyclicity in temperature and locomotion[4–6]. These effects are mediated by estrogen receptor α (ERα) signaling: eliminating ERα either globally or in the central nervous system leads to obesity due increased feeding, reduced movement, and reduced thermogenesis[7–9]. While estrogen-based hormone therapy can improve metabolic profiles after menopause, it is associated with higher cardiovascular disease risk[10] and, in the case of estrogen plus progestogen therapy, higher breast cancer risk[11]. To ultimately circumvent the risks associated with systemic estrogen therapy, we aim to pinpoint neurons that control systemic energetic balance and define their responses to estrogen signaling.

Recent work has begun to define the neuron populations that mediate the effects of ERα signaling on energy balance. Conditional knockout mouse models suggest that ERα signaling modulates feeding in female mice via neurons of the pro-opiomelanocortin (*Pomc*) lineage, possibly located in the arcuate nucleus (ARC)[5,9,12,13] or outside the medial basal hypothalamus[14]. Additionally, ERα signaling modulates two types of energy expenditure, spontaneous physical activity and thermogenesis, via neurons of the steroidogenic factor 1 (*Sf1/Nr5a1*) lineage in the ventromedial hypothalamus (VMH)[9,15–17]. However, ERα-expressing neurons of the VMH have many functions. In addition to female-specific roles in energy expenditure, ERα^+ VMH neurons

control fear, territorial aggression, and self defense in males, maternal aggression in females, and mating behaviors in both sexes[18–23]. We hypothesize that these diverse and sex-specific functions are mediated by distinct subpopulations of ERα$^+$ neurons. Consistent with this notion, distinct neuronal ensembles are activated in the ventrolateral region of the VMH (VMHvl) of male mice during interactions with male or female conspecifics[18,24]. While these neuron populations remain to be defined, a subset of ERα$^+$ neurons in the VMH, which co-express tachykinin 1 (*Tac1*) and oxytocin receptor (*Oxtr*), drive estrogen-dependent changes in physical activity in females[17,25]. However, the VMHvl populations that control other sex-specific behaviors, such as estrogen-dependent increases in thermogenesis, have not been identified.

The VMH is sexually dimorphic with respect to hormone responsiveness, gene expression, neurochemistry, synaptic organization, and neuron function[26–28]. Here, we use RNA sequencing with single cell resolution to test the hypothesis that neurons in this region are heterogeneous and sexually dimorphic. We define six major neuron populations in the VMH and a new sexually dimorphic transcript in the VMHvl, reprimo (*Rprm)*, which regulates core body temperature. Collectively, these studies demonstrate that estrogen regulates energy expenditure in females through two intermingled but distinct neuronal subsets, and suggest that the VMH serves as a hormone-responsive nexus of distinct neural circuits controlling metabolic homeostasis.

Results

Single Cell Transcriptomics Reveals Neuronal Heterogeneity in the VMH

We used a fluorescent reporter strategy to isolate neurons of the VMH and single cell RNA sequencing to cluster neurons by transcriptional signature. To selectively label

VMH neurons, the *Sf1Cre* driver[29] was crossed to mice carrying a latent allele of tdTomato *(Ai14)*[30] (Figure 2.1a). Importantly, this strategy yields tdTomato expression in neurons of the entire VMH upon Cre expression, including in the ventrolateral VMH where it overlaps with ERα immunoreactivity in both males and females (Figure 2.1b, c) as in [31]. tdTomato expression in surrounding hypothalamic regions, the dorsomedial hypothalamus (DMH) and the arcuate nucleus (ARC), was detectable but scattered and infrequent. Fluorescence-activated cell sorting (FACS) was performed on single cell suspensions of hypothalami to isolate live neurons of the *Sf1* lineage for single cell transcriptomic analysis (Figure 1d).

Unicellular transcriptional analysis of 530 single cells from 3 male and 3 female postnatal day (P) 10 mice detected an average (median) of 2556 genes per single cell and revealed strong and consistent expression of the neuronal markers β3-tubulin (*Tubb3*) and neurofilament light peptide (*Nefl*), while very few cells exhibited detectable expression of the glial markers *Gfap* and *Olig1* (Figure 2.2a). Consistent with the VMH being predominantly glutamatergic, high expression of the glutamatergic marker *Slc17a2* and consistently low expression of the GABAergic marker *Gad2* was observed in all samples (Figure 2.2a). Finally, to assess how dissociation and FACS sorting may have affected gene expression, we examined immediate early gene expression. Expression of *Fos* and *Arc*, used as a readout for isolation stress and activation[32,33], appears undetectable in the majority of cells from suspensions obtained from different animals and sexes (Figure 2.2a). Overall, we conclude that the *Sf1Cre*-mediated fluorescent reporter strategy primarily yields healthy VMH glutamatergic neurons.

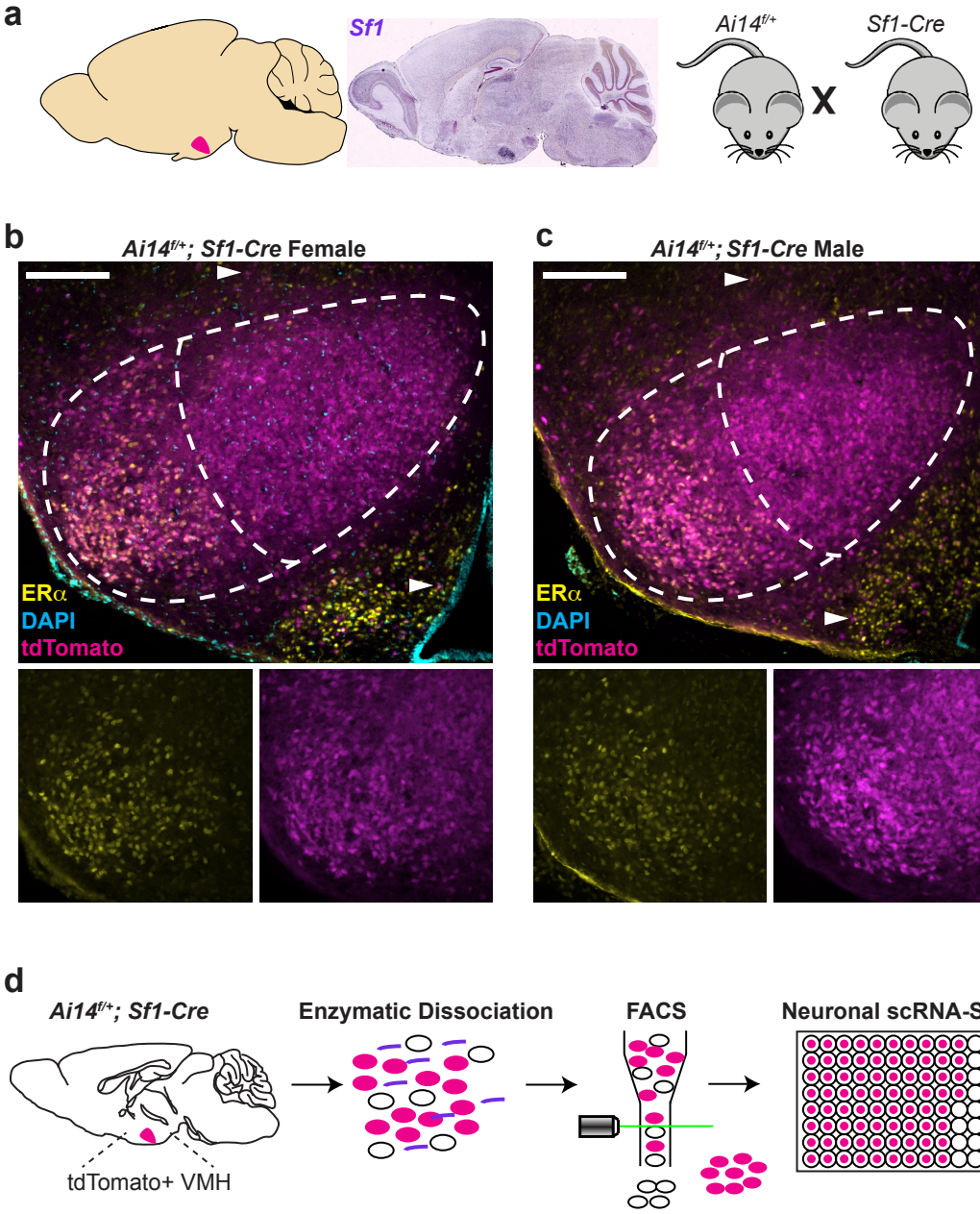
a
Sf1
Ai14f/+
X
Sf1-Cre
b
Ai14f/+; Sf1-Cre Female
ERα
DAPI
tdTomato
c
Ai14f/+; Sf1-Cre Male
ERα
DAPI
tdTomato
d
Ai14f/+; Sf1-Cre
tdTomato+ VMH
Enzymatic Dissociation
FACS
Neuronal scRNA-Seq

Figure 2.1 *Sf1* lineage tracing allows for targeted scRNA-seq of the VMH. a, In-situ hybridization of *Sf1* transcripts in sagittal section of mouse brain (from Allen Brain Atlas) shows a pattern of expression restricted to the VMH. b,c, Mice harboring both the *Sf1-Cre* allele and a latent allele of tdTomato (*Ai14*) show VMH specific fluorescence within the hypothalamus: coronal sections taken from P10 mice, scale bars = 200um. Both female (b) and male (c) VMH show expression of ERa in the VMHvl. As expected, females show higher immunoreactivity. White arrowheads highlight scattered *Sf1* lineage cells outside of the VMH. **d,** Strategy for dissociation followed by FACS and VMH targeted scRNA-seq.

To determine if VMH neurons show heterogeneity in gene expression profiles, we used a Shared Nearest Neighbor (SNN) algorithm to identify clusters comprised of transcriptionally similar cells[34]. A uniform manifold approximation and projection (UMAP) revealed a main cluster and two divergent clusters (Figure 2.2b). Within the main cluster, UMAP-based separation was less pronounced, as may be expected when examining neurons of a single transcription factor lineage (*Sf1Cre*). Nevertheless, we detected distinct clusters marked by differential expression of genes that have known and unknown significance in the VMH. We identified a total of eight clusters, hereby identified by the top most differentially expressed transcript within each cluster (Figure 2.2b, c): *Tac1*, which has been previously demonstrated to promote physical activity in female mice[17]; reprimo (*Rprm*), a TP53 and ERα regulated gene[35] with no described role in the brain; prodynorphin (*Pdyn*), a gene encoding an endogenous opioid precursor with described roles in leptin-regulated energy homeostasis throughout the

hypothalamus[36]; somatostatin (*Sst*), a neuropeptide precursor gene which has hypothalamic roles in the negative regulation of growth hormone axis[37] and feeding[38]; hippocalcin-like protein 1 (*Hpcal1*) encoding a neuron-specific calcium binding protein; and galanin (*Gal*), a neuropeptide precursor gene shown to increase food consumption when injected into the VMH of rats[39]. In addition to the subpopulations in the principal six clusters, we identified two divergent clusters: a cluster marked by differential expression of proopiomelanocortin (*Pomc*) and many other markers indicating an ARC derived origin, and one marked by differential expression of apolipoprotein E (*Apoe*) and many other markers of glial-like signature.

Comparing overall transcriptional signatures amongst the eight clusters (Figure 2.2d), the most divergent population are the cells with glial-like signature (*Apoe*$^{+}$), followed by neurons expected to be from the ARC (*Pomc*). Neuron clusters expected to arise from the VMH are more closely related in overall expression signature. Remarkably, the expression of cluster-defining markers appears largely mutually exclusive (Figure 2.2e), suggesting distinct molecular signatures among neuron clusters of the VMH.

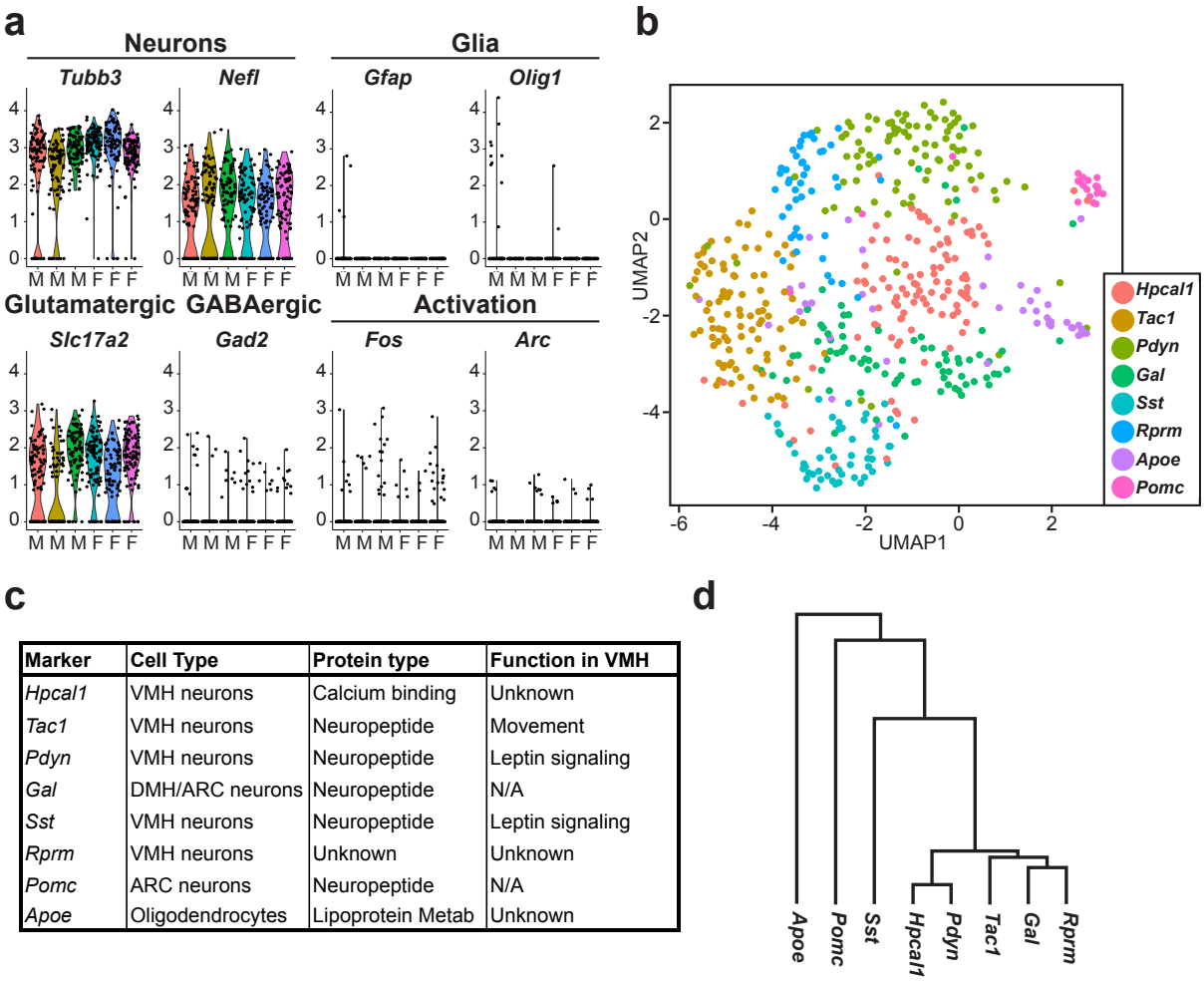

c

Marker	Cell Type	Protein type	Function in VMH
Hpcal1	VMH neurons	Calcium binding	Unknown
Tac1	VMH neurons	Neuropeptide	Movement
Pdyn	VMH neurons	Neuropeptide	Leptin signaling
Gal	DMH/ARC neurons	Neuropeptide	N/A
Sst	VMH neurons	Neuropeptide	Leptin signaling
Rprm	VMH neurons	Unknown	Unknown
Pomc	ARC neurons	Neuropeptide	N/A
Apoe	Oligodendrocytes	Lipoprotein Metab	Unknown

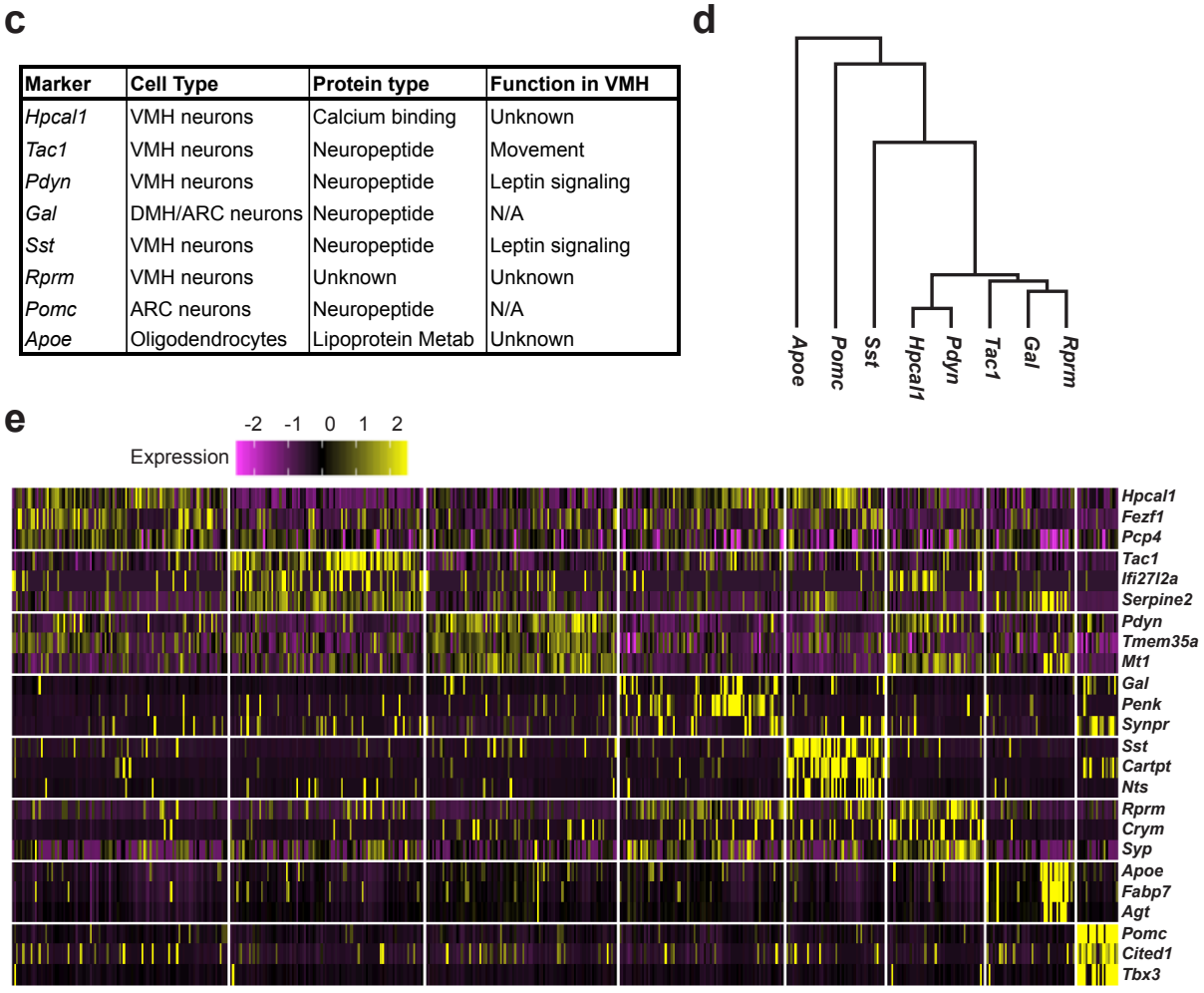

Figure 2.2 Single cell RNA sequencing reveals non-overlapping gene expression signatures in the VMH. a, scRNA sequencing results from (n = 3 female, 3 male) P10 mice showing high expression levels of the neuron specific markers *Tubb3* and *Nefl* with only scattered cells expressing the glial markers *Gfap* and *Olig1*. Cells also express high levels of the glutamatergic marker *Slc17a2*, low levels of the GABAergic marker *Gad2*, and limited expression of the immediate early genes *Fos* and *Arc*. b, UMAP showing clusters as defined by marker with highest expression relative to other clusters.

All the neuron clusters identified in the unicellular analysis of the VMH were obtained by analyzing males and females together (Figure S2.1a). We then compared the gene expression profiles between males and females to determine whether sex-specific signatures existed in VMH neurons. The paternally-expressed gene necdin (*Ndn*) had the highest enrichment in males, whereas the proto-oncogene *Araf* had the highest enrichment in females (Figure S2.1b). *Ndn* expression was consistently higher across all clusters in males (Figure S2.1c) and RNA *in situ* hybridization (ISH) confirmed enrichment of *Ndn* transcripts in the male VMH as compared to females (Figure S2.1d). *Araf* expression was detected to be consistently higher in neurons from females across clusters, compared to those from males (Figure S2.1e). ISH of *Araf* was unable to clearly confirm the female biased expression in the VMH, though it appears that *Araf* expression in females might be slightly higher in the VMHvl (Figure S2.1f). As *Araf* is a direct effector of the RAF/MEK/ERK MAPK cascade, we sought to determine if this pathway is activated differentially in females. Intriguingly, we found female-specific phosphorylation of MEK in the VMHvl that co-localizes with ERα (Figure S2.1g). This

result supports a female specific role of MAPK signaling in the VMHvl as well as *Araf* as a target to be explored to induce changes in energy balance.

Sex differences established by gonadal hormones

To test the prediction that each neuron cluster generated by gene expression would have a correspondingly distinct spatial distribution within the intact VMH, we detected and localized the expression of the cluster-defining markers using ISH. Further confirming the efficiency of VMH neuron isolation used in the scRNA-seq, expression of all marker genes except *Pomc* was detected within the anatomical boundaries of the VMH (Figure 2.3 and Figure S2.2a, b). The most restricted expression patterns were observed with *Tac1*, *Rprm*, *Pdyn,* and *Sst*. Sexually dimorphic expression of *Tac1*, *Rprm*, and *Pdyn* was detected in the VMHvl (Figure 2.3a-c). Specifically, *Tac1* and *Rprm* expression were both significantly enriched in females within the VMHvl (Figure 2.3a, b). In contrast, *Pdyn* expression was significantly enriched in males within the VMHvl, although both males and females showed robust expression of *Pdyn* in the dorsomedial VMH (VMHdm, Figure 2.3c). Finally, we did not detect any major differences in expression of *Sst* between males and females (Figure 2.3d).

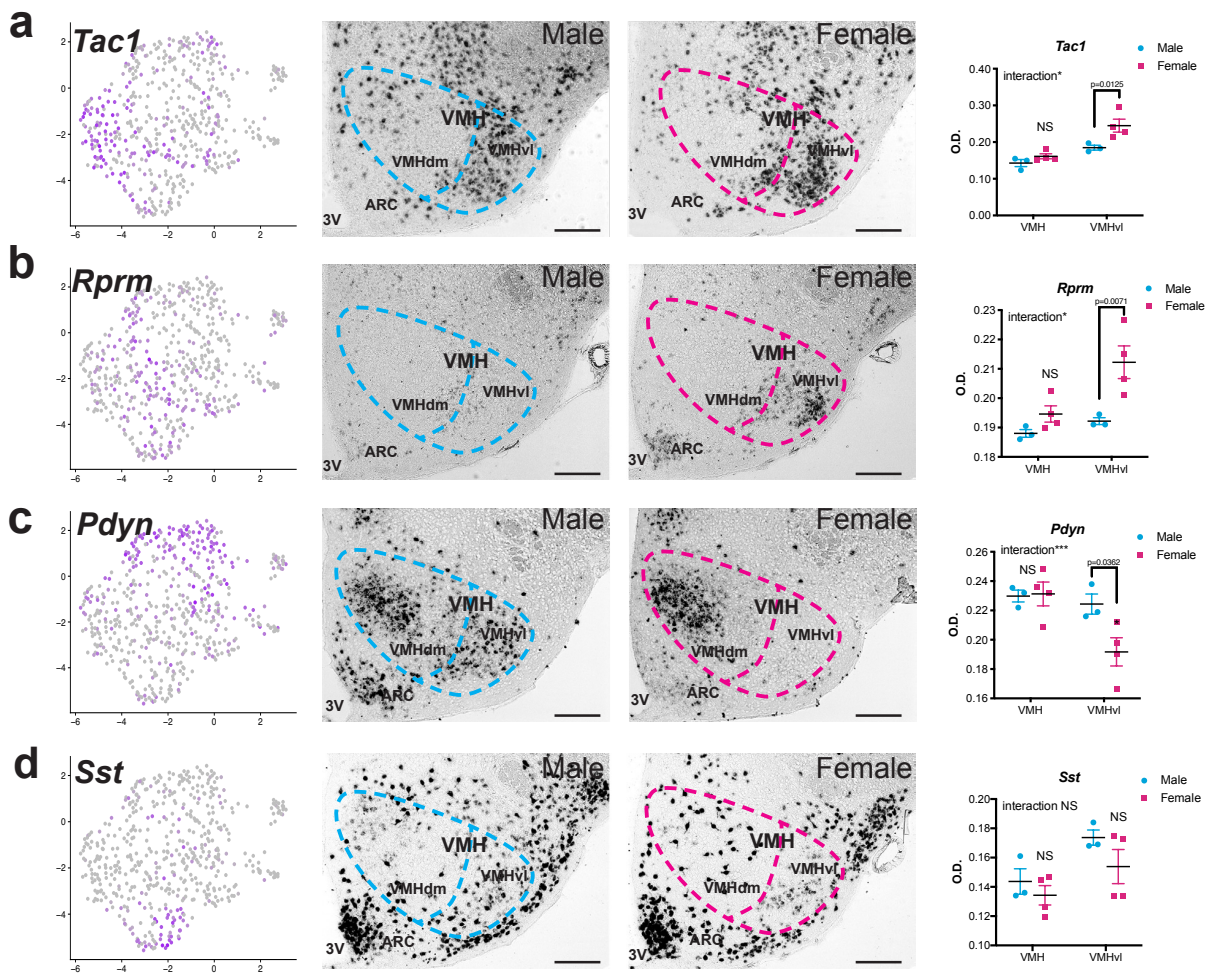

Figure 2.3 Spatial organization of cluster marker within the VMH. Cells positive for a, *Tac1*, b, *Rprm*, c, *Pdyn*, and d, *Sst* are identified in purple within the UMAP (left panels). Spatial localization of each cluster marker along the rostral-caudal axis of the VMH in intact males (n = 3 mice) and females (n = 3-4 mice) by chromogenic ISH (right panels). mRNA levels were quantified within the caudal VMH and caudal VMHvl subregion. A statistically significant interaction between sex and ROI was determined for *Tac1* (*F(1,5) = 8.932, p = 0.0305*), *Rprm (F(1,5) = 13.23, p = 0.0149)*, and *Pdyn* (*F(1,5) = 65.84, p = 0.0005*). Post-hoc Sidak's multiple comparison tests revealed statistically significant sex

differences in expression in the caudal VMHvl (*p = 0.0125 for Tac1, p = 0.0071 for Rprm, p = 0.0362 for Pdyn*). Dashed line shows boundary of VMH and VMHvl, in blue for male and magenta for female. Scalebars = 200μm, * = p<0.05, ** = p<0.01, *** = p<0.001.

Sex hormones mediate permanent (organizational) differentiating effects on the brain during development, as well as reversible (activational) effects during adulthood, with additional contributions to sex differences caused by sex chromosome genes expressed within brain cells. To delineate how sexually dimorphic expression of cluster markers develops in the VMHvl, we used the four-core genotypes model[40] to reveal i) organizational effects of hormones, by comparing XX female vs. XX male or XY male vs. XY female, all gonadectomized (GDX) upon sexual maturity, ii) activational effects of hormones, by comparing GDX vs. intact XX females or XY males, and iii) the effects of sex chromosomes, by comparing XX female vs. XY female or XX male vs. XY male, all GDX, as illustrated in Figure 2.4a. Expression patterns of both *Tac1* and *Rprm* were unchanged by GDX in females, showing that hormonal activation is not essential for dimorphic expression. Moreover, the presence of the Y chromosome in females did not change *Tac1* or *Rprm* expression, suggesting that the Y chromosome did not have a repressive role on these genes. However, gonadal sex was critical for determining these sexually dimorphic expression patterns, suggesting that these patterns are established during development and are maintained in adulthood (Figure 2.4b, c). In contrast, the expression pattern of *Pdyn* was distinct between GDX or intact females and gonad-intact males, but not GDX males (Figure 2.4d, and Figure S2.3), suggesting that *Pdyn*

expression is maintained by differences in testicular sex hormone signaling in adulthood. Finally, we did not observe any sex differences in *Sst* along any of the three phenotypic comparisons (Figure 2.4e).

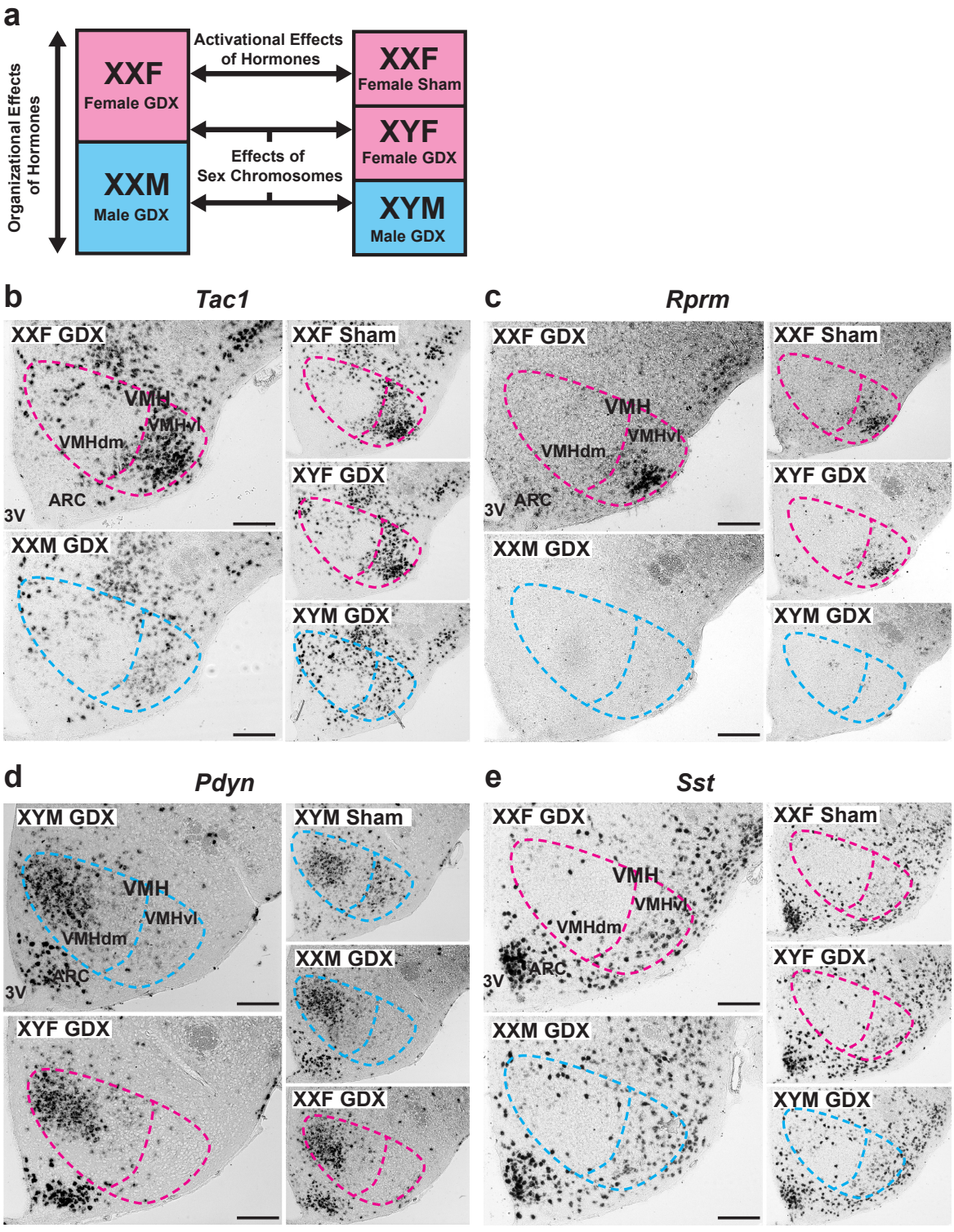
a
Organizational Effects of Hormones
XXF
Female GDX
XXM
Male GDX
Activational Effects of Hormones
Effects of Sex Chromosomes
XXF
Female Sham
XYF
Female GDX
XYM
Male GDX
b
Tac1
XXF GDX
XXF Sham
XYF GDX
XXM GDX
XYM GDX
VMH
VMHvl
VMHdm
ARC
3V
c
Rprm
d
Pdyn
XYM GDX
XYM Sham
XXM GDX
XYF GDX
XXF GDX
e
Sst

Figure 2.4 Organizational effects of hormones establish sexual dimorphic expression of cluster markers. a, The Four-Core Genotypes (FCG) mouse model, which produces littermates of XX gonadal females (XXF), XX gonadal males (XXM) with an autosomal transgene of the testis-determining gene *Sry* (*Sry Tg*), XY gonadal males (XYM), and XY gonadal females (XYF) with the *Sry Tg*, can be used to determine if the origin of sexually dimorphic gene expression arises due to organizational effects of hormones, activational effects of hormones, or effects due to differences in sex chromosome complement. Expression of b, *Tac1*, c, *Rprm*, d, *Pdyn*, and e, *Sst* in the caudal VMH of gonadectomized (GDX) or sham FCG mice (n= 2-3 mice per group) by chromogenic ISH. Dashed line shows boundary of VMH and VMHvl, in blue for male and magenta for female. Scalebars = 200μm.

Two major estrogen-sensitive populations in the female VMHvl

Estradiol, as a metabolite of testosterone from the testes, plays a major role in the early permanent masculinization of the mammalian brain in males and the expression of male-specific behaviors. To determine if any of the organizational and activational effects of sex hormones on neuronal cluster markers, specifically *Tac1*, *Rprm*, and *Pdyn*, could be related to estradiol action on ERα, we first examined the expression of ERα by fluorescent ISH (FISH) within each cluster. In females, ERα immunoreactivity was frequent in *Tac1*$^+$ cells and *Rprm*$^+$ cells (Figure 2.5a, b), but rare in *Sst*$^+$ and Pdyn$^+$ cells (Figure S2.4a, b). In males, also we found that ERα immunoreactivity was frequent in Tac1$^+$ cells, despite lower ERα protein expression compared to females (Figure 2.5c). In contrast to females, however, ERα

immunoreactivity was also frequent in *Pdyn*$^+$ cells (Figure 2.5d) but rare *Rprm*$^+$ cells in males (Figure S2.5c). We then investigated the spatial relationship of these ERα^+ neuron populations. In females, *Tac1*$^+$ and *Rprm*$^+$ cells were highly intermingled within the VMHvl (Figure 2.5d), but largely spatially distinct from *Sst*$^+$ cells (Figure S2.4e, f). Finally, we asked if ERα is required for the sexually dimorphic expression of *Rprm* in females, as previous studies showed that *Tac1* expression was independent of ERα status in the VMHvl. We compared mice with genetic ablation of ERα in the *Sf1* lineage, which results in a substantial loss of ERα^+ cells in the VMH[9], and a second mouse model lacking ERα in the *Nkx2-1* lineage, which shows near complete elimination of ERα both in the VMH and ARC[17]. Interestingly, we found that *Rprm* expression, similar to *Tac1* expression, was insensitive to ERα ablation in the female VMHvl (Figure 2.5f, g). Together, these findings are in line with evidence that early brain masculinization, rather than feminization, following the perinatal testosterone surge is dependent on ERα-induced regulation of gene expression (Nugent et al 2015).

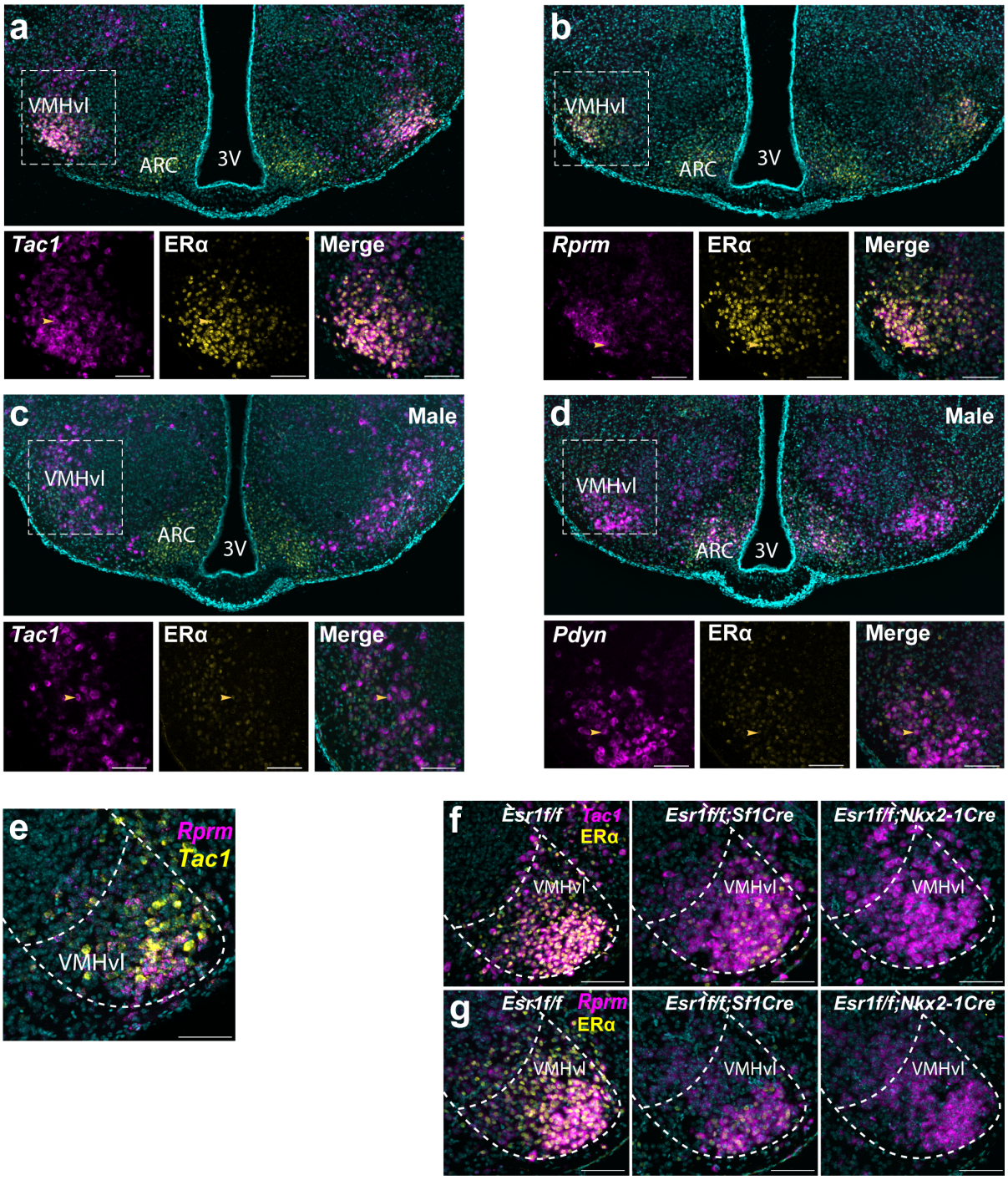

Figure 2.5 *Tac1*$^{+}$ and *Rprm*$^{+}$ cells are principal ERα-expressing neurons in the female VMHvl. Transcript expression (magenta) of a, *Tac1*, and b, *Rprm* is shown together with ERα immunoreactivity (yellow) in the VMHvl using fluorescent ISH (FISH, n = 5 female mice). Scalebars on insets = 100μm. Transcript expression of *Pdyn* (magenta) in the

VMHvl of c, female mice (n = 5) and d, male mice (n = 5) and ERα immunoreactivity (yellow) using FISH/IHC. Scalebars on insets = 100μm. Yellow arrows indicate colocalized signals. e, *Rprm* (magenta) and *Tac1* (yellow) transcript expression is visualized using TSA-FISH (n = 5 female mice) in the rostral (top panel) and caudal (bottom panel) VMH. Scalebars = 100μm. Transcript expression (magenta) of f, *Tac1* and g, *Rprm* together with ERα immunoreactivity (yellow) is visualized in *Esr1*$^{f/f}$ mice (n = 6 female mice, left panel), and mice with genetic ablation of ERα in neurons of *Sf1* lineage (*Esr1*$^{f/f}$*;Sf1Cre*, n = 4 female mice, middle panel) and in neurons of *Nkx2-1* lineage (*Esr1*$^{f/f}$*;Nkx2-1Cre*, n = 3 mice, right panel). Scalebars = 100μm. Images are merged with DAPI (cyan).

VMH Expression of Reprimo Regulates the Central Control of Temperature

To discern the role of ERα^{+} VMHvl neurons in energy expenditure, we first chemogenetically activated ERα neurons using the Cre-dependent DREADD (AAV-DIO-hM3Dq[41]) delivered bilaterally to the VMHvl of *Esr1Cre* knockin mice[20]. Administration of the DREADD ligand, clozapine-N-oxide (CNO), elicited a sustained (6 hour) increase in both heat and physical activity in *Esr1Cre* females compared to saline administration in the same mice on a different day and compared to CNO administration to wild-type littermates (Figure 2.6a, b Figure S2.5).

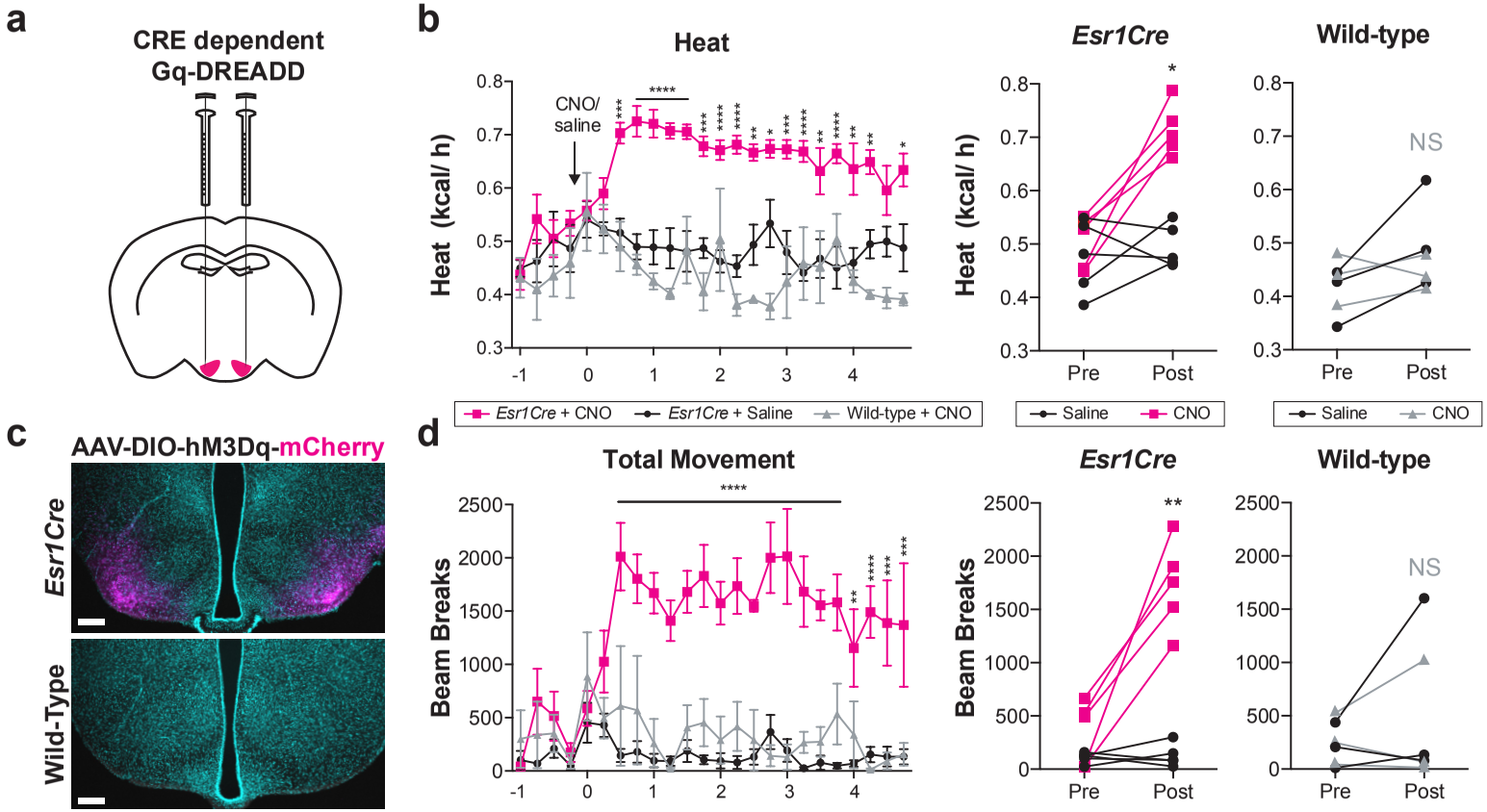
a
CRE dependent
Gq-DREADD
b
Heat
CNO/
saline
Heat (kcal/ h)
Esr1Cre + CNO
Esr1Cre + Saline
Wild-type + CNO
Esr1Cre
Wild-type
Pre
Post
NS
Saline
CNO
c
AAV-DIO-hM3Dq-mCherry
Esr1Cre
Wild-Type
d
Total Movement
Beam Breaks

Figure 2.6 Specific activation of *Esr1*$^{+}$ neurons in the VMHvl causes enhanced movement and thermogenesis. a,c, Strategy for and validation of stereotaxic injection of AAVs harboring Cre dependent Gq-coupled DREADDs in the VMHvl b, Heat generation increases acutely in *Esr1-Cre* animals after CNO injection but not after saline injection (n = 5 females). Two way RM ANOVA: Time (*F(23,92) = 4.542, p < 0.0001)*, CNO *(F(1,4) = 57.19, p = 0.0016)*, Interaction *(F(23,92) = 3.517, p < 0016).* Wild-type littermate controls stereotaxically injected with the Cre dependent Gq-coupled DREADD show no significant increase in thermogenesis after CNO treatment (n = 3). d, Movement increases acutely in *Esr1-Cre* animals after CNO injection but not after saline injection. Two way RM ANOVA: Time (*F(23,92) = 6.361, p < 0.0001)*, CNO *(F(1,4) = 47.17, p = 0.0024)*, Interaction *(F(23,92) = 4.945, p < 0001).* Wild-type animals stereotaxically injected with the Cre dependent Gq-coupled DREADD show no significant increase in movement after CNO treatment. Within-subject changes in average heat and average total movement are shown as averages 0-60 minutes prior to (Pre) and 30-90 minutes following the disturbance to deliver CNO (Post). All subjects were female wild-type mice, ages 10-18 weeks, and singly housed in indirect calorimetry chambers. Posthoc Sidak's multiple comparison tests were used for pairwise comparisons: * = p<0.05, ** = p<0.01, *** = p<0.001, **** = p<0.0001.

Previous studies suggest that *Tac1*$^{+}$ neurons mediate estrogenic effects on physical activity but not thermogenesis, and that these neurons require *Tac1* expression to fully induce movement[17]. The neuronal population controlling thermogenesis in a sexual dimorphic manner, however, was still elusive. Thus, we hypothesized that the

specific role of these newly identified *Rprm*$^{+}$ neurons was to control thermogenesis in females. To test this hypothesis, we silenced *Rprm* gene function within the VMHvl using cell permeable siRNA pools delivered via bilateral stereotaxic injections (Figure 2.7a, inset). When compared to animals injected with a non-targeting siRNA, females injected with *Rprm* targeting siRNA showed a significant increase in body temperature (Figure 2.7a, left). The increase in temperature was persistent across time points and was significant both in the active night phase and the inactive day phase (Figure 2.7a, right). In contrast, males injected with *Rprm* targeting siRNA showed no difference in body temperature to animals injected with the non-targeting siRNA during any phase of the light cycle (Figure 2.7b). Importantly, *Rprm* knockdown also did not induce changes in physical activity in females or males (Figure 2.7c), suggesting that the body temperature increase in females was distinct from a movement phenotype.

To determine the origin of the *Rprm* knockdown-induced body temperature increase, we examined BAT and inguinal WAT depots for markers of thermogenesis. These data suggest that increased BAT thermogenesis could be a mediator of increased body temperature. Finally, we examined if the effect of *Rprm* knockdown on BAT thermogenesis was dependent on the presence of ovarian hormone by thermogenic image analysis (Figure 2.7d. Interestingly, simple main effects analysis showed that siRNA type significantly contributed to BAT temperature (three-way ANOVA, $p=0.0208$), but not hormone status ($p= 0.5229$), time of day ($p=0.9113$), or interactions between siRNA type, hormone status, and time of day (Figure 2.7e). These data demonstrate that *Rprm* knockdown in the VMH is sufficient to increase BAT thermogenesis in females, even in the absence of circulating ovarian hormone.

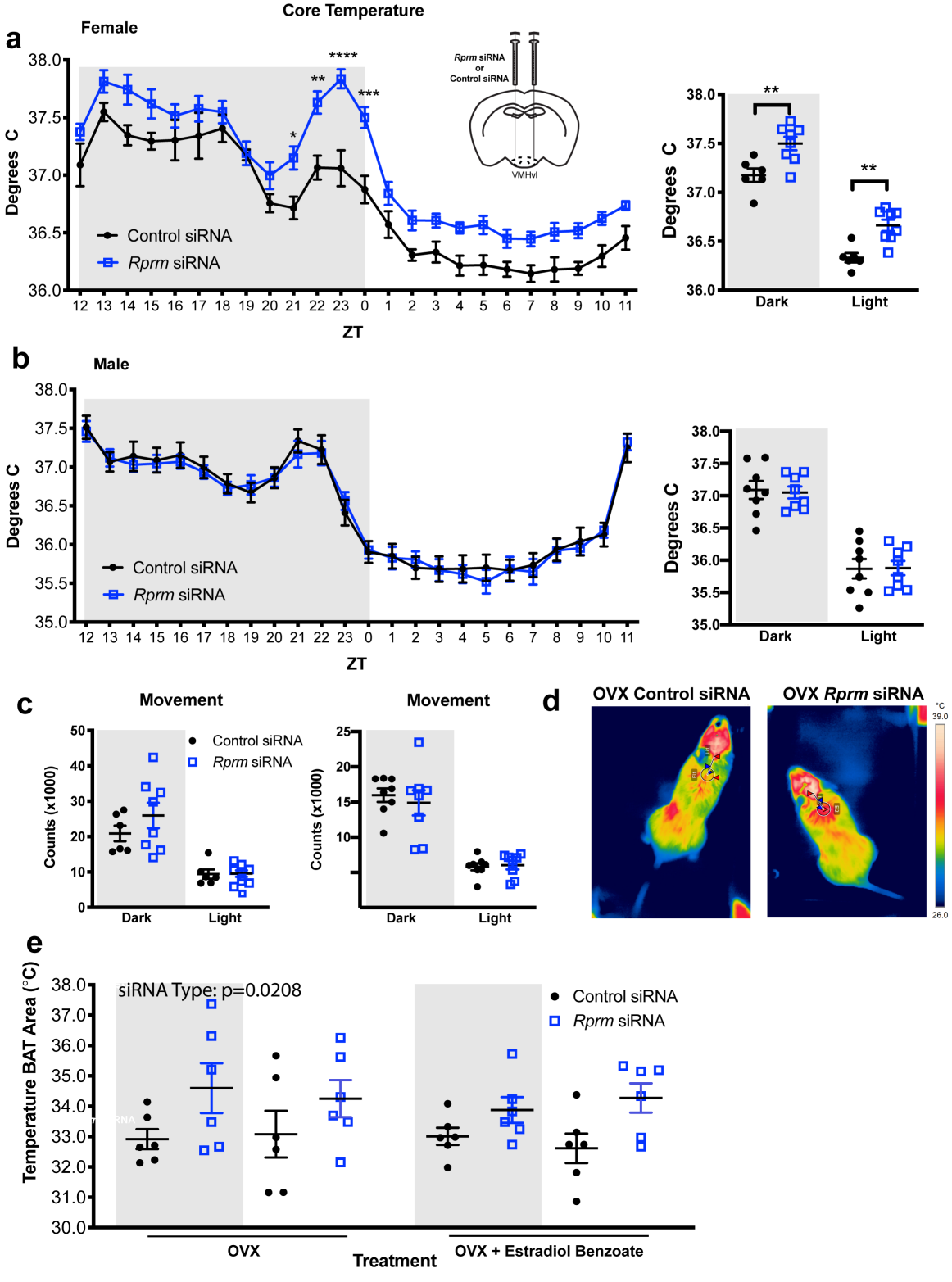
a
Female
Core Temperature
Degrees C
ZT
Control siRNA
Rprm siRNA
Rprm siRNA or Control siRNA
VMHvl
Dark
Light
b
Male
c
Movement
Counts (x1000)
d
OVX Control siRNA
OVX Rprm siRNA
e
siRNA Type: p=0.0208
Temperature BAT Area (°C)
OVX
OVX + Estradiol Benzoate
Treatment

Figure 2.7 Core body temperature is dysregulated in mice lacking *Rprm.* a, Strategy for stereotaxic injection of cell-permeable siRNA pools either targeting *Rprm* (n = 6) or non-targeting (n = 8) to female mice. Left panel, core temperature is significantly increased in animals injected with *Rprm* targeting siRNA pools compared to animals injected with non-targeting siRNA pools. Two way RM ANOVA: Interaction (*F(23,276) = 1.653, p = 0.0329)*, Time *(F(23,276) = 67.31, p <0.0001)*, siRNA *(F(1, 12) = 18.31, p = 0011)*. Right panel, the effect of *Rprm* depletion on core temperature is significant in both the sleep (day) phase and active (night) phase compared to non-targeting controls. Two way RM ANOVA: Interaction (*F(1,12) = 1.653, p = 0.9408)*, Time *(F(1,12) = 330.1, p <0.0001)*, siRNA *(F(1, 12) = 18.31, p = 0011)* b. No significant difference in core body temperature between male mice receiving stereotaxic injection of cell-permeable siRNA pools either targeting *Rprm* (n = 8) or non-targeting (n = 8). c,. *Rprm* depletion showed no significant effect on movement in females or males in either sleep or active phase when compared to non-targeting controls. All subjects were wild-type mice, ages 10-20 weeks, and singly housed. d. Representative thermographic image analysis of ovariectomized mice following stereotaxic injection of siRNA pools. The BAT ROI was defined as a standard distance from the base of the ears. e. Temperature of skin in BAT area of mice following stereotaxic injection of siRNA pools targeting *Rprm* (n=6) or non-targeting (n=6) following ovariectomy and hormone replacement (estradiol benzoate, 20µg). Three way RM ANOVA: siRNA F (1, 10) = 7.509, p=0.0208). No significant effects of treatment, time of day, or interaction between the factors. Three Posthoc Sidak's multiple comparison tests were used for pairwise comparisons: * = p<0.05, ** = p<0.01, *** = p<0.001, **** = p<0.0001.

Discussion

This study used the power of single cell RNA sequencing as a starting point for a high resolution atlas of the VMH, one of the brain's longest known sexually dimorphic regions. By performing our sequencing ten days after birth, we were able to discover populations established in development, before they are altered by hormonal changes associated with experience or puberty. Extensive validation experiments confirm all of the populations identified by sequencing analysis. Additionally, *in situ* hybridization comparing the sexes revealed novel sexually dimorphic populations in the VMHvl that scRNA sequencing did not resolve. We detected only scattered reads from *Esr1* in our sequencing, but combining immunohistochemistry with in situ hybridization clearly identified specific populations that overlap with ERα expression, notably including the sexually dimorphic subpopulations of the VMH. Finally, *in vivo* validation experiments confirm that ERα^{+} neurons in the VMHvl play unique roles in regulating energy expenditure in females, and extend this finding by functionally and molecularly subdividing these neurons. Functional dissection of sex differences in the neural circuits that control food intake and energy expenditure is critical to understanding the biological basis of gender differences in the control of body weight.

Single cell RNA sequencing has led to dramatic improvements in understanding diverse cell populations of the hypothalamus, using dissociated brain tissue without purification of cell types [42,43]. Here, we extend these studies by using mice harboring a genetically encoded fluorescent lineage tracer (*Sf1-Cre; Ai14*). This approach was tailored to allow specific purification of VMH neurons by FACS prior to scRNA-Seq. We identified six major and two minor clusters of cells with distinct transcriptional

signatures. Notably, previous studies do not identify the two clusters marked *Hpcal1* or *Rprm*, nor do they assign *Tac1*, *Pdyn*, *Sst,* or *Gal* populations to the VMH [42,43]. In contrast, targeted profiling of the *Sf1* lineage allows the study of the VMH with unprecedented resolution.

As the overall anatomy of the VMH is conserved between males and females (Figure 2.1b-c, 2.3, Figure S2.1), it is curious how activation of equivalent neurons can evoke sex specific behaviors. It is now generally accepted that sexually dimorphic behaviors are sexually differentiated by sex hormones during critical developmental periods (reviewed in [44,45]). Estrogen signaling in the VMH has clearly demonstrated roles in coordinating the increased movement and thermogenesis that accompany the sexually receptive period in female mice[16,46]. Indeed, partial ablation of *Esr1*$^+$ neurons in the VMH impairs BAT thermogenesis in females[9]. Additionally, activation of neurons in the VMHvl increases physical activity in females, but not in males, in a manner that is dependent on both circulating estrogens and hypothalamic expression of ERα[17]. Here, we find that specific activation of *Esr1*$^+$ neurons in female VMHvl increases physical activity and body temperature, supporting the notion that *Esr1*$^+$ VMHvl neurons coordinate estrogen-dependent energy expenditure.

The present results suggest that sex hormone signaling during development drives the emergence of two female-specific subpopulations of *ERa*α^+ neurons, defined by largely mutually exclusive expression of either *Tac1* or *Rprm*. Previous studies link the *Tac1*$^+$ subset of ERα^+ neurons to the regulation of physical activity in females, without affecting thermogenesis[17]. To date, several lines of evidence have also implicated estrogen signaling in the VMH, primarily dependent on inhibition of AMP-

kinase (AMPK), in enhanced BAT thermogenesis through activation of the sympathetic nervous system (SNS)[16,47]. We now report that silencing *Rprm* function selectively alters core body temperature without significantly affecting movement in females but not males. Furthermore, we detected markers indicative of increase BAT thermogenesis, suggesting that this increase in temperature was at least partially mediated by BAT. Together, our expression analyses and functional studies suggest a model in which estrogens act on the *Tac1* and *Rprm* neuron clusters to increase energy expenditure in females by two distinct mechanisms. The intermingling of *Tac1*$^+$ and *Rprm*$^+$ neurons within the VMHvl is intriguing. In the future, it will be very interesting to examine whether *Rprm*$^+$ neurons and *Tac1*$^+$ neurons exhibit crosstalk and how their circuit wiring differs, but this will require currently unavailable tools, such as a *Rprm-Cre* mouse, to allow for specific labeling, activation, and inhibition of these populations.

These studies also uncovered a male-specific pattern of expression in the VMHvl, defined by the expression of *Pdyn*. A notable difference between the *Pdyn* and *Tac1* or *Rprm* subpopulations is that maintenance of *Pdyn* in the VMHvl expression requires circulating testicular hormones. This result is made more striking by the observation that *Pdyn* expression in the dorsomedial VMH (VMHdm) is contrastingly unaffected by castration. Dynorphins, the products of *Pdyn*, are potent endogenous opioid peptides[48] with demonstrated roles in reward, addiction, and stress[49]. It will be very interesting in future studies to examine the role of VMH *Pdyn* expression in male behavior, and how these behaviors might be modified by circulating levels of testosterone. In addition to the observed sub-specialization of the VMHvl, we observed a limited number of VMH-wide sex differences in gene expression, including male-

biased expression of *Ndn*, which appears to be due to fewer *Ndn*$^{+}$ cells in the VMH of females compared to males.

Entry into menopause is associated with significant increases in visceral abdominal fat and body weight. Surprisingly, this is not associated with an increase in caloric intake. Instead, adiposity correlates with a decrease in overall energy expenditure, which manifests most strikingly during sleep[1], implying that an increasingly sedentary lifestyle cannot be the primary determinant. Because postmenopausal obesity confers enhanced risks of cardiovascular disease and breast cancer, there is a clear and urgent need to find new strategies to combat weight gain. Replacing hormones lost during menopause, such as estrogen and progesterone, can bring about weight loss, but these treatments themselves carry potential cardiovascular and cancer risks. We speculate that *Tac1*$^{+}$ and *Rprm*$^{+}$ neurons are important nodes in the dysregulation of energy expenditure accompanying the abrupt decline in circulating sex hormones experienced during menopause. Interestingly, we found that manipulation of *Rprm* expression leads to an increase in BAT thermogenesis regardless of peripheral hormone status, suggesting the cellular mechanism of *Rprm* on BAT can be activated even without ERα signaling. As such, the molecular mechanism whereby these neurons control thermogenesis will be of interest for the treatment of post-menopausal obesity.

Experimental Procedures

Mice

All studies were carried out in accordance with the recommendations in the Guide for the Care and Use of Laboratory Animals of the National Institutes of Health.

UCLA is AALAS accredited and the UCLA Institutional Animal Care and Use Committee (IACUC) approved all animal procedures. Mice expressing the *Sf1Cre* driver transgene (*Tg(Nr5a1-cre)7Lowl*), the *Nkx2-1Cre* driver transgene (*Tg(Nkx2-1-cre)2Sand*), and the *Ai14*-tdTomato reporter with loxP-flanked STOP cassette (*Gt(ROSA)26Sort*$^{m14(CAG-tdTomato)Hze}$) were maintained on a C57BL/6 genetic background. The *Esr1 floxed* allele (*Esr1*^{tm1Sakh}) was maintained on a CD-1;129P2 mixed background. Breeder male "Four Core Genotypes" mice (FCG, background C57BL/6J) possess a Y chromosome deleted for the testis-determining gene *Sry*, and an *Sry* transgene inserted into chromosome 3. The four genotypes include XX and XY gonadal males (XXM and XYM), and XX and XY gonadal females (XXF and XYF). Genotypes were discriminated using genomic PCR as described in [50]. All other experiments were carried out on C57BL/6J mice (JAX 000664). Except for gonadectomy studies, all experiments were performed in intact males and intact cycling females.

scRNA sequencing

We labeled all VMH neurons by crossing the Cre-dependent tdTomato reporter (*Ai14*)[30] to the *Sf1Cre* driver[29] to generate *Ai14*$^{f/f}$*; Sf1Cre* mice. Because the tdTomato signal is largely restricted to the VMH, a fairly large hypothalamic region was collected under fluorescent illumination. Cells were dissociated using a papain-based enzymatic process (Worthington Biochemical). VMH neurons were sorted by FACS using parameters that select for tdTomato signal. Because tdTomato is expressed in processes and projections, we enriched for cell bodies using a nuclear DNA dye (cell permeant DRAQ5, ThermoFisher). Dead cells were excluded by eliminating cells

stained by NucBlue (cell impermeant DAPI). Doublet discrimination was used to ensure single cells were deposited into each well. Individual tdTomato^{+} neurons were sorted into each well of a 96-well plate (Precise WTA kits, BD). The Precise WTA single cell sequencing kits include a well index to identify each cell and a unique molecular index (UMI) to identify each transcript and reduce bias due to PCR amplification. Libraries were prepared according to manufacturer's instructions and sequenced on an Illumina NextSeq 500 using paired end 2 x 75 bp mode.

Expression data were analyzed using the R package Seurat[51]. Normalized data were scaled with a linear regression model based on number of unique molecular identifiers (UMIs) per cell and percentage of reads from the mitochondrial genome to remove unwanted sources of variability and to normalize gene expression data. Analyses included all genes expressed in ≥ 2 cells, and all cells expressing ≥ 500 genes and a fraction of mitochondrial reads < 0.17. To cluster cells based on transcriptome similarity, we used Shared Nearest Neighbor (SNN) algorithm[52]. For each cell cluster, marker genes were determined by comparing expression in the given cluster against all other clusters using the smart local moving algorithm to iteratively group clusters together[52]. To determine sex differences, all female neurons passing initial filtering were compared to all male neurons passing initial filtering.

Mouse Procedures

Mice were anaesthetized with isofluorane and received analgesics (0.01mg/mL buprenorphine, 0.58mg/mL carprofen) pre- and post- surgery. Bilateral ovariectomy and castration surgery with complete removal of the ovaries or the testes was performed on

adult mice. For Figure 2.4, sham or gonadectomized control mice (XXF and XYM) and gonadectomized FCG mice from separate experimental batches are shown together. The Cre-dependent AAV8-hM3Dq-mCherry DREADD (Addgene, titer ≥ 4×10^{12} vg/mL, 200 nL to each side) was injected bilaterally into the VMHvl of adult female mice (coordinates: A-P: -1.56 mm from Bregma; lateral: ±0.85 mm from Bregma; D-V: 5.6 mm from the cortex). After 2 weeks of recovery, mice received i.p. injections of CNO (0.3 mg/kg) or vehicle (saline, 0.15% DMSO) 3 hr after the onset of the light phase. Saline and CNO were administered on consecutive days in a randomized balanced design. SiRNA pools against *Rprm* or non-targeting controls (Dharmacon, 0.4 mM, 350 nL to each side) were delivered to the VMHvl as described above. Indirect calorimetry was performed in Oxymax metabolic chambers (Columbus Instruments). Gross movement and core body temperature were measured using an IP-implanted G2 eMitter and VitalView software (Starr Life Sciences).

RNA probe generation

Digoxigenin (DIG)- or fluorescein (FITC)-labeled sense and antisense riboprobes for somatostatin (*Sst),* reprimo (*Rprm),* tachykinin 1 (*Tac1),* prodynorphin (*Pdyn),* necdin (*Ndn),* and proto-oncogene, serine/threonine kinase A-Raf (*Araf)* were in vitro transcribed from template cDNA using T7/T3/SP6 RNA polymerase (DIG/FITC RNA labeling kit, Roche) and purified with RNA Clean & Concentrator (Zymo Research). For template cDNA generation, PCR products for individual genes were amplified from a hypothalamic cDNA library and cloned into pCR 2.1-TOPO or pCR II-TOPO (Invitrogen) for all probes except *Tac1*, which was previously described[17]. Plasmid DNA was

isolated from bacterial cultures using ZymoPURE II Plasmid Midiprep kit (Zymo Research), linearized by restriction digest, and purified with DNA Clean & Concentrator (Zymo Research). All PCR products, except *Araf*, were generated using reference primer sequences from the Allen Brain Institute. For *Araf*, cDNA was generated from bases 639-942 (NM_009703.2).

In situ hybridization

The ISH protocol was partially adapted from previously published methods[17]. 18µm-thick cryosections containing the VMH were obtained from paraformaldehyde-fixed mouse brains. Day 1: Upon defrosting to room temperature (rt), slides were washed in PBS, postfixed in 4% PFA, and washed again. TSA-fluorescent ISH (FISH) slides were also incubated in 3% H_2O_2 for 30min to quench endogenous peroxidase activity. To permeabilize the tissues, slides were incubated in proteinase K (1ug/mL) for TSA-FISH and chromogenic ISH (CISH), or 0.3% Triton X-100 in PBS for combined FISH-IHC. CISH slides were postfixed again in 4% PFA for 5 min. Slides were incubated in hyb solution containing probe overnight at 65C. Day 2: Coverslips were removed in solution containing 5x SSC heated to 65C. Slides were then subject to a series of stringency washes, then blocked in NTT containing 2% blocking reagent and HISS for 2 h at rt. Slides were incubated in antibody solution containing either anti-DIG-AP (1:5,000), anti-FITC-AP (1:5,000), or anti-DIG-POD (1:4,000) in 4C overnight. FISH-IHC slides were additionally incubated in anti-ERα (Rb, 1:1000). Day 3: Slides were washed in NTT, then NTTML (0.15M NaCl, 0.1M Tris pH 9.5, 50mM $MgCl_2$, 2mM levamisole, and 0.1% Tween-20) to quench endogenous phosphatase activity. Slides

were developed in INT/BCIP solution (Roche). FISH-IHC slides were blocked in 10% normal goat serum for 1hr at rt, and incubated with anti-rabbit 647 for 2 h at rt, and incubated in HNPP/Fast red working solution according to manufacturer's instructions (HNPP Fluorescent Detection Set, Roche). To stop the reaction, the slides were washed 3x 5min in PBS, counterstained with DAPI, and immediately stored in -20C to prevent HNPP/Fastred diffusion. TSA-FISH slides were incubated in working solution containing Cy5 Plus tyramide according to manufacturer's instructions (Perkin Elmer). Slides were then washed in NTT and incubated in 3% H_2O_2 for 30min to quench the first tyramide reaction. Slides were then washed 3x 5min in NTT, blocked in in NTT containing 2% blocking reagent and HISS for 2 h at rt, and incubated overnight in anti-FITC-POD (1:4,000). Day 4: TSA-FISH slides were washed in NTT, and incubated in working solution containing FITC Plus tyramide according to manufacturer's instructions (Perkin Elmer). The reaction was terminated with NTT and slides were counterstained in DAPI. Control experiments using sense riboprobes and no probes showed negligible signal. Additionally, performing the TSA reaction following 3% H_2O_2 for 30min in the absence of a second POD incubation confirmed adequate quenching. Probes with weaker signal intensity were developed first in TSA-FISH.

Image Acquisition and Quantification

All CISH experiments with imaged in brightfield on a DM1000 LED microscope (Leica) using 5X or 10X objectives. Semi-quantitative optical density (O.D.) measurements of mRNA in CISH slides were obtained with ImageJ (NIH) following calibration with a calibrated step tablet (Kodak), according to standard protocols[53].

Measurements from the left and right VMH were averaged to calculate the mean O.D. for each animal using predetermined ROIs based on the Franklin and Paxinos Mouse Brain Atlas. Sex differences in O.D. between the whole VMH and VMHvl were determined by two-way ANOVA with Bonferroni multiple-comparison correction. FISH and IHC experiments were imaged on a LSM780 confocal microscope (Zeiss) using 10X or 20X objectives. Tile-scanned images were stitched using Zen Black (Zeiss). All images were taken with the same z-sampling interval for a given objective and z-stacks were merged to obtain maximum intensity projections. Cyan/magenta/yellow pseudo-colors were applied to all fluorescent images for accessibility. Image processing, limited to brightness and contrast, was performed using the Leica Application Suite (Leica), Zen Black (Zeiss), ImageJ (NIH), and Photoshop (Adobe). Infrared images were captured using the FLIR e60bx at a distance of 30 cm. Temperature of BAT area was analyzed using the FLIR Tools software. A predefined size for BAT region of interest (ROIs) was used for all images. The BAT ROI was defined as the interscapular region a standardized distance from the base of the ears[54].

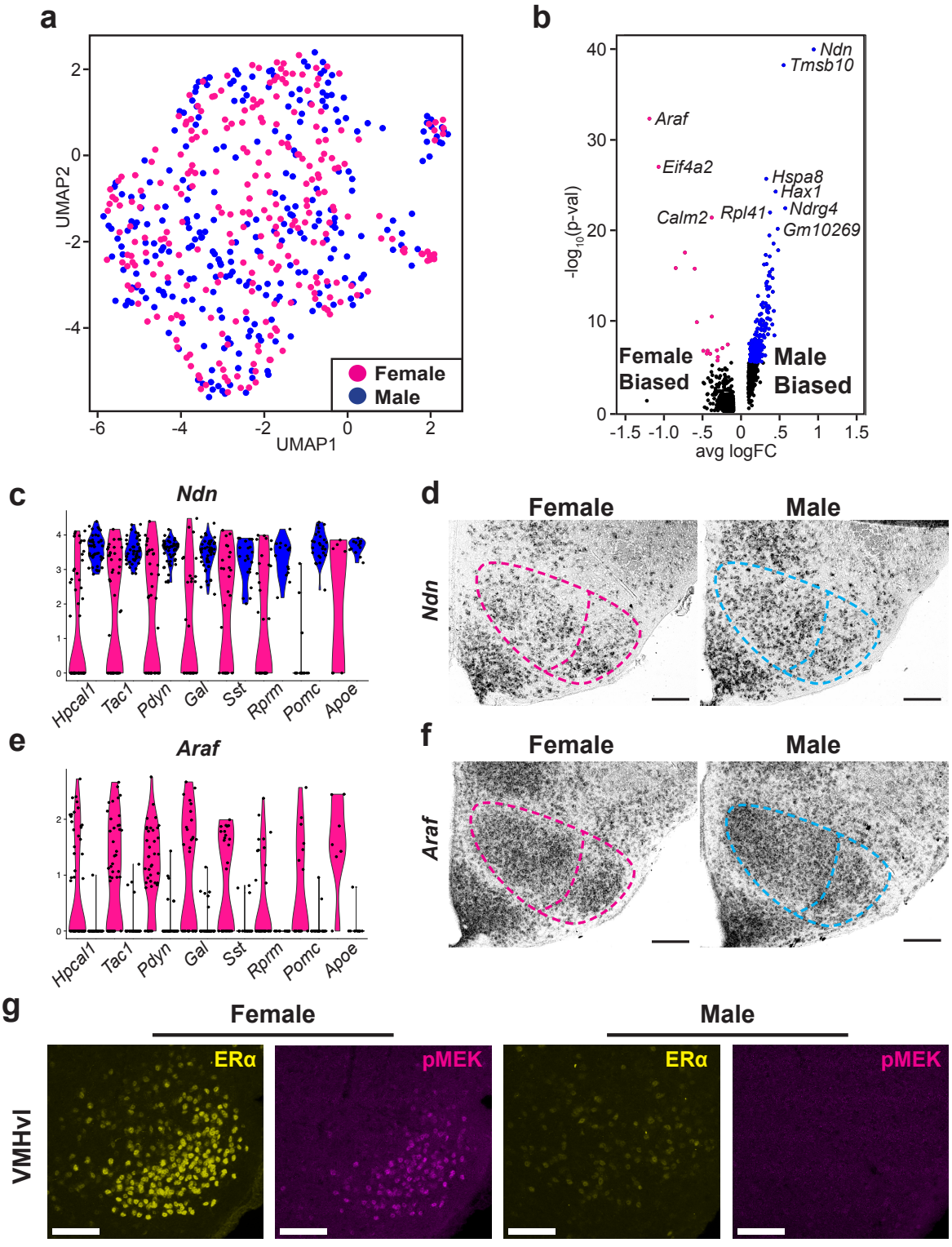
a
UMAP2
UMAP1
Female
Male
b
-log10(p-val)
avg logFC
Ndn
Tmsb10
Araf
Eif4a2
Hspa8
Hax1
Calm2
Rpl41
Ndrg4
Gm10269
Female Biased
Male Biased
c
Ndn
Hpcal1
Tac1
Pdyn
Gal
Sst
Rprm
Pomc
Apoe
d
Female
Male
Ndn
e
Araf
f
Female
Male
Araf
g
Female
Male
VMHvl
ERα
pMEK
ERα
pMEK

Figure S2.1 The overall architecture of the VMH is conserved between males and females. a, UMAP showing that male and female neurons are present in all clusters identified. b, Volcano plot showing differences in gene expression when comparing male and female VMH transcriptomes. Female biased (Adj. P < .05) genes shown in pink, male biased (Adj. P < .05) shown in blue. c, Violin plots showing male biased expression of *Ndn* across all VMH clusters. d, ISH validating male biased expression of *Ndn* in the VMH, scalebars = 200μm. e, Violin plots showing female biased expression of *Araf* across all clusters identified. f, ISH showing expression of *Araf* in male and female VMH, scalebars = 200μm. g, Immunofluorescence demonstrating strong pMEK immunoreactivity in a subset of ERα expressing female neurons in the VMHvl, but no observable pMEK staining in the male VMHvl, scalebars = 100μm.

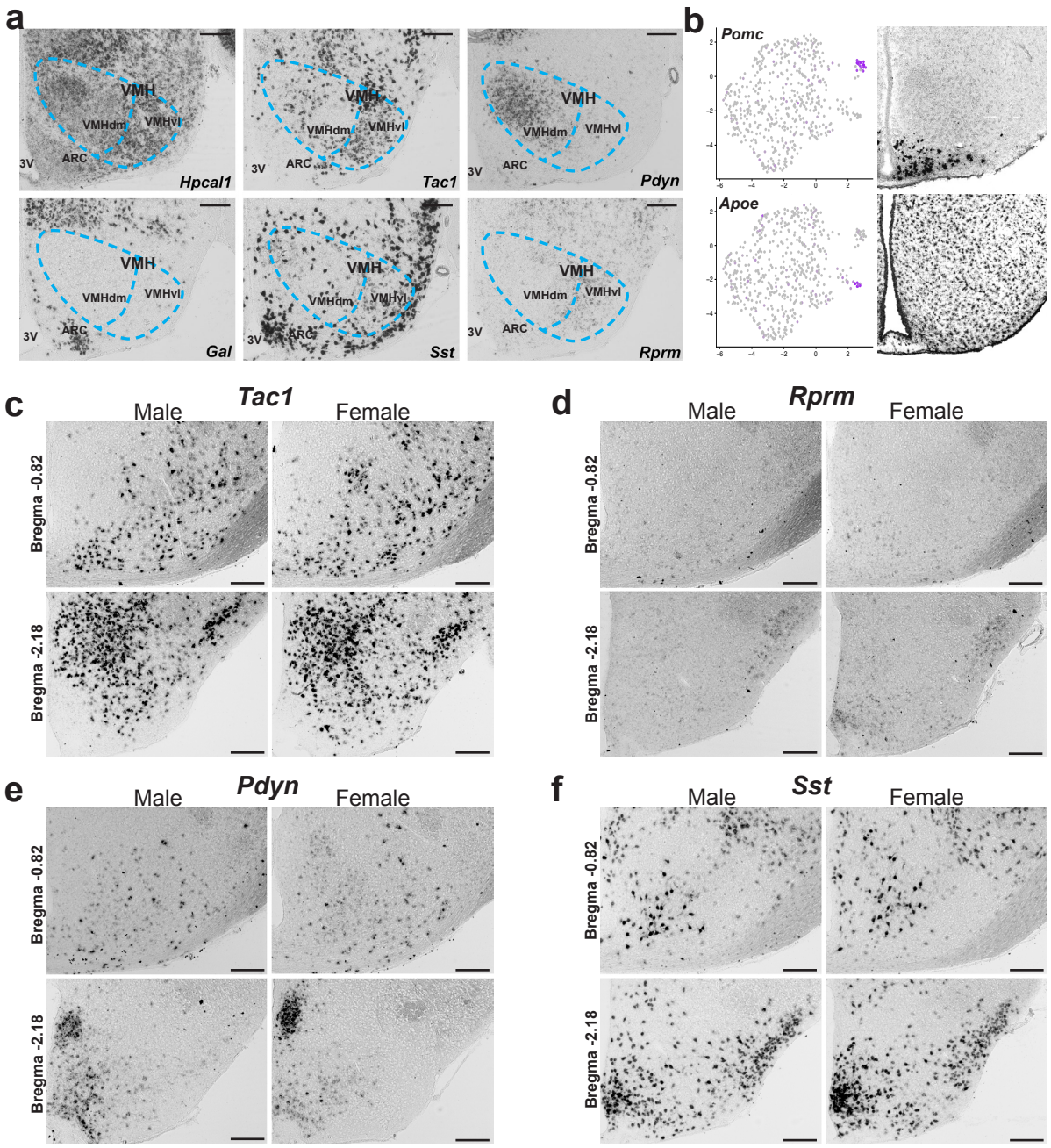

Figure S2.2 Clustering and expression of non-specific markers and markers outside of the VMH. a, Expression of *Hpcal1*, *Tac1*, *Pdyn*, *Gal*, *Sst*, and *Rprm* detected within the anatomical boundaries of the VMH of a P10 male. b, Top panel, ISH shows *Pomc* expression strongest in the ARC. Bottom panel, ISH shows *Apoe* expression with no

particular pattern. e, expression of *Tac1*, *Rprm*, *Pdyn*, and *Sst* in brain areas adjacent to the VMH along the rostral-caudal axis in males (n=3) and females (n=4). Scalebars = 200μm. Images in b from Allen Brain Atlas.

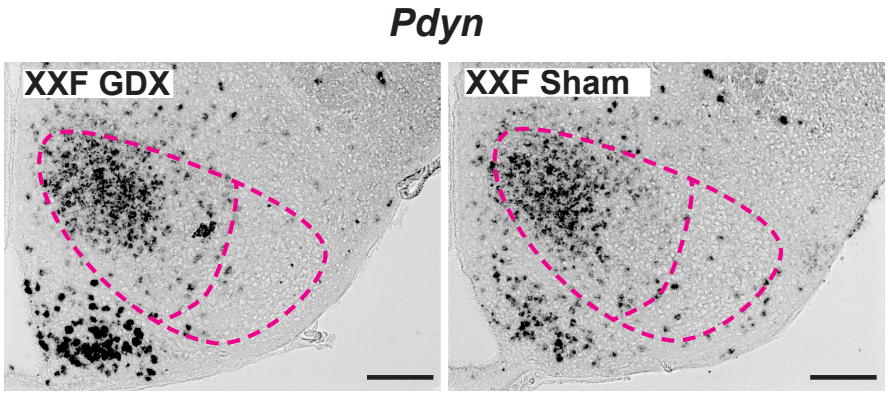

Figure S2.3 Sexually dimorphic expression of *Pdyn* in the VMHvl is not maintained by differences in ovarian sex hormone signaling in adulthood. Expression of *Pdyn* in the VMH of gonadectomized (GDX) or sham XXF FCG mice (n=3 mice) by chromogenic ISH. Dashed line shows boundary of VMH and VMHvl, in magenta. Scalebars = 200μm.

a
VMHvl
ARC
3V
Sst
ERα
Merge
b
VMHvl
ARC
3V
Pdyn
ERα
Merge
c Rprm
Male
ERα
Merge
e
Rprm
Sst
f
Tac1
Sst

Figure S2.4 *Sst*$^{+}$ cells show limited ERα immunoreactivity in the female VMHvl. a, Transcript expression of *Sst* (magenta) is shown together with ERα immunoreactivity (yellow) in the VMHvl using fluorescent ISH (FISH, n=5 female mice). Yellow arrow indicates colocalized signal. b. Transcript expression of *Pdyn* (magenta) is shown together with ERα immunoreactivity (yellow) in the VMHvl using fluorescent ISH (FISH, n=5 female mice). c. Transcript expression of *Rprm* (magenta) is shown together with ERα immunoreactivity (yellow) in the VMHvl using fluorescent ISH (FISH, n=4 male mice). Transcript expression (magenta) of e, *Rprm*, and f, *Tac1* is visualized with *Sst* transcript expression (yellow) using TSA-FISH (n=5 female mice) in the VMH. Scalebars = 100μm. Images are merged with DAPI (cyan).

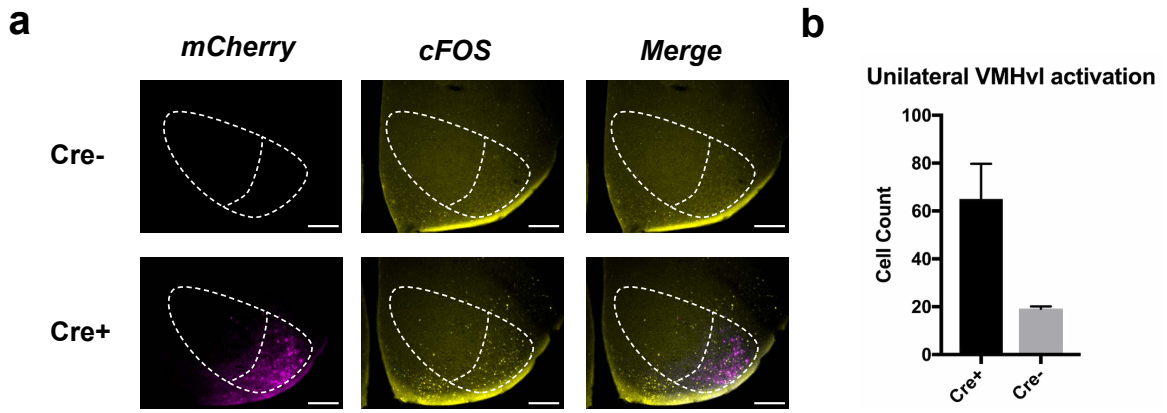

Figure S2.5 DREADD activation increases cFOS immunoreactivity. Representative images of increased mCherry (magenta) and cFOS (yellow) in the VMHvl of *Esr1Cre* (Cre+, n = 5) mice compared to wild-type (Cre-, n = 3) injected with a viral, cre-dependent mCherry-fused Gq-coupled DREADD. b, cFOS immunoreactivity in the VMHvl (quantified on one side per animal) is increased in Cre+ subjects 90 minutes following CNO injection. Scalebars = 200μm.

REFERENCES

1. Lovejoy, J. C., Champagne, C. M., de Jonge, L., Xie, H. & Smith, S. R. Increased visceral fat and decreased energy expenditure during the menopausal transition. *Int J Obes (Lond)* **32**, 949–58 (2008).
2. Slonaker, J. R. The effect of copulation, pregnancy, pseudopregnancy and lactation on the voluntary activity and food consumption of the albino rat. *Am J Physiol* **71**, (1925).
3. Brobeck, J. R., Wheatland, M. & Strominger, J. L. Variations in regulation of energy exchange associated with estrus, diestrus and pseudopregnancy in rats. *Endocrinology* **40**, 65–72 (1947).
4. Kopp, C., Ressel, V., Wigger, E. & Tobler, I. Influence of estrus cycle and ageing on activity patterns in two inbred mouse strains. *Behavioural brain research* **167**, 165–74 (2006).
5. Olofsson, L. E., Pierce, A. A. & Xu, A. W. Functional requirement of AgRP and NPY neurons in ovarian cycle-dependent regulation of food intake. *Proceedings of the National Academy of Sciences of the United States of America* **106**, 15932–7 (2009).
6. Sanchez-Alavez, M., Alboni, S. & Conti, B. Sex- and age-specific differences in core body temperature of C57Bl/6 mice. *Age (Dordr)* **33**, 89–99 (2011).
7. Heine, P. A., Taylor, J. A., Iwamoto, G. A., Lubahn, D. B. & Cooke, P. S. Increased adipose tissue in male and female estrogen receptor-alpha knockout mice. *Proceedings of the National Academy of Sciences of the United States of America* **97**, 12729–34 (2000).

8. Park, C. J. *et al.* Genetic rescue of nonclassical ERalpha signaling normalizes energy balance in obese Eralpha-null mutant mice. *The Journal of clinical investigation* **121**, 604–12 (2011).
9. Xu, Y. *et al.* Distinct hypothalamic neurons mediate estrogenic effects on energy homeostasis and reproduction. *Cell metabolism* **14**, 453–65 (2011).
10. Hulley, S. *et al.* Randomized Trial of Estrogen Plus Progestin for Secondary Prevention of Coronary Heart Disease in Postmenopausal Women. *JAMA* **280**, 605–613 (1998).
11. Writing Group for the Women's Health Initiative Investigators. Risks and Benefits of Estrogen Plus Progestin in Healthy Postmenopausal WomenPrincipal Results From the Women's Health Initiative Randomized Controlled Trial. *JAMA* **288**, 321–333 (2002).
12. Smith, A. W., Bosch, M. A., Wagner, E. J., Rønnekleiv, O. K. & Kelly, M. J. The membrane estrogen receptor ligand STX rapidly enhances GABAergic signaling in NPY/AgRP neurons: role in mediating the anorexigenic effects of 17β-estradiol. *American Journal of Physiology-Endocrinology and Metabolism* **305**, E632–E640 (2013).
13. Ismael González-García *et al.* mTOR signaling in the arcuate nucleus of the hypothalamus mediates the anorectic action of estradiol. *Journal of Endocrinology* **238**, 177–186 (2018).
14. Herber, C. B. *et al.* Estrogen signaling in arcuate Kiss1 neurons suppresses a sex-dependent female circuit promoting dense strong bones. *Nature Communications* **10**, 163 (2019).

15. Musatov, S. *et al.* Silencing of estrogen receptor alpha in the ventromedial nucleus of hypothalamus leads to metabolic syndrome. *Proceedings of the National Academy of Sciences of the United States of America* **104**, 2501–6 (2007).
16. Martinez de Morentin, P. B. *et al.* Estradiol Regulates Brown Adipose Tissue Thermogenesis via Hypothalamic AMPK. *Cell metabolism* **20**, 41–53 (2014).
17. Correa, S. M. *et al.* An estrogen-responsive module in the ventromedial hypothalamus selectively drives sex-specific activity in females. *Cell Rep* **10**, 62–74 (2015).
18. Hashikawa, K. *et al.* Esr1+ cells in the ventromedial hypothalamus control female aggression. *Nature Neuroscience* **20**, 1580 (2017).
19. Lin, D. *et al.* Functional identification of an aggression locus in the mouse hypothalamus. *Nature* **470**, 221–6 (2011).
20. Lee, H. *et al.* Scalable control of mounting and attack by Esr1+ neurons in the ventromedial hypothalamus. *Nature* **509**, 627–32 (2014).
21. Yang, C. F. *et al.* Sexually dimorphic neurons in the ventromedial hypothalamus govern mating in both sexes and aggression in males. *Cell* **153**, 896–909 (2013).
22. Wang, L. *et al.* Hypothalamic Control of Conspecific Self-Defense. *Cell Reports* **26**, 1747-1758.e5 (2019).
23. Silva, B. A. *et al.* Independent hypothalamic circuits for social and predator fear. *Nature neuroscience* **16**, 1731–3 (2013).
24. Remedios, R. *et al.* Social behaviour shapes hypothalamic neural ensemble representations of conspecific sex. *Nature* **550**, 388–392 (2017).

25. Narita, K., Murata, T. & Matsuoka, S. The ventromedial hypothalamus oxytocin induces locomotor behavior regulated by estrogen. *Physiology & behavior* **164**, 107–12 (2016).
26. Flanagan-Cato, L. M. Sex differences in the neural circuit that mediates female sexual receptivity. *Frontiers in neuroendocrinology* **32**, 124–36 (2011).
27. Yang, T. & Shah, N. M. Molecular and neural control of sexually dimorphic social behaviors. *Curr Opin Neurobiol* **38**, 89–95 (2016).
28. Krause, W. C. & Ingraham, H. A. Origins and Functions of the Ventrolateral VMH: A Complex Neuronal Cluster Orchestrating Sex Differences in Metabolism and Behavior. in *Sex and Gender Factors Affecting Metabolic Homeostasis, Diabetes and Obesity* (ed. Mauvais-Jarvis, F.) 199–213 (Springer International Publishing, 2017). doi:10.1007/978-3-319-70178-3_10
29. Dhillon, H. *et al.* Leptin directly activates SF1 neurons in the VMH, and this action by leptin is required for normal body-weight homeostasis. *Neuron* **49**, 191–203 (2006).
30. Madisen, L. *et al.* A robust and high-throughput Cre reporting and characterization system for the whole mouse brain. *Nature neuroscience* **13**, 133–40 (2010).
31. Cheung, C. C., Kurrasch, D. M., Liang, J. K. & Ingraham, H. A. Genetic labeling of steroidogenic factor-1 (SF-1) neurons in mice reveals ventromedial nucleus of the hypothalamus (VMH) circuitry beginning at neurogenesis and development of a separate non-SF-1 neuronal cluster in the ventrolateral VMH. *J Comp Neurol* **521**, 1268–88 (2012).
32. Sheng, M. & Greenberg, M. E. The regulation and function of c-fos and other immediate early genes in the nervous system. *Neuron* **4**, 477–485 (1990).

33. Wu, Y. E., Pan, L., Zuo, Y., Li, X. & Hong, W. Detecting Activated Cell Populations Using Single-Cell RNA-Seq. *Neuron* **96**, 313-329.e6 (2017).
34. McInnes, L., Healy, J. & Melville, J. UMAP: Uniform Manifold Approximation and Projection for Dimension Reduction. *arXiv:1802.03426v2*
35. Malik, S. *et al.* Histone deacetylase 7 and FoxA1 in estrogen-mediated repression of RPRM. *Mol Cell Biol* **30**, 399–412 (2010).
36. Allison, M. B. *et al.* TRAP-seq defines markers for novel populations of hypothalamic and brainstem LepRb neurons. *Molecular Metabolism* **4**, 299–309 (2015).
37. Tannenbaum, G. S. & Bowers, C. Y. Interactions of growth hormone secretagogues and growth hormone-releasing hormone/somatostatin. *Endocrine* **14**, 21–27 (2001).
38. Luo, S. X. *et al.* Regulation of feeding by somatostatin neurons in the tuberal nucleus. *Science* **361**, 76 (2018).
39. Schick, R. R. *et al.* Effect of galanin on food intake in rats: involvement of lateral and ventromedial hypothalamic sites. *American Journal of Physiology-Regulatory, Integrative and Comparative Physiology* **264**, R355–R361 (1993).
40. Arnold, A. P. & Chen, X. What does the 'four core genotypes' mouse model tell us about sex differences in the brain and other tissues? *Front Neuroendocrinol* **30**, 1–9 (2009).
41. Dong, S., Allen, J. A., Farrell, M. & Roth, B. L. A chemical-genetic approach for precise spatio-temporal control of cellular signaling. *Molecular bioSystems* **6**, 1376–80 (2010).
42. Chen, R., Wu, X., Jiang, L. & Zhang, Y. Single-Cell RNA-Seq Reveals Hypothalamic Cell Diversity. *Cell Rep* **18**, 3227–3241 (2017).

43. Romanov, R. A. *et al.* Molecular interrogation of hypothalamic organization reveals distinct dopamine neuronal subtypes. *Nature Neuroscience* **20**, 176 (2016).
44. Yang, C. F. & Shah, N. M. Representing sex in the brain, one module at a time. *Neuron* **82**, 261–78 (2014).
45. McCarthy, M. M., Pickett, L. A., VanRyzin, J. W. & Kight, K. E. Surprising origins of sex differences in the brain. *Hormones and Behavior* **76**, 3–10 (2015).
46. Clegg, D. J. *et al.* Estradiol-dependent decrease in the orexigenic potency of ghrelin in female rats. *Diabetes* **56**, 1051–8 (2007).
47. Contreras, C. *et al.* The brain and brown fat. *Ann Med* **47**, 150–68 (2015).
48. Chavkin, C., James, I. & Goldstein, A. Dynorphin is a specific endogenous ligand of the kappa opioid receptor. *Science* **215**, 413 (1982).
49. Bruchas, M. R., Land, B. B. & Chavkin, C. The dynorphin/kappa opioid system as a modulator of stress-induced and pro-addictive behaviors. *Brain Research* **1314**, 44–55 (2010).
50. Burgoyne, P. S. & Arnold, A. P. A primer on the use of mouse models for identifying direct sex chromosome effects that cause sex differences in non-gonadal tissues. *Biology of sex differences* **7**, 68–68 (2016).
51. Satija, R., Farrell, J. A., Gennert, D., Schier, A. F. & Regev, A. Spatial reconstruction of single-cell gene expression data. *Nat Biotechnol* **33**, 495–502 (2015).
52. Blondel, V. D., Guillaume, J.-L., Lambiotte, R. & Lefebvre, E. Fast unfolding of communities in large networks. *Journal of Statistical Mechanics: Theory and Experiment* **2008**, P10008 (2008).

53. Robbins, E. *et al.* Quantitative non-radioactive in situ hybridization of preproenkephalin mRNA with digoxigenin-labeled cRNA probes. *Anat Rec* **231**, 559–62 (1991).

54. Crane, J. D., et al. (2014). "A standardized infrared imaging technique that specifically detects UCP1-mediated thermogenesis in vivo." Mol Metab 3(4): 490-494.

Chapter 3

Generation of a novel mouse model to study the regulation of thermogenesis by the ventromedial hypothalamus

Abstract

Reprimo *(Rprm)* and tachykinin-1 (*Tac1)*-expressing neurons in the ventromedial hypothalamus (VMH) contribute to female-specific regulation of energy expenditure. Mouse models that allow for specific activation and inhibition of *Tac1* neurons are commercially available. However, no mouse models have been developed that specifically target *Rprm* neurons, limiting the ability to further investigate the relationship between *Rprm* neuron activity and energy balance, including in long-term metabolic studies. Here, we used a CRISPR-based approach for rapid and efficient generation of a *Rprm*-Cre driver knock-in, with the additional modification of FRT sites flanking the *Rprm* exon to allow for permanent gene knockout. Ultimately, this model will be pivotal towards establishing the mechanistic role of *Rprm* neurons and mapping the circuits that emanate from this new estrogen-sensitive and female-specific population.

Main

Reprimo *(Rprm)* is a 327bp, single-exon gene on murine chromosome 2 that encodes a 109 amino acid, cytosolic protein (Wichmann et al 2016). *Rprm* is involved in tumor suppression by mediating p53-dependent cell cycle arrest at G2 by the inhibition of the Cdc2-cyclin B1 activity (Ohki et al 2000). Hypermethylation of *Rprm* and decreased transcript expression has been reported in several human cancers, including

ERα-positive breast cancer (Buchegger et al 2017), and *Rprm* is a known target of ERα-mediated repression (Malik et al 2010). Recently, *Rprm*$^{+}$ neurons in the VMH were implicated in female-specific regulation of core body temperature and BAT thermogenesis (Van Veen Kammel et al 2019). However, the transient nature of siRNA gene knockdown used in these studies precludes long-term study of the metabolic phenotype, and is insufficient to answer mechanistic questions about thermogenesis or map the circuitry of these neurons. Further interpretation of these studies is also confounded by the lack of dissociation between *Rprm* gene function from the activity of *Rprm*$^{+}$ neurons. Here, we designed a repair cassette that drives the expression of the Cre gene following the *Rprm* coding sequence, and additionally flanks the *Rprm* exon with FRT sites. Mouse transgenesis was then performed via pronuclear injection of our construct using a CRISPR-based strategy (Miura et al 2018). Finally, genomic DNA from resulting offspring was tested for the fidelity of insertion and off-target effects.

Results

Donor construct design

We first introduce the coding sequence for P2A peptide following a deleted stop codon in the *Rprm* CDS. 2A peptide sequences induce ribosome skipping, which results in the generation of distinct peptide products from a single multicistronic construct. Unlike other methods for inducing multiple gene products like IRES, 2A sequences have the advantage of being very short (66bp) and allow for stoichiometric expression of flanking genes, and P2A has the highest cleavage efficiency among the 2A peptide genes (Kim et al 2011). We then add the coding sequence for codon-improved Cre

recombinase (iCre) protein (1026bp) following the P2A break. The 5' end of the iCre sequence also contains a 21-bp nuclear localization sequence (NLS). We then appended ~2000bp homology arms upstream and downstream of the 5' and 3' UTRs of the *Rprm* exon, respectively, to guide insertion. Finally, we inserted FLP Recognition Target (FRT) sites in the homology arms within 250bp of the 5' and 3' exons. This will allow us to additionally use the mouse as a *Rprm* knockout model following stereotaxic delivery of FLP recombinase (Figure 3.1).

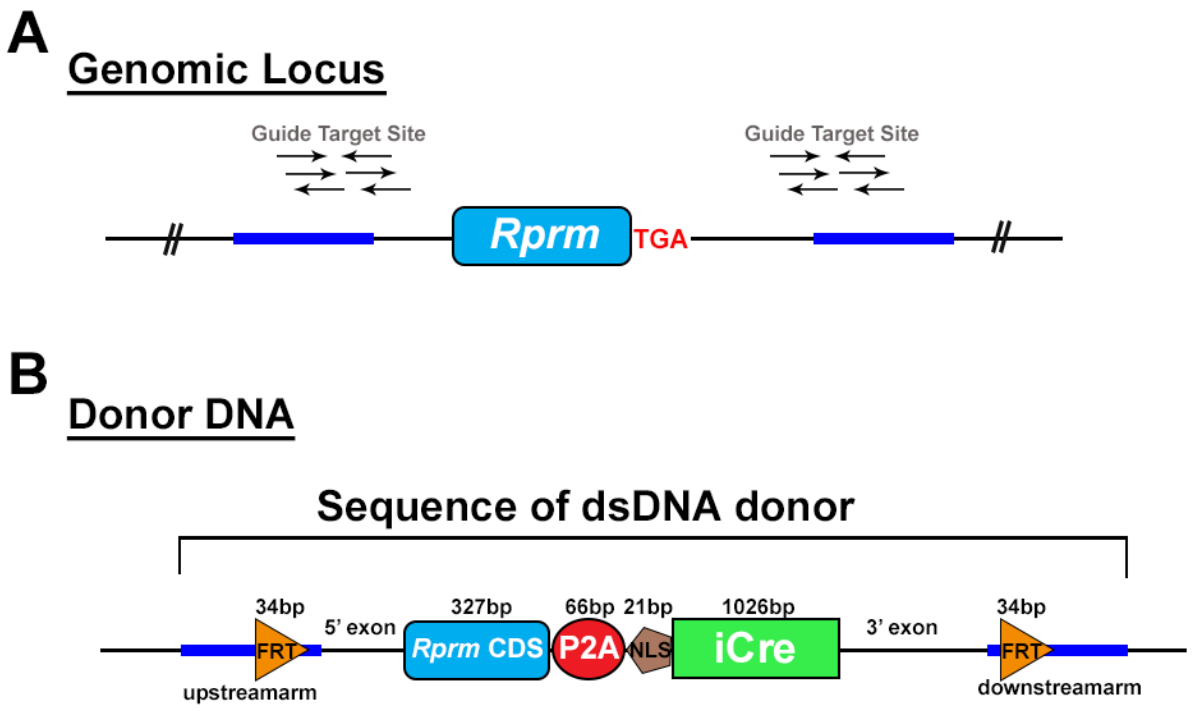

Figure 3.1 Schematic of *Rprm* Cre-FRT knock-in design. A. Genomic locus of the single *Rprm* exon. Arrows show potential guide RNAs that target within 250bp of the 5' and 3' UTRs. Blue box indicates flanking homology arms. B. Double stranded DNA (dsDNA) was used for the repair cassette. The dsDNA sequence contains an upstream homology arm containing the 5' FRT site, followed by the 5' exon with a deleted TGA stop codon

at the terminus of the *Rprm* CDS. Then, we add a P2A sequence followed by iCre. Finally, we include another homology arm containing the 3' FRT site downstream of the 3' exon.

Founder selection

The initial round of mouse transgenesis produced 20 live pups. However, one male suffered hydrocephalus and was excluded from further testing. Of the remaining pups, we successfully obtained 2 offspring that expressed iCre (one male and one female) (Figure 3.2a). We then wanted to confirm that the FRT sites were also faithfully integrated. We designed separate PCR screens for the 5' and 3' FRT sites, and we were able to detect the 5' FRT band in both mice (Figure 3.2b). However, we could only detect the 3' FRT site in the female, suggesting the male contained a truncated construct due to possible recleavage at the guide target site (Figure 3.2b). Finally, to identify if the construct was integrated in the correct genomic locus, we designed a primer pair from within the iCre sequence to a native site downstream of our 3' homology arm. We were able to detect the proper integration band for the female, but not the male (Figure 3.2c). Therefore, we successfully generate one female mouse with the complete and correctly integrated genetically engineered transgenic cassette, and one male transgenic mouse with *Rprm*-driven iCre expression. The female was used to propagate the line by breeding with a male wild-type C57Bl/6J mouse.

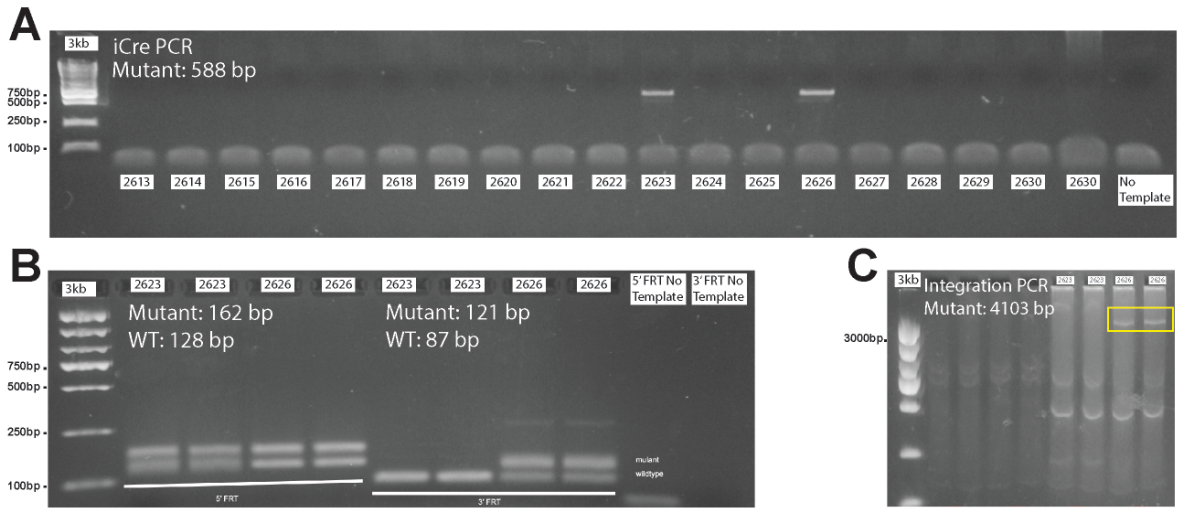

Figure 3.2 PCR screen for iCre, FRT sites, and integration of the transgenic cassette. Genomic DNA was extracted from mouse ear biopsies. a. Of 19 mice analyzed, two (male 2623, female 2626) showed a product of the expected band size for iCre (588bp). b. In the two iCre-positive mice, both showed a product of the expected band size for the 5' FRT (162bp), but only the female showed a product of the expected band size for the 3' FRT (121bp). c. A PCR screen for integration of the targeting cassette to the *Rprm* genomic locus showed a product of the expected band size (4103bp) for female mouse, but not the male mouse.

Discussion

Here, we generated a genetically engineered *Rprm*-Cre-FRT mouse model to begin assessing if the VMHvl neuronal population marked by *Rprm* is specialized to regulate thermogenesis. *Rprm* neurons in the VMH were recently identified to contribute to female-specific regulation of energy balance. Stereotaxic delivery a Cre-dependent Gq-DREADD to the VMHvl of *Rprm*-Cre mice followed by administration of the

DREADD agonist clozapine N-oxide (CNO) can be used to begin to obtain acute and longterm changes related to activity of *Rprm* neurons. For instance, mice can be observed in a CLAMS chamber to obtain comprehensive physiological and behavioral monitoring. We would anticipate seeing significant alterations in measures of thermogenesis, such as calorimetry and core body temperature, upon CNO treatment compared to vehicle-injected animals. Additionally, the *Rprm*-Cre-FRT model will allow for the study of *Rprm* neuron inhibition, through stereotaxic delivery of an inhibitory DREADD (Gi-KORD), on metabolic outcomes. This model can also be used to test the prediction that *Rprm* neuron activation will protect against diet-induced obesity, and that *Rprm* silencing will lead to obesity on regular chow.

This model can be also be used to identify *Rprm* neurons *ex vivo*. Experiments requiring fluorescent detection of Cre cells can be performed by either crossing the mice with a reporter strain for lineage detection, or by stereotaxically injecting with an AAV-FLEX-GFP in adults. Fluorescent labeling would allow for FACS of isolated cells, to perform bulk and single-cell transcriptome analysis of this population purified under various physiological conditions, including hormonal manipulation. Fluorescent labeling would also identify *Rprm* neurons in slices, which would allow for electrophysiological studies. It would allow for the tracing of the circuitry of these neurons within the hypothalamus. Finally, an additional benefit of this model is that we have been unable to generate an antibody against *Rprm* due to its short size and highly conserved sequence among host species. The 2A peptide would add an additional epitope, which would enable immunogenic probing of *Rprm*, for immunoprecipitation, as well subcellular localization studies (van Veen et al 2016). Together, this model would allow for a

comprehensive characterization of the functional attributes of this novel neuronal population, as well as the role of *Rprm* gene in transcriptional repression of *ERα*. Finally, we will make our mouse model available to other investigators as a shared resource.

Experimental Procedures

Mice

All studies were carried out in accordance with the recommendations in the Guide for the Care and Use of Laboratory Animals of the National Institutes of Health. UCLA is AALAS accredited and the UCLA Institutional Animal Care and Use Committee (IACUC) approved all animal procedures. All experiments were carried out on C57BL/6J mice (JAX 000664). The UCSD Transgenic Core Facility performed microinjection of one-cell embryos and embryo implantation into pseudo-pregnant females.

CRISPR reagents

Custom 20bp guides were chosen based on offtarget and ontarget scores, and designed as two-part crRNA and tracrRNA molecules (Alt-R™ CRISPR guide RNAs, Integrated DNA Technologies, Inc. (IDT)). Because of the flanking FRT sites, two CRISPR guide RNAs rather than one were designed targeting near the FRT insertion sites: Guide 1—ACTTAAGAGAGGGTGTGATC, Guide 2—ATAGATCCTTAGATCCATGG. The targeting construct was custom synthesized and cloned into pUC57-Kan by Genewiz, Inc. Unlinearized dsDNA was used as the donor.

Preparation of CRISPR mix

The crRNA/tracrRNA/Cas9 complexes were prepared based on a protocol provided by the UCSD Transgenic Core Facility. Briefly, Hi-Fi Cas9 (Integrated DNA Technologies, Inc. (IDT), tracrRNA, crRNA, and IDTE ((Integrated DNA Technologies, Inc. (IDT)) were incubated for 5 min at RT. Donor dsDNA was added to the mix, and incubates at RT for another 5 min. Finally, mix was centrifuged at 10,000rpm for 1 min. Supernatant was extracted and transferred to the UCSD Transgenic Core Facility for microinjection.

Genomic DNA screening

Ear biopsies were obtained from mice and genomic DNA was extracted using an NaOH-based extraction method (Truett et al 2000). The following primer pairs were used for the PCR screen. iCre, F: 5'-GCCTTCTCTGAACACACCTGGA-3'
R: 5'-AGCCACACCAGACACAGAGATC-3'; 3' FRT, F: 5'-
AGCTGCGATTCTAGAAGTTCCT-3'
R: 5'-TCTCCCTAAAGACTGGCTTGGC-3'; 5' FRT
F: 5'-CAGCCTTTCTCTGAAGTTCCT-3'
R: 5'-TCTCAAGAACCTCTTCAGGGC-3'; Rprm-iCre Integration
F: 5'-TCCTGTACAGTCTTGCTTGGGG-3'
WTR: 5'-CTTCTTCCTTGGCTGCAACCTG-3'. Genotyping reactions were performed using Q5 High-Fidelity 2X Master Mix (New England Biolabs, USA) and DreamTaq Green PCR (2X) Master Mix (Thermo Fisher Scientific, USA). Amplification was achieved using a touchdown PCR strategy, as in Van Veen Kammel et al. 2019.

CRISPR Injection

CRISPR reagents and donor construct were injected into pronuclear stage embryos based on (Yang et al. 2014). The UCSD Transgenic Core Facility performed microinjection embryos and embryo implantation into foster females. 10-day-old pups and their foster mothers were then transferred to the UCLA mouse facilities.

References

Buchegger K, Riquelme I, Viscarra T, Ili C, Brebi P, et al. 2017. Reprimo, a Potential p53-Dependent Tumor Suppressor Gene, Is Frequently Hypermethylated in Estrogen Receptor alpha-Positive Breast Cancer. *Int J Mol Sci* 18

Malik S, Jiang S, Garee JP, Verdin E, Lee AV, et al. 2010. Histone deacetylase 7 and FoxA1 in estrogen-mediated repression of RPRM. *Mol Cell Biol* 30: 399-412

Miura H, Quadros RM, Gurumurthy CB, Ohtsuka M. 2018. Easi-CRISPR for creating knock-in and conditional knockout mouse models using long ssDNA donors. *Nat Protoc* 13: 195-215

Ohki R, Nemoto J, Murasawa H, Oda E, Inazawa J, et al. 2000. Reprimo, a new candidate mediator of the p53-mediated cell cycle arrest at the G2 phase. *The Journal of biological chemistry* 275: 22627-30

Truett GE, Heeger P, Mynatt RL, Truett AA, Walker JA, Warman ML. 2000. Preparation of PCR-quality mouse genomic DNA with hot sodium hydroxide and tris (HotSHOT). *Biotechniques* 29: 52, 54

van Veen JE, Pringle DR, McMahon M. 2016. P2A-Fluorophore Tagging of BRAF Tightly Links Expression to Fluorescence In Vivo. *PloS one* 11: e0157661

Wichmann IA, Zavala K, Hoffmann FG, Vandewege MW, Corvalan AH, et al. 2016. Evolutionary history of the reprimo tumor suppressor gene family in vertebrates with a description of a new reprimo gene lineage. *Gene* 591: 245-54

Yang, H., et al. 2014. Generating genetically modified mice using CRISPR/Cas-mediated genome engineering. Nat Protoc 9(8): 1956-1968.

Chapter 4

Limitations and Future Directions

To date, no literature has described a role for *Rprm* in neurons or in the hypothalamus, although transcript expression of *Rprm* has been reported in the murine hypothalamus (Ferran et al 2015). Here, I report that a *Rprm*-expressing neuron population in the VMHvl may contribute to the regulation of core body temperature in females by modulating BAT thermogenesis. This population, together with a *Tac1*-expressing population that our lab has previously found to regulate female-specific locomotor activity, identifies a class of estrogen-sensitive, sexually differentiated neurons that play distinct roles in regulating energy balance in females.

Interestingly, estrogen-sensitive neurons that co-express *Rprm* were virtually undetectable by our methodologies in the male VMHvl. We did find that estrogen-sensitive *Tac1* neurons also exist in the VMHvl, but *Tac1* expression is overall significantly lower than in females and activation of this same population is insufficient to drive physical activity in males (Correa et al. 2015). The male VMHvl does, however, contain a population of estrogen-sensitive neurons that co-express *Pdyn*, the expression of which is absent in females (ovariectomized or intact), in prepubertal males, and in castrated males. This supports the idea that *Pdyn* expression in the male VMHvl is dependent on the presence of circulating testosterone in adulthood. Interestingly, the onset of puberty in female rats, a physiologic process that is in part cued by positive energy balance, was recently reported to coincide with increasing levels of *Pdyn* expression in the arcuate nucleus of the hypothalamus (Marajune et al

2019). It remains to be determined if the VMH *Pdyn* population also has a role related to energy balance in males.

Female mice have an overall elevated core body temperature compared to male mice throughout their lifespan, and experience a sustained elevation in core body temperature during the dark cycle of estrus resulting from a shift in their temperature profile from a biphasic to monophasic curve (Sanchez-Alavez et al 2011). Anecdotally, many women also use their basal body temperature to predict ovulation. This suggests the intriguing possibility that the sex-specific role of *Rprm* on core body temperature may have a specific biological function, particularly in relation to the reproductive cycle and fertility. Furthermore, it could help explain why loss of estrogen signaling at menopause, the termination of the reproductive period, can lead to profound metabolic deficits. Future studies will be necessary to determine whether *Rprm* neurons contribute to dynamic body temperature changes during the estrus cycle or rather play a role in homeostatic body temperature regulation.

One line of evidence that may help resolve these questions is to determine if and how ERα regulates *Rprm* expression in the VMHvl. Rprm was previously reported to be a target of ERα-mediated repression in human breast cancer cells (Malik et al 2010), but it is unclear if a similar mechanism is true in VMH neurons. Neither ovariectomy nor knockout of ERα in VMH lineage neurons is sufficient to suppress *Rprm* expression in female VMH. However, my preliminary evidence suggests that bolus E2 given to ovariectomized mice can briefly repress *Rprm* transcript expression in the VMHvl (Figure 4.1). Interestingly, chronic high levels of ovarian hormones such as during late pregnancy and lactation are associated with an inhibition of BAT thermogenesis,

potentially at the benefit of reserving nutrients for offspring development (Puerta et al. 1994). Further studies are therefore necessary to determine if my results more closely resemble the physiological regulation of *Rprm* during pregnancy or non-pregnancy, and whether chronic treatment E2 would mediate different results.

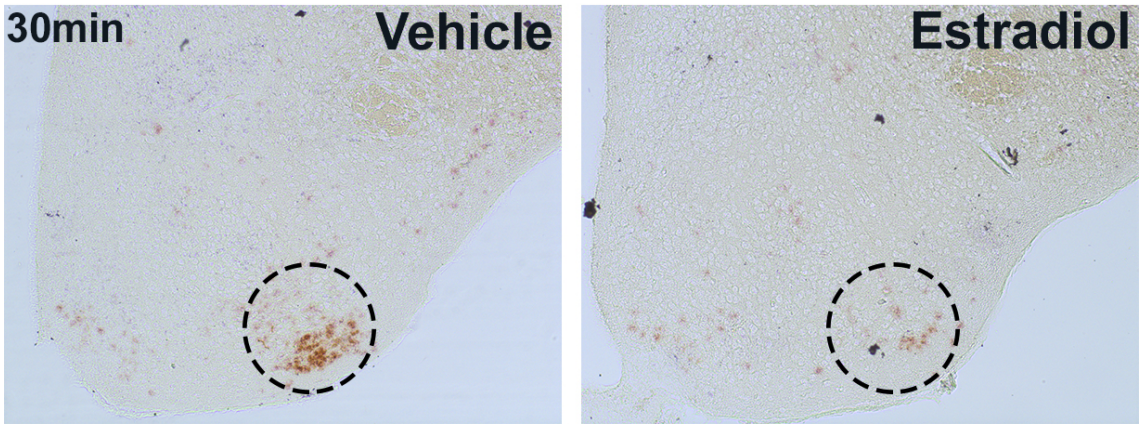

Figure 4.1 E2 may dynamically regulate *Rprm* transcript expression in the female VMHvl. Adult, ovariectomized mice were treated with a bolus of estradiol (1μg, subcutaneous) or oil. *Rprm* transcript expression in the VMH was evaluated 30min, 4hrs, 12hrs, and 24hrs post treatment by chromagen ISH. Reduced *Rprm* transcript expression was detected within 30min post treatment. Levels returned to baseline by 12hrs post treatment (not shown). Circle indicates ventrolateral region of the VMH.

Another line of evidence that could aid in our understanding of *Rprm* neuron function is to differentiate the role of the *Rprm* gene/protein function from the activity of neurons that express *Rprm*. In other words, is the E2-mediated increase in thermogenesis inherently dependent on *Rprm* downregulation or does *Rprm* simply perform such an essential function that downregulation alters the activity and thus

functionality of these neurons? This is an important distinction because we have previously seen phenotypic inconsistencies between the knockout of the gene *Tac1* and the chemogenetic manipulation of *Tac1*-expressing neurons on locomotor activity. It will also be important when considering the therapeutic potential of *Rprm* for the treatment of post-menopausal obesity. With my siRNA-based manipulations of *Rprm* transcript expression in particular, we cannot clearly distinguish between the two mechanisms. Using the *Rprm*-Cre-FRT mouse, however, we will be able to selectively activate and inhibit these neurons independent of *Rprm* gene expression manipulation. This new mouse will also allow for immunofluorescence and immunoprecipitation experiments that will enable us to resolve the intracellular localization of the *Rprm* protein as well as its binding partners, which will help determine its function *in vivo*.

Finally, the relevance of BAT thermogenesis to humans has not been without controversy. Although the presence of metabolically active brown adipose tissue has been demonstrated in adults, the ability of exploiting BAT activation to stimulate glucose uptake and combat obesity is far less clear. In humans, only a very small proportion of the total adipose tissue mass is made up of brown adipocytes (Leitner et al. 2018), and its distribution in the body is significantly different from rodents. In fact, very little is found in the interscapular region by adulthood, although interscapular BAT does contribute to heat production in infants (Astrup, 1986, reviewed in Carpentier et al. 2018). Furthermore, although optogenetic stimulation of sympathetic fibers innervating BAT has been shown to activate BAT and lower blood glucose level in mice (Jeong et al. 2018), the contribution of BAT to postprandial heat production in humans is minor (Din et al. 2018). However, as technologies that accurately quantify dynamic glucose

uptake by BAT are limited, its contribution may currently be underestimated. Finally, the idea that BAT significantly contributes to diet-induced thermogenesis in any organism has been contested from an evolutionary standpoint (reviewed in Kozak 2010). Nevertheless, estrogen-mediated regulation of BAT in rodents is well supported (Martínez de Morentin et al. 2014). Therefore it seems quite plausible that targeting BAT in humans is a reasonable strategy for mitigating post-menopausal obesity, if not diet-induced obesity.

References

Astrup, A. 1986. Thermogenesis in human brown adipose tissue and skeletal muscle induced by sympathomimetic stimulation. Acta Endo Suppl (Copenh) 278: 1-32.

Carpentier, A. C., et al. 2018. Brown Adipose Tissue Energy Metabolism in Humans. Front Endocrinol (Lausanne) 9: 447.

M, U. D., et al. 2018. Postprandial Oxidative Metabolism of Human Brown Fat Indicates Thermogenesis. Cell Metab 28(2): 207-216 e203.

Ferran, J. L., et al. 2015. Molecular codes defining rostrocaudal domains in the embryonic mouse hypothalamus. Front Neuroanat 9: 46.

Kozak, L. P. 2010. Brown fat and the myth of diet-induced thermogenesis. Cell Metab 11(4): 263-267.

Leitner, B. P., et al. 2017. Mapping of human brown adipose tissue in lean and obese young men. Proc Natl Acad Sci U S A 114(32): 8649-8654.

Majarune, S., et al. 2019. Ad libitum feeding triggers puberty onset associated with increases in arcuate Kiss1 and Pdyn expression in growth-retarded rats. J Rep Dev.

Martinez de Morentin, P. B., et al. 2014. Estradiol regulates brown adipose tissue thermogenesis via hypothalamic AMPK. Cell Metab 20(1): 41-53.

Malik, S., et al. 2010. Histone deacetylase 7 and FoxA1 in estrogen-mediated repression of RPRM. Mol Cell Biol 30(2): 399-412.

Puerta, M. et al. 1994. Effects of sex steroids in thermogenic tissues. *Thermal Balance in Health and Disease* pp 115-119

Sanchez-Alavez, M., et al. 2011. Sex- and age-specific differences in core body temperature of C57Bl/6 mice. Age (Dordr) 33(1): 89-99.

Chapter 5

Enhanced GABAergic tonic inhibition reduces intrinsic excitability of hippocampal CA1 pyramidal cells in experimental autoimmune encephalomyelitis

NEUROSCIENCE
RESEARCH ARTICLE
L. G. Kammel et al. / Neuroscience 395 (2018) 89–100

Enhanced GABAergic Tonic Inhibition Reduces Intrinsic Excitability of Hippocampal CA1 Pyramidal Cells in Experimental Autoimmune Encephalomyelitis

Laura G. Kammel, [a,b†] **Weizheng Wei,** [c†] **Shekib A. Jami,** [a,c] **Rhonda R. Voskuhl** [b] **and Thomas J. O'Dell** [c,d*]

[a] *Molecular, Cellular, and Integrative Physiology Graduate Program, University of California, Los Angeles, Los Angeles, CA, United States*

[b] *Multiple Sclerosis Program and Department of Neurology, David Geffen School of Medicine at UCLA, Los Angeles, CA, United States*

[c] *Department of Physiology, David Geffen School of Medicine at UCLA, Los Angeles, CA, United States*

[d] *UCLA Integrative Center for Learning and Memory, Brain Research Institute, Los Angeles, CA, United States*

Abstract—Cognitive impairment (CI), a debilitating and pervasive feature of multiple sclerosis (MS), is correlated with hippocampal atrophy. Findings from postmortem MS hippocampi indicate that expression of genes involved in both excitatory and inhibitory neurotransmission are altered in MS, and although deficits in excitatory neurotransmission have been reported in the MS model experimental autoimmune encephalomyelitis (EAE), the functional consequence of altered inhibitory neurotransmission remains poorly understood. In this study, we used electrophysiological and biochemical techniques to examine inhibitory neurotransmission in the CA1 region of the hippocampus in EAE. We find that tonic, GABAergic inhibition is enhanced in CA1 pyramidal cells from EAE mice. Although plasma membrane expression of the GABA transporter GAT-3 was decreased in the EAE hippocampus, an increased surface expression of α5 subunit-containing $GABA_A$ receptors appears to be primarily responsible for the increase in tonic inhibition during EAE. Enhanced tonic inhibition during EAE was associated with decreased CA1 pyramidal cell excitability and inhibition of α5 subunit-containing $GABA_A$ receptors with the negative allosteric modulator L-655,708 enhanced pyramidal cell excitability in EAE mice. Together, our results suggest that altered GABAergic neurotransmission may underlie deficits in hippocampus-dependent cognitive function in EAE and MS.

Key words: multiple sclerosis, experimental autoimmune encephalomyelitis, hippocampus, inhibitory synaptic transmission, tonic inhibition, intrinsic excitability, long-term potentiation.

INTRODUCTION

Cognitive impairment (CI) is a debilitating feature of multiple sclerosis (MS) that presents in both relapsing remitting and progressive MS subtypes (Ruano et al., 2016), and is associated with reduced quality of life due to impacts on employment and social engagement (Rao et al., 1991). Brain magnetic resonance imaging studies show atrophy within the hippocampus, disproportionately affecting the CA1 region (Sicotte et al., 2008). Importantly, both total and regional hippocampal atrophy (Sicotte et al., 2008, Longoni et al., 2015) are correlated with impairments in visuospatial/verbal learning, one of the primary cognitive domains affected by MS (Litvan et al., 1988, Denney et al., 2005, Ruano et al., 2016, for reviews see Chiaravalloti and DeLuca, 2008, Guimaraes and Sa, 2012). Therefore, the vulnerability of the hippocampus and CA1 subregion to pathologic processes during MS may contribute to the clinical presentation of CI.

Although the molecular mechanisms underlying hippocampal dysfunction in MS are unclear, findings from postmortem MS hippocampi indicate a downregulation of genes involved in excitatory synaptic transmission, including NMDA receptor (NMDAR) and AMPA receptor subunits, but an upregulation of genes involved in inhibitory synaptic transmission, including α5, β3, and γ2 subunits of $GABA_A$ receptors (Dutta et al., 2011). Consistent with these findings, alterations in both

*Correspondence to: T. J. O'Dell, Department of Physiology, David Geffen School of Medicine at UCLA, 53-231 Center for the Health Sciences, Box 951751, Los Angeles, CA 90095-1751, United States. Fax: +1-310-206-5661.
E-mail address: todell@mednet.ucla.edu (T. J. O'Dell).
† These authors contributed equally to this work.

Abbreviations: ACSF, artificial cerebrospinal fluid; CI, cognitive impairment; DPI, days post-induction; EAE, experimental autoimmune encephalomyelitis; EDTA, ethylenediaminetetraacetic acid; EGTA, ethylene glycol-bis(β-aminoethyl ether)-N,N,N′,N′-tetraacetic acid; fEPSP, field excitatory postsynaptic potential; HEPES, 4-(2-hydroxyethyl)-1-piperazineethanesulfonic acid; IPSC, inhibitory postsynaptic current; LTP, long-term potentiation; MS, multiple sclerosis; NMDAR, NMDA receptor; PM, plasma membrane; sIPSC, spontaneous inhibitory postsynaptic current.

https://doi.org/10.1016/j.neuroscience.2018.11.003
0306-4522/

excitatory (Centonze et al., 2009, Ziehn et al., 2012, Grasselli et al., 2013, Mandolesi et al., 2013) and phasic forms of inhibitory synaptic transmission (Rossi et al., 2011, Mandolesi et al., 2012, Nistico et al., 2013), have been reported in the MS model experimental autoimmune encephalomyelitis (EAE). Interestingly, α5/β3/γ2 subunit-containing $GABA_A$ receptors give rise to an extrasynaptic pool of $GABA_A$ receptors that mediate a distinct form of inhibitory transmission, called tonic inhibition, in hippocampal CA1 pyramidal cells (Caraiscos et al., 2004; Zarnowska et al., 2015). Although studies of inhibitory synaptic dysfunction in MS have focused on alterations in phasic forms of inhibition (Mandolesi et al., 2015), changes in $GABA_A$ receptor subunit expression that occur in MS suggest that tonic forms of inhibition might be altered as well. By regulating neuronal excitability, tonic inhibition not only influences neuronal information processing (Mitchell and Silver, 2003, Chadderton et al., 2004, Pavlov et al., 2009), but also opposes the induction of activity-dependent forms of synaptic plasticity involved in memory formation, such as long-term potentiation (LTP) (Martin et al., 2010, Whissell et al., 2013). Furthermore, pharmacological inhibition of α5 subunit-containing $GABA_A$Rs (α5-$GABA_A$Rs) improves performance on hippocampus-dependent learning tasks (Atack et al., 2006; Etherington et al., 2017), and α5 subunit null mutant mice exhibit enhanced spatial learning (Collinson et al., 2002). Therefore, an increase in tonic inhibition might contribute to deficits in LTP (Kim do et al., 2012; Di Filippo et al., 2013; Novkovic et al., 2015; Di Filippo et al., 2016; Planche et al., 2016), as well as learning and memory (Ziehn et al., 2010; Acharjee et al., 2013; Novkovic et al., 2015; Di Filippo et al., 2016), observed during EAE.

To determine whether alterations in GABAergic inhibition might contribute to disruption of hippocampal function in MS, we examined phasic and tonic inhibition in EAE. We find that both forms of inhibition are significantly enhanced in hippocampal CA1 pyramidal cells during EAE. We then examined how changes in plasma membrane levels of α5-$GABA_A$Rs and GABA transporters might contribute to enhanced tonic inhibition in EAE and explored the functional effects of enhanced tonic inhibition on pyramidal cell intrinsic excitability and LTP induction.

EXPERIMENTAL PROCEDURES

All experimental protocols used in this study were approved by UCLA's Chancellor's Animal Research Committee and are consistent with PHS Policy on Humane Care and Use of Laboratory Animals.

Active EAE induction

Active EAE was induced in C57BL/6 mice (Jackson labs) using myelin oligodendrocyte glycoprotein (MOG) amino acids 35–55 peptide (MOG35-55), as described (Itoh et al., 2018). Briefly, female mice at 8–15 weeks of age underwent subcutaneous injection of MOG35-55 (200 μg/animal, Mimotopes, San Diego, CA, USA) emulsified in Complete Freund's Adjuvant, supplemented with Mycobacterium Tuberculosis H37Ra (200 μg/animal, Difco Laboratories, Detroit, MI, USA), over two sites drained by left inguinal and auxiliary lymph nodes on day 0 (0.1 ml/mouse). A booster immunization was applied subcutaneously on day 7 over contralateral lymph nodes. Pertussis toxin (500 ng/mouse) (List Biological Laboratories) was injected intraperitoneally on days 0 and 2. Animals were monitored daily and scored based on a standard EAE 0–5 scale scoring system: 0, healthy; 1, complete loss of tail tonicity; 2, loss of righting reflex; 3, partial paralysis; 4, complete paralysis of one or both hind limbs; and 5, premoribund state. Whole-cell voltage-clamp recordings of phasic and tonic inhibitory transmission were performed 21–42 days post-induction (DPI). The induction of LTP by theta pulse stimulation was examined at both early (16–29 DPI) and late (starting at 40 DPI) time points post EAE induction. Whole-cell current-clamp recordings were used to examine CA1 pyramidal cell intrinsic excitability starting at 42 DPI and tissues for western blotting were collected at 40 DPI.

Inhibitory synaptic transmission

Mice were deeply anesthetized with isoflurane, decapitated, and the brain was rapidly removed and placed into ice-cold, oxygenated (bubbled with 100% O_2) cutting solution containing 135 mM N-methyl-D-glucamine, 10 mM D-glucose, 4.0 mM $MgCl_2$, 0.5 mM $CaCl_2$, 1.0 mM KCl, 1.2 mM KH_2PO_4, and 26 mM HEPES (pH = 7.4). Coronal brain slices (320-μm-thick) containing the dorsal hippocampus and striatum were cut using a Campden 7000SMZ-2 Vibratome. Slices were then maintained in an interface-slice type chamber perfused at 2–3 ml/min with a warm (30 °C), oxygenated (95% O_2/5% CO_2) artificial cerebrospinal fluid (ACSF) containing 124 mM NaCl, 4.4 mM KCl, 25 mM $NaHCO_3$, 1.0 mM NaH_2PO_4, 2.0 mM $CaCl_2$, 1.2 mM $MgSO_4$, and 10 mM glucose (pH = 7.4). Slices were allowed to recover for at least 1 h prior to electrophysiological recordings. For each experiment, slices were transferred to a submerged-slice type recording chamber (Warner Instruments, Hamden, CT, USA) perfused with warm (30 °C), oxygenated ACSF and individual cells were visualized using infrared differential interference contrast microscopy (Zeiss Axio Examiner D1 fitted with 40× water-immersion objective) and a CMOS camera (QImaging Rolera Bolt). Low-resistance electrodes (3–6 MΩ) filled with an internal solution containing 120 mM $CsMeSO_4$, 10 mM CsCl, 5 mM TEA-Cl, 1.5 mM $MgCl_2$, 10 mM HEPES, 0.1 mM EGTA, 2 mM Na-ATP, 0.5 mM Na-GTP, and 5 mM QX-314 (pH = 7.3, osmolarity = 275–285 mOsm) were used to record spontaneous inhibitory postsynaptic currents (sIPSCs) in CA1 pyramidal cells or medium spiny neurons in the striatum. Whole-cell voltage-clamp recordings were performed using a Multiclamp 700B amplifier and pClamp 10 (Molecular Devices, San Jose, CA, USA) and series resistance and whole-cell capacitance were automatically compensated. Recordings were discontinued if series resistance increased by > 20%. Pyramidal cells were voltage-clamped at the reversal potential for excitatory postsynaptic currents (+10 mV)

to record sIPSCs. Bath application of 100 μM SR-95531 (Caymen Chemical) blocked sIPSCs, confirming that inhibitory synaptic currents were adequately isolated using this approach. Data analysis was performed using Clampfit (Molecular Devices, San Jose, CA, USA). The EVAN LabView-based program developed by the Moody laboratory at UCLA was used for the detection, and measurement of peak amplitudes, 10–90% rise times, weighted decay time constants, and frequency of sIPSCs.

Tonic inhibition was measured by the change in the holding current needed to voltage-clamp cells at +10 mV induced by bath application of ≥100 μM SR-95531. In our initial experiments examining tonic inhibition in CA1 pyramidal cells (Fig. 2A, B), slices were continuously bathed in ACSF containing 5.0 μM GABA to enhance tonic inhibitory currents. All other experiments were performed without supplemental GABA in the ACSF. In experiments examining the effects of the $GABA_AR$ modulators L-655,708 and DS2 (Tocris) or the GABA transporter inhibitor nipecotic acid (Tocris) on tonic inhibition, drugs were bath applied until changes in holding current needed to clamp cells at +10 mV reached steady state and SR-95531 was then bath applied. The current needed to clamp cells in the presence of SR-95531 was then subtracted from the amplitude of the holding current before and after application of L-655,708, DS2, or nipecotic acid to determine drug effects on tonic inhibition.

Intrinsic excitability

Intrinsic excitability was examined using 400-μm-thick dorsal hippocampal slices prepared using previously described techniques (Babiec et al., 2017) and maintained at 30 °C in interface-type chambers perfused with ACSF at 2–3 mL/min. Slices were transferred to a submerged-slice recording chamber perfused with ACSF and whole-cell current-clamp recordings from CA1 pyramidal cells were performed using patch electrodes (4–8 MΩ) containing 122.5 mM K-gluconate, 17.5 mM KCl, 10 mM HEPES, 0.2 mM EGTA, 10 mM Na_2-phosphocreatine, 4 mM Mg-ATP, 0.3 mM Na-GTP (pH = 7.3, 290 mOsm). The number of action potentials elicited by 500-ms depolarizing current pulses (50–150 pA) was used to determine neuronal excitability and the peak change in membrane potential elicited by a 500-ms-long hyperpolarizing current pulse (−100 pA) was used to measure membrane input resistance. Reported membrane potentials have not been corrected for an estimated liquid junction potential of 13.4 mV.

LTP induction protocol

Standard extracellular recording techniques (Babiec et al., 2017) were used to examine LTP in slices maintained in interface-slice recording chambers. In these experiments, a glass microelectrode filled with ACSF (resistance = 5–10 MΩ) was placed in stratum radiatum of the CA1 region to record field excitatory postsynaptic potentials (fEPSPs) evoked by single pulses of presynaptic fiber stimulation (0.2 ms in duration, stimulation rate = 0.02 Hz) delivered by a bipolar stimulating electrode placed in stratum radiatum. At the start of each experiment, the intensity of presynaptic fiber stimulation was varied to determine the maximum fEPSP amplitude and the stimulation strength was then set to evoke fEPSPs that were 50% of maximum. After a stable baseline recording of 20 min, LTP was induced by a 150-pulse train of theta-frequency stimulation (single stimulation pulses delivered at 5 Hz). fEPSPs were recorded for 45 min post-LTP induction. fEPSP slopes were normalized to the pre-5-Hz stimulation baseline and fEPSP slopes averaged over the final 5 min were used for statistical comparisons.

Plasma membrane protein isolation

Dorsal portions of the hippocampus were dissected free from rest of the brain and immediately frozen on dry ice. Frozen hippocampi were pulverized using a mechanical tissue grinder, and further processed for either plasma membrane or whole lysate fractions. Plasma membrane fractions were prepared using a commercially available plasma membrane protein extraction kit (Abcam, Cambridge, United Kingdom, ab65400) according to manufacturer's instructions. Briefly, pulverized tissue was resuspended in homogenization buffer containing 1:500 protease inhibitor cocktail, and homogenized using a glass Dounce homogenizer. Homogenates were centrifuged for 10 min at 700 rcf to remove debris and the nuclear fraction. The supernatants were then centrifuged for 30 min at 10,000 rcf, to separate the cytosol fraction from total cellular membrane protein. The pellets from this spin were resuspended in upper phase and lower phase solutions provided in the kit. The upper phase, containing plasma membrane proteins, was purified after three, 5-min centrifugation steps at 1000 rcf. The purified upper phase was then diluted in water (5×), and centrifuged for 10 min at 13,500 rpm. The resulting pellet was resuspended in modified RIPA (mRIPA) buffer, containing 50 mM Tris (pH 7.4), 150 mM NaCl, 1% NP-40, 0.5% DOC, 0.1% SDS, 10 mM EGTA, 10 mM EDTA, 25 mM sodium pyrophosphate, 10 μM cantharidin, and cocktails of both protease (Sigma–Aldrich, St. Louis, MO, USA) and protein phosphatase inhibitors (Phosphatase Inhibitor Cocktails 2 and 3 from Sigma–Aldrich, St. Louis, MO, USA). For whole lysate protein isolation, mechanically pulverized hippocampi were resuspended in mRIPA buffer and briefly homogenized with a handheld sonicator. Protein concentrations were determined by the Bradford assay.

Western blotting

Whole hippocampal lysate and plasma membrane protein fractions were diluted in 2× loading buffer (National Diagnostics, Atlanta, GA, USA) and denatured by boiling for 5 min. Samples containing 10 μg of protein were separated by SDS–PAGE, using 4% and 12% acrylamide stacking and resolving gels, respectively. Proteins were transferred onto a 0.2-μm nitrocellulose membrane and blocked for 1 h at room temperature in

4% nonfat dry milk dissolved in Tris-buffered saline containing 0.05% Tween-20 (TBST). Nitrocellulose membranes were incubated overnight at 4 °C in milk/TBST containing the antibodies: anti-α5-$GABA_A$R (Aviva Systems Biology, San Diego, CA, USA, RRID:AB_2046033), anti-GAT3 (Abcam, Cambridge, United Kingdom, RRID:AB_304437), anti-GAT1 (Abcam, Cambridge, United Kingdom, RRID:AB_2189971), anti-Flotillin-1 (Santa Cruz Biotechnology, Dallas, TX, USA, RRID:AB_2106567), and anti-GSTπ (Enzo Life Science, Farmingdale, NY, USA, RRID:AB_2039146). Blots were then washed three times in TBST and incubated for 3 h at room-temperature in milk/TSBT containing HRP-conjugated secondary antibodies (1:2000, GE Healthcare catalog no. NA934V, NA931V). To image blots, membranes were immersed in ProtoGlow ECL (National Diagnostics, Atlanta, GA, USA), and immunoreactive bands were detected using a 12-bit cooled CCD camera and Image Lab software (Bio-Rad, Hercules, CA, USA). Densitometry analysis was performed using ImageJ (NIH). For quantification, density values from α5-$GABA_A$R, GAT1, and GAT3 bands were normalized to values for either the membrane-associated protein flotillin-1, for plasma membrane fractions, or βIII tubulin (Millipore, Burlington, MA, USA, RRID:AB_309804), for whole lysate proteins, to control for loading variations. Levels of α5-$GABA_A$R and GAT1/3 were expressed as a percentage of control. To estimate molecular weights, MagicMark XP (Thermo Fisher Scientific, Waltham, MA, USA) standard lanes were imaged together with sample lanes. To confirm enrichment of plasma membrane proteins, dorsal hippocampal lysates containing total protein from controls were run together with plasma membrane fractions during Western immunoblotting. In addition, immunoblots were probed with a glutathione S-transferase π (GSTπ) antibody to confirm the absence of significant cytosolic protein contamination in plasma membrane fractions.

Statistical analyses

All values are reported as mean ± SEM. Student's *t* tests as well as two-way and three-way ANOVAs (followed by Bonferroni's *t*-tests for specific comparisons) were used to determine statistical significance. All statistical analyses were performed using Prism 6 (GraphPad Software) or SigmaPlot (SPSS).

RESULTS

Phasic inhibitory synaptic transmission in CA1 pyramidal cells is enhanced in EAE

Previous studies have found that the frequency of sIPSCs in striatal medium spiny neurons (Rossi et al., 2011), cerebellar Purkinje cells (Mandolesi et al., 2012), and hippocampal CA1 pyramidal cells (Nistico et al., 2013) is significantly reduced during early stages of EAE (20–25 DPI). Thus, to determine how inhibitory transmission in hippocampal CA1 region is altered at later stages of EAE, we first examined sIPSCs in CA1 pyramidal cells from healthy, age-matched control mice and EAE mice 21–42 days post-induction (Fig. 1A, B). Strikingly, at these time points post-EAE induction, sIPSC frequency was significantly higher in CA1 pyramidal cells from EAE mice (Fig. 1B, C) There was no difference, however, in the amplitude, rise time, or decay time course of sIPSCs in cells from EAE and control mice (Fig. 1C). Although our findings, along with those of Nistico et al (2013), suggest that phasic inhibition in the hippocampal CA1 region undergoes distinct changes during EAE, phasic inhibitory synaptic transmission in striatal medium spiny neurons is significantly reduced at both early (20 DPI) and later stages of EAE (up to 90 DPI) (Rossi et al., 2011). Thus, the increase in sIPSC frequency in CA1 pyramidal cells during EAE suggested that there might be regional differences in how inhibitory synaptic transmission is altered in EAE. To examine this possibility we next recorded sIPSCs in striatal medium spiny neurons from both EAE (21–42 DPI) and control mice. Consistent with previous findings (Rossi et al., 2011), the frequency of sIPSCs was significantly reduced in medium spiny neurons from EAE mice (Fig. 1D, E). Together, these results suggest that there are significant time- and brain-region-dependent effects of EAE on phasic inhibitory synaptic transmission.

Increased surface expression of α5-$GABA_A$Rs contributes to enhanced tonic inhibition in EAE

To examine whether tonic inhibition is altered during EAE, we measured the decrease in the steady-state current needed to voltage-clamp CA1 pyramidal cells at +10 mV induced by the $GABA_A$ receptor antagonist SR-93551 (gabazine) (Fig. 2A). As shown in Fig. 2B, tonic inhibition in cells from EAE mice was approximately twofold larger compared to control cells. Tonic inhibition in CA1 pyramidal cells is primarily mediated by α5 subunit-containing receptors (Caraiscos et al., 2004; Zarnowska et al., 2015). Thus, to determine whether differences in the expression of extrasynaptic $GABA_A$Rs might contribute to the enhanced tonic inhibition in EAE, we measured plasma membrane levels of α5 subunits in hippocampal samples from control and EAE mice. Interestingly, plasma membrane levels of α5 subunits were significantly increased in EAE compared to normal (Fig. 2C, D). In a separate series of experiments, we found that total levels of $GABA_A$R α5 subunit expression were also significantly elevated in hippocampal lysates prepared from EAE mice (levels in samples from EAE mice were 131 ± 11% of control, $n = 5$ EAE and 6 control mice, $t(9) = 2.39$, $p = 0.04$). This suggests that the increased plasma membrane levels of α5 subunits is due, at least in part, to increased total levels of α5 subunit protein. To test whether enhanced α5-$GABA_A$Rs expression is responsible for increased tonic inhibition during EAE, we examined the effects of L-655,708, an inverse-agonist of the α5 subunit-containing $GABA_A$Rs (Quirk et al., 1996) on tonic inhibition in CA1 pyramidal cells from EAE and control mice. Following bath application of L-655,708 (5 μM) tonic inhibition was reduced to a greater extent in cells from EAE mice than from control mice (Fig. 2E). Moreover, in the presence

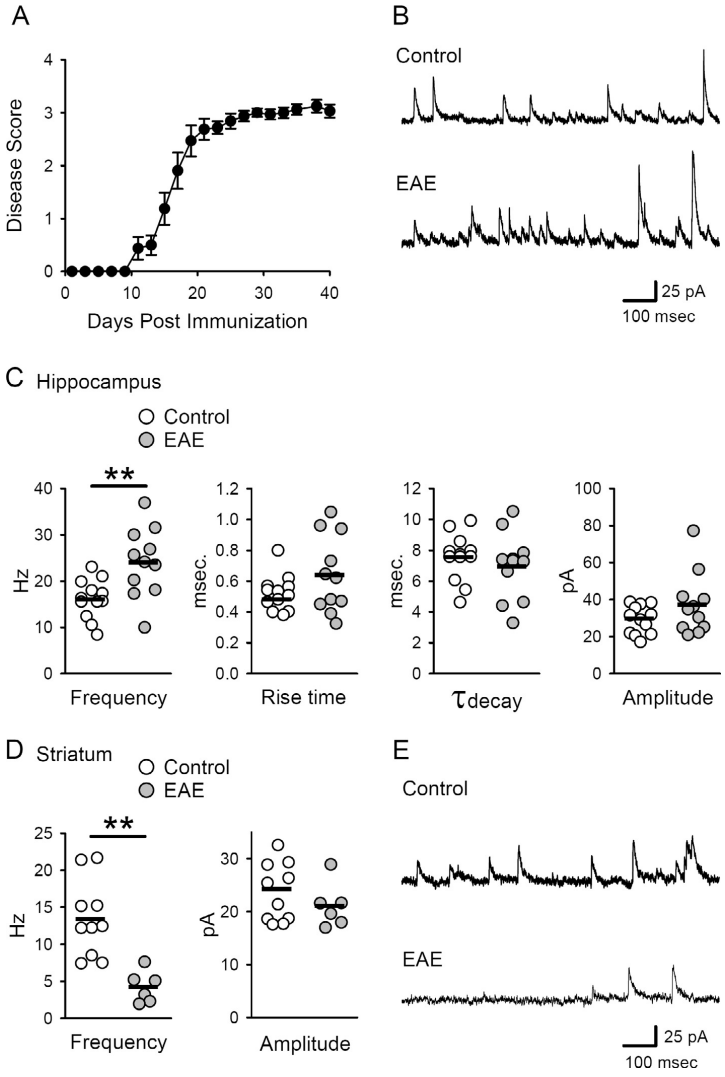

Fig. 1. Phasic inhibition is altered in EAE. (A) Disease scores for EAE animals used in experiments investigating phasic and tonic inhibition (n = 17). Disease scores were averaged across all animals, yielding a mean disease score per group. (B) Examples of sIPSCs in CA1 pyramidal cells in slices from control and EAE mice. (C) Frequency, amplitude, rise time, and decay time of sIPSCs in cells from healthy control and EAE mice. Plots show results from all cells, bars indicate mean values. The frequency of sIPSCs in cells from EAE mice (24 ± 2.3 Hz, n = 12 cells from 4 mice) was significantly higher than the sIPSC frequency in cells from controls (16.2 ± 1.2 Hz, n = 11 cells from 3 mice, $t(21) = 3.139$, $^{**}p = 4.96 \times 10^{-3}$). Peak sIPSC amplitudes were 29.2 ± 2.2 pA in control cells and 37.3 ± 5.1 pA in EAE cells ($t(21) = 1.503$, $p = 0.148$). Rise times (10–90% of peak amplitude) were 0.52 ± 0.03 msec in control cells and 0.64 ± 0.08 msec in EAE cells ($t(21) = 1.503$, $p = 0.148$). Decay time constants derived from single exponential fits to the decaying phase of sIPSCs were 7.5 ± 0.5 msec in control cells and 6.9 ± 0.7 msec in EAE cells ($t(21) = 0.767$, $p = 0.45$). (D) Frequency and amplitude of sIPSCs in striatal medium spiny neurons. The frequency of sIPSCs in cells from EAE mice (4.2 ± 0.9 Hz, n = 6 cells from 3 mice) was significantly reduced compared to control cells (13.4 ± 1.6 Hz, n = 10 cells from 3 mice, $t(14) = 4.11$, $^{**}p = 0.001$). Peak sIPSC amplitudes were 23.7 ± 1.8 pA in control cells and 21.0 ± 1.7 pA in cells from EAE mice ($t(14) = 0.96$, $p = 0.353$). (E) Examples of sIPSCs in medium spiny neurons in slices from control and EAE mice.

of L-655,708, tonic inhibition in cells from EAE mice was not significantly different from control cells ($t(26) = 1.792$, $p = 0.08$). Because δ subunit-containing $GABA_A$Rs also contribute to tonic inhibition in CA1 neurons (Scimemi et al., 2005), we examined the effects of DS2, a positive allosteric modulator of δ subunit-containing $GABA_A$Rs (Wafford et al., 2009) on tonic inhibition in EAE and control cells. The increase in tonic inhibition produced by bath application of DS2 (2 μM) was the same in control cells (26.1 ± 3.8%, n = 14 cells from 3 mice) and cells from EAE mice (22.5 ± 4.0%, n = 11 cells from 3 mice, $t(23) = 0.653$, $p = 0.52$). Together, these results indicate that an increase in plasma membrane expression of α5 subunit-containing $GABA_A$Rs has an important role in enhanced tonic inhibition during EAE.

Plasma membrane expression of the GABA transporter GAT-3 is reduced in EAE

The GABA transporters GAT-1 and GAT-3 are the primary neuronal and astrocytic GABA transporters, in hippocampal pyramidal cells (Cembrowski et al., 2016) and astrocytes (Chai et al., 2017). Moreover, both of these transporters are thought to have important roles in regulating tonic inhibition by controlling extracellular levels of GABA (Nusser and Mody, 2002; Jensen et al., 2003; Semyanov et al., 2003; Kersante et al., 2013). In contrast, the GAT-2 GABA transporter is not expressed in hippocampal pyramidal cells or astrocytes (Durkin et al., 1995; Evans et al., 1996; Cembrowski et al., 2016; Chai et al., 2017). Thus, to investigate whether deficits in GABA uptake might also contribute to enhanced tonic inhibition during EAE, we examined whether the expression of GAT-1 and/or GAT-3 is altered during EAE. Both plasma membrane (Fig. 3A) and total GAT-1 levels in whole hippocampal lysates from EAE mice were not significantly different from controls (total levels in lysates from EAE mice were 129 ± 14.3% of control,

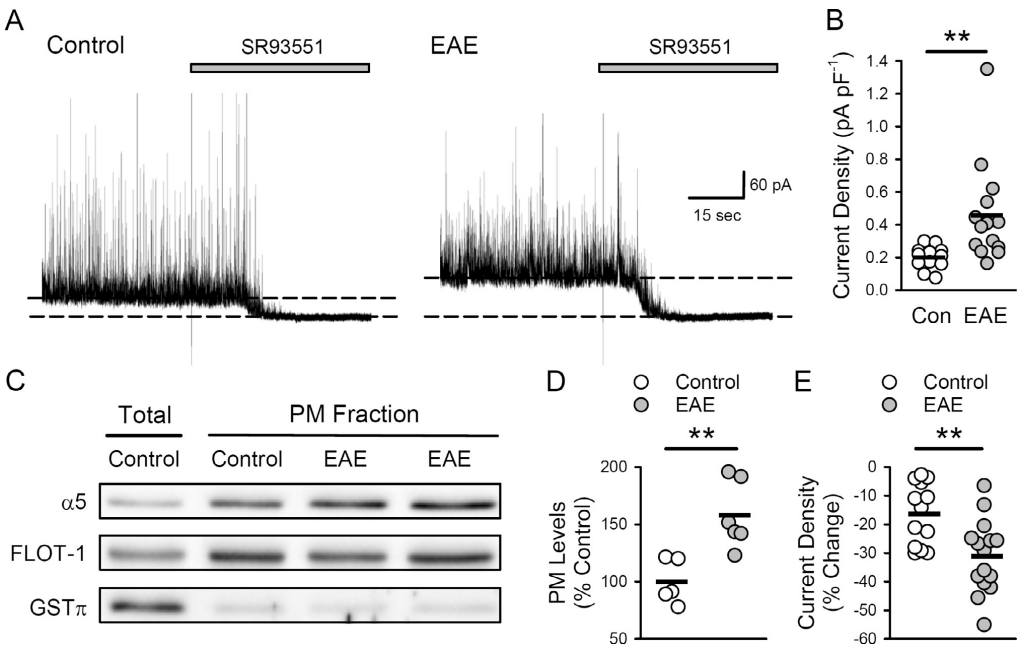

Fig. 2. Tonic inhibition and plasma membrane levels of α5 $GABA_AR$ subunits are increased in EAE. (A) Examples of tonic inhibition in cells from control and EAE mice (slices were continuously bathed in ACSF containing 5.0 μM GABA). Tonic inhibition is revealed by the change in the holding current needed to voltage-clamp cell at + 10 mV (indicated by the dashed lines) before and after blocking $GABA_A$ receptors with bath application of SR93551 (100 μM, indicated by the bar). (B) Tonic inhibition is significantly enhanced in CA1 pyramidal cells from EAE mice. Tonic inhibitory current density was 0.2 ± 0.02 pA/pF in control cells (n = 12 cells from 4 mice) and 0.46 ± 0.08 pA/pF in EAE cells (n = 14 cells from 4 mice, $t(24) = 2.845$, $^{**}p = 8.93 \times 10^{-3}$). Plot shows results from all cells, bars indicate mean values. (C) Immunoblots showing total and plasma membrane (PM) levels of α5 subunit levels in samples prepared from control and EAE hippocampi. Comparison of total and plasma membrane fractions shows enrichment in the membrane fraction while GSTπ levels show extent of cytosolic protein contamination in membrane fractions. Levels of α5 subunits were normalized to FLOT-1 levels. (D) Plot shows results from all experiments, bars indicate mean values. Plasma membrane levels of α5 $GABA_AR$ subunits in hippocampal homogenates prepared from EAE mice (n = 6) were 157.9 ± 12.0% of levels in homogenates from control animals (n = 5, $t(9) = 3.753$, $^{**}p = 0.005$). (E) A 10-min bath application of L-655,708 (5 μM) reduced tonic inhibition to a greater extend in pyramidal cells from EAE mice compared to controls. Plot shows results from all cells, bars indicate mean values. Tonic inhibition was reduced by 31.2 ± 3.3% in cells from EAE mice (n = 15 cells from 3 mice) compared to 16.3 ± 3.0% in control cells (n = 13 cells from 3 mice, $t(26) = 3.284$, $^{**}p = 2.93 \times 10^{-3}$).

n = 6 EAE and 6 control mice, $t(10) = 1.437$, $p = 0.181$). In contrast, GAT-3 plasma membrane expression was significantly decreased in the EAE hippocampus (Fig. 3B). There was no difference, however, in total levels of GAT-3 in lysates from EAE and control mice (levels were 96 ± 6.7% of control in EAE lysates, n = 6 EAE and 6 control mice, $t(10) = 0.371$, $p = 0.718$). This suggests that the decrease in plasma membrane GAT-3 levels during EAE is due to an alteration in GAT-3 membrane trafficking. To address the functional significance of decreased GAT-3 membrane expression during EAE, we next determined whether the increase in tonic inhibition induced by GAT-1 and GAT-3 inhibitor nipecotic acid (Pandit et al., 2013) was blunted in CA1 pyramidal cells from EAE mice (Fig. 3C). As shown in Fig. 3D, bath application of nipecotic acid (10 μM) induced a robust increase in tonic inhibition in both control and EAE cells. Though this finding does not rule out a potential role for deficits in GABA transporter function in the enhancement of tonic inhibition in EAE, it does suggest that an increase in α5 subunit-containing $GABA_AR$ is likely to have a more important role.

Decreased CA1 pyramidal cell excitability and LTP deficits in EAE

Tonic inhibition acts as a form of shunting inhibition that can potently reduce neuronal excitability. Thus, to begin to explore the impact of enhanced tonic inhibition in EAE on hippocampal function we first examined whether intrinsic excitability of CA1 pyramidal cells is reduced in EAE. Although resting membrane potentials in cells from control and EAE mice were similar (Fig. 4A), membrane input resistance was significantly lower in cells from EAE mice (Fig. 4B). Consistent with previous findings (Novkovic et al., 2015), there was also a robust, right-shift in action potential firing-to-current injection curves in cells from EAE mice, indicating a significant decrease in intrinsic excitability (Fig. 4C, D). To determine whether the decrease in pyramidal cell

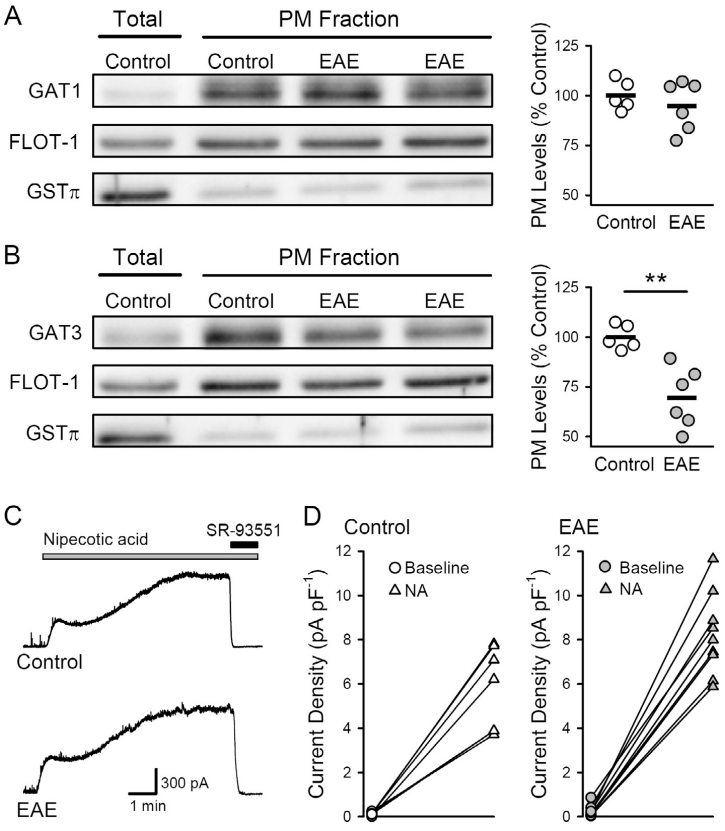

Fig. 3. Plasma membrane levels of the GABA transporter GAT-3 are reduced in EAE. (A, B) Plasma membrane (PM) levels of GAT-1 (A) and GAT-3 (B) in hippocampal samples from control (n = 5) and EAE mice (n = 6). GAT-1 and GAT-3 levels were normalized to levels of plasma membrane protein FLOT-1. Total protein levels in hippocampal lysates were used to confirm enrichment in the plasma membrane fraction, and GSTπ levels were used to monitor the extent of cytosolic contamination. Plots show results from all experiments, bars indicate mean values. Although plasma membrane levels of GAT-1 were not altered (levels were 95 ± 5% of control, $t(9) = 0.827$, $p = 0.43$), membrane levels of GAT-3 were significantly reduced in samples from EAE mice (levels were 69 ± 6% of control, ($t(9) = 4.192$, $^{**}p = 0.002$). (C) Examples of outward currents induced by bath application of the GAT-1/3 inhibitor nipecotic acid (10 μM, indicated by the bar) in CA1 pyramidal cells from control and EAE mice (V_{hold} = +10 mV). The contribution of $GABA_A$Rs to the outward current (tonic inhibition) was determined by bath application of 100 μM SR-93551 at the end of the recording (indicated by the bar). (D) Increase in tonic inhibition induced by nipecotic acid (NA) in CA1 pyramidal cells from control (n = 7 cells from 2 mice) and EAE mice (n = 9 cells from 2 mice).

excitability in EAE is due to enhanced tonic inhibition, we next examined resting membrane potential, input resistance, and excitability in cells continuously bathed in ACSF containing 5.0 μM L-655,708. Although L-655,708 had no effect on resting membrane potential (Fig. 4E), membrane input resistance in cells from control and EAE mice were no longer significantly different (Fig. 4F). Moreover, L-655,708 significantly enhanced depolarization-induced action potential firing in cells from EAE mice but had no effect on excitability in cells from control mice (Fig. 4G, H), indicating that the decrease in CA1 pyramidal cell excitability in EAE is due to enhanced tonic inhibition.

Because enhanced inhibition and decreased excitability can oppose the postsynaptic depolarization needed for activation of NMDARs and LTP induction, we next examined whether enhanced tonic inhibition is responsible for LTP deficits seen in EAE. Compared to slices obtained from healthy controls, the induction of LTP by a brief train of theta-pulse stimulation (150 pulses at 5 Hz) was significantly reduced in slices obtained from EAE mice at both early and later time points post-EAE induction (16–29 and > 40 days, respectively) (Fig. 5A, B). However, reducing tonic inhibition with L-655,708 failed to enhance LTP induction in slices obtained from mice > 40 day post-EAE induction (Fig. 5B), a time point post-EAE induction where L-655,708 strongly enhances CA1 pyramidal cell excitability (Fig. 4G, H). L-655,708 also had no effect on theta-pulse stimulation-induced LTP induction in slices obtained from healthy control mice (in the presence of L-655,708, fEPSPs in were potentiated to 143 ± 7% of baseline, n = 7 slices from 5 mice, $t(16) = 0.595$, $p = 0.56$ compared to vehicle controls). Thus, the LTP deficits that occur during EAE are not simply due to changes in tonic inhibition but instead likely involve additional pathophysiological changes in excitatory synaptic function.

DISCUSSION

In this study, we assessed the role of GABAergic transmission in modifying hippocampal function in EAE. We found that CA1 pyramidal cells exhibit both enhanced phasic and tonic currents during EAE. Although decreased surface expression of the GAT-3 GABA transporter may contribute, our results indicate that enhanced tonic inhibition during EAE is mediated primarily by increased surface expression of α5-$GABA_A$Rs. Importantly, tonic inhibition regulates neuronal excitability and thus can strongly influence information transmission through neural circuits (Semyanov et al., 2004). For example, in

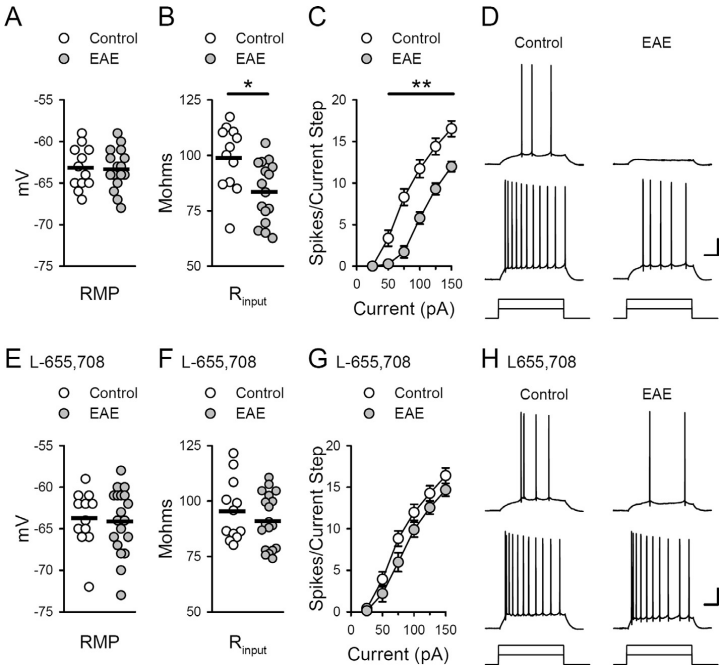

Fig. 4. Enhanced tonic inhibition reduces CA1 pyramidal cell excitability in EAE. (A) Resting membrane potential (RMP) in cells from EAE and control mice. Resting membrane potentials were −63.3 ± 0.6 mV in 16 cells from 7 EAE mice and −63.2 ± 0.7 mV in 12 cells from 5 control mice. (B) Membrane input resistance (R_{in}) was significantly lower in cells from EAE mice (83.6 ± 3.4 MΩ) compared to controls (98.9 ± 4.2 MΩ, $^{*}p < 0.01$, Bonferroni's *t*-test comparison). Plots in A and B show results from all cells, bars indicate mean values. (C) Action potential firing induced by somatic current injections is significantly reduced in cells from EAE mice ($n = 17$ cells from 7 EAE mice and 12 cells from 5 control mice, $^{**}p < 0.001$, Bonferroni's *t*-test comparison). (D) Traces show examples of action potentials elicited by 50- and 100-pA current injections in cells from control and EAE mice. Calibration: 20 mV, 100 ms. (E) Resting membrane potentials in cells from EAE and control mice in the presence of 5.0 μM L-655,708. Resting membrane potentials were -63.8 ± 0.9 mV in 12 cells from 5 control mice and −64.2 ± 0.9 mV in 19 cells from 6 EAE mice. A two-way ANOVA analysis of resting membrane potentials in cells from EAE and control mice in the presence and absence (panel A) of L-655,708 revealed no effect of group (EAE vs. control), $F_{(1,55)} = 0.086$, $p = 0.77$, or L-655,708, $F_{(1,55)} = 0.652$, $p = 0.423$, and no group × L-655,708 interaction, $F_{(1,55)} = 0.156$, $p = 0.903$. (F) Membrane input resistance in cells from EAE and control mice in the presence of L-655,708. Input resistance was 91.1 ± 2.8 MΩ in cells from EAE mice and 95.5 ± 3.9 MΩ in cells from control mice. A two-way ANOVA analysis of membrane input resistance in cells from EAE and control mice in the presence and absence (panel B) of L-655,708 revealed a significant difference between cells from EAE and control mice, $F_{(1,55)} = 7.582$, $p = 0.0008$. Post-hoc Bonferroni's *t*-tests: cells from EAE vs. control mice in the absence of L-655,708, $t = 2.971$, $p = 0.004$; cells from EAE vs. control mice in the presence of L-655,708, $t = 0.887$, $p = 0.379$. Plots in E and F show results from all cells, bars indicate mean values. (G) Depolarization-induced action potential firing in cells from control and EAE mice in the presence of L-655,708 ($n = 13$ cells from 5 control mice and 19 cells from 6 EAE mice). A three-way ANOVA analysis of the action potential firing-to-current injection curves in the presence and absence (panel C) of L-655,708 revealed a significant effect of group (EAE vs. control) $F_{(1,342)} = 81.705$, $p < 0.001$), L-655,708 ($F_{(1,342)} = 25.081$, $p < 0.001$), and a significant group × L-655,708 interaction ($F_{(1,342)} = 20.521$, $p < 0.001$). Post-hoc Bonferroni's *t*-tests: EAE vs. control cells in the absence of L-655,708, $t = 9.38$; $p < 0.001$), L-655,708 had no effect on excitability in control cells ($t = 0.307$, $p = 0.759$) but significantly enhanced excitability in cells from EAE mice ($t = 7.441$, $p < 0.001$). (H) Traces show examples of action potential firing in response to 50 and 100 pA current injections in cells from control and EAE mice in the presence of L-655,708. Calibration: 20 mV and 100 ms.

the cerebellar cortex, $GABA_A$-mediated tonic inhibition is the main inhibitory influence regulating the transfer of information at mossy fiber synapses onto granule cells, and is thought to have a crucial role in the sparse coding of sensory information in the cerebellar cortex (Hamann et al., 2002, Chadderton et al., 2004). Tonic inhibition also regulates the excitability of hippocampal pyramidal cells (Glykys and Mody, 2006, Bonin et al., 2007, Pavlov et al., 2009, Groen et al., 2014). Thus, alterations in network activity and information processing due to increased tonic inhibition and decreased neuronal excitability may contribute to cognitive disability in MS.

Although our study is the first to identify changes in tonic inhibition in EAE, previous studies have found that phasic inhibitory synaptic transmission is also altered in EAE (Rossi et al., 2011, Mandolesi et al., 2012, Nistico et al., 2013). Interestingly, although sIPSPC frequency in CA1 pyramidal cells is reduced relatively soon after EAE induction (Nistico et al., 2013), we find that the frequency of sIPSCs is enhanced at later time points post-EAE induction. Although differences in EAE induction protocols might contribute to this difference, our results, along with those of Nistico et al. (2013), suggest that phasic inhibitory synaptic transmission in the hippocampus undergoes distinct, time-dependent changes during the course of EAE. In contrast to the changes in phasic inhibitory synaptic transmission that occur in hippocampal CA1 pyramidal cells during EAE, sIPSC frequency is strongly reduced in striatal medium spiny neurons at both early and later time points post-EAE induction (Rossi et al., 2011). Thus, EAE may lead to brain-region-specific alterations in phasic inhibition, perhaps due to region and/or cell type-specific effects on expression of distinct $GABA_AR$ subtypes. Indeed, there are brain region differences in EAE-induced changes in astrocyte gene expression (Itoh et al., 2018). Notably, loss of parvalbumin (PV)-positive inhibitory interneurons occurs in both MS (Clements et al., 2008) and EAE (Ziehn et al., 2010; Rossi et al., 2011; Nistico et al., 2013). Although loss of PV-positive interneurons is

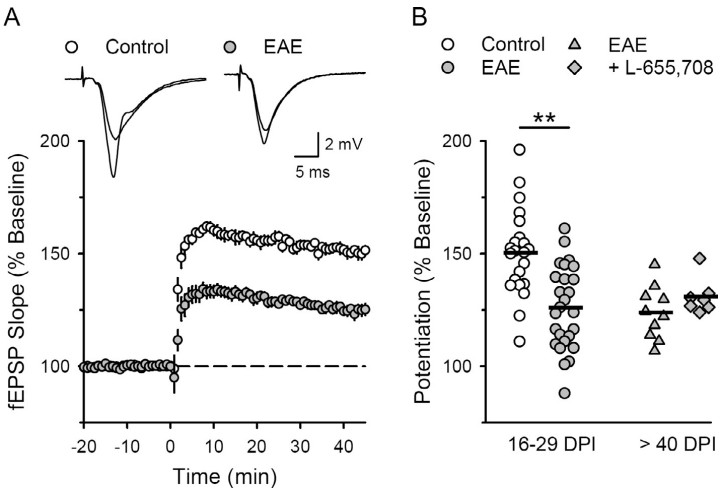

Fig. 5. LTP is impaired in the CA1 region of the hippocampus during EAE. (A) LTP was induced by theta-frequency stimulation (150 presynaptic fiber stimulation pulses at 5 Hz, delivered at time = 0) in the CA1 region of hippocampal slices obtained from healthy control and EAE mice (16–29 days post EAE induction). Traces show superimposed fEPSPs recorded during baseline and 45 min post-LTP induction. (B) Plot shows results from all LTP experiments, bars indicate mean values. In hippocampal slices obtained from EAE mice 16–29 days post induction (DPI), fEPSPs were potentiated to 125 ± 4% of baseline in slices from EAE mice (26 slices from 7 mice) and to 150 ± 4% of baseline in slices from healthy controls (22 slices from 5 mice, $t(46) = 4.498$, $^{**}p = 4.64 \times 10^{-5}$). In experiments where hippocampal slices from EAE mice (> 40 days post induction) were continuously bathed in ACSF containing 5.0 μM L-655,708 fEPSPs were potentiated to 131 ± 3% of baseline ($n = 7$ slices from 5 mice) compared to 124 ± 4% of baseline in vehicle control experiments (0.1% DMSO, $n = 10$ slices from in 7 mice, $t(15) = 1.39$, $p = 0.185$).

thought to underlie the reduction in sIPSC frequency in medium spiny neurons (Rossi et al., 2011), we observed an increase is sIPSC frequency in CA1 pyramidal cells even though the number of PV-positive interneurons is also reduced in hippocampal CA1 region during EAE (Ziehn et al., 2010; Nistico et al., 2013). Thus, the mechanisms responsible for increased sIPSCs in CA1 pyramidal cells during EAE are unclear. It is interesting, however, that PV-positive, basket and bistratified interneurons in the CA1 region form inhibitory synaptic connections onto both pyramidal cells and other inhibitory neurons (Bezaire and Soltesz, 2013). For example, nearly 30% of all inhibitory synapses onto PV-positive interneurons in the CA1 region arises from other, PV-positive cells (Gulyás et al., 1999, for review see Hu et al., 2014). Thus, the increase in sIPSC frequency we observed during EAE may reflect disinhibition of inhibitory interneuron networks due to partial loss of PV-positive interneurons.

Tonic inhibition in hippocampal CA1 pyramidal cells is primarily mediated by α5β3γ2 subunit-containing $GABA_A$Rs (Caraiscos et al., 2004; Zarnowska et al., 2015), although α5β2 subunit-containing receptors may also be involved (Ju et al., 2009). Thus, although our results are consistent with the notion that up-regulation of α5β3γ2 subunit-containing receptors has an important role in the increase in tonic inhibition in EAE, additional experiments are needed to better define how the expression of β3/2 and γ2 subunits changes during EAE. The molecular mechanisms responsible for increases in α5-$GABA_A$Rs during EAE are also unclear. However, our finding that α5-$GABA_A$R-mediated tonic inhibition is enhanced in the hippocampal CA1 during EAE parallels other studies suggesting that inflammatory molecules acting on $GABA_A$Rs can effect cell excitability, excitatory neurotransmission and synaptic plasticity. For example, the pro-inflammatory cytokine interleukin-1beta (IL-1β) induces a rapid increase in $GABA_A$R surface expression in hippocampal neurons (Serantes et al., 2006) and mediates the increase in α5-$GABA_A$Rs surface expression and tonic inhibition in CA1 pyramidal cells following systemic inflammation induced by the bacterial endotoxin lipopolysaccharide (Wang et al., 2012). Although other inflammatory cytokines, such as tumor necrosis factor alpha and interleukin 6, can regulate inhibitory synaptic transmission (Stellwagen et al., 2005, Garcia-Oscos et al., 2012), these cytokines have little, if any, effect on tonic inhibition in cultured hippocampal neurons (Wang et al., 2012). Interestingly, extrasynaptic α5-$GABA_A$R expression and tonic inhibition are also strongly increased in dentate gyrus granule cells in the 5xFAD model of Alzheimer's disease (Wu et al., 2014). Moreover, enhanced α5-$GABA_A$R-mediated tonic inhibition in cortical pyramidal neurons found within the peri-infarct region contributes to reduced cortical plasticity and motor recovery in a rodent stroke model (Clarkson et al., 2010). Together with these findings, our results suggest that enhanced α5-$GABA_A$R-mediated tonic inhibition may be a common pathological response that occurs during neurodegeneration and brain injury.

Because GABAergic inhibition potently regulates the induction of LTP at glutamatergic synapses (Wigstrom and Gustafsson, 1983, Davies et al., 1991, Arima-Yoshida et al., 2011), we investigated if the enhanced tonic inhibition in EAE leads to LTP deficits in the hippocampal CA1 region. Consistent with previous findings showing that LTP is reduced in EAE (Kim do et al., 2012, Di Filippo et al., 2013, Novkovic et al., 2015), the induction of LTP by a theta-frequency stimulation protocol was significantly reduced in hippocampal slices from EAE mice. However, reducing tonic inhibition with L-655,708 had little effect on theta frequency stimulation-induced LTP. This suggests that the LTP deficits that occur during EAE are not simply due to enhanced tonic inhibition but instead are more likely to reflect alterations in the NMDAR-dependent signaling pathways involved in the

induction and/or maintenance of LTP. Notably, there is considerable controversy regarding how LTP induction is altered in EAE. Although the deficits in theta-frequency stimulation-induced LTP observed in our experiments are consistent with deficits in high-frequency stimulation-induced LTP seen in previous studies (Kim do et al., 2012; Di Filippo et al., 2013, Novkovic et al., 2015), other studies have found either no change (Ziehn et al., 2010; Prochnow et al., 2013) or even an enhancement of LTP in EAE (Nistico et al., 2013). A number of experimental variables, such as differences in the pattern of synaptic stimulation used to induce LTP and methods for EAE induction, might contribute to these disparate findings. Interestingly, although we find significant deficits in the induction of LTP by relatively modest theta pulse stimulation protocols at early time points following EAE induction, recent findings indicate that the induction of LTP by stronger, high-frequency synaptic stimulation in the hippocampal CA1 region becomes progressively impaired as disease progresses (Novkovic et al., 2015). Moreover, LTP induction in the dentate gyrus is impaired early in EAE when high-frequency stimulation-induced LTP in CA1 is intact, suggesting that hippocampal dysfunctions may extend through the trisynaptic loop as the disease progresses (Planche et al., 2016). These findings parallel the clinical observation that cognitive deficits accumulate with aging and progression of other MS disabilities (Ruano et al., 2016). Thus, future studies examining how deficits in the induction of LTP by different patterns of synaptic stimulation and how alterations in tonic inhibition evolve with time during EAE should provide important insights into the synaptic and molecular mechanisms underlying CI in MS.

ACKNOWLEDGMENTS

We thank Voskuhl lab members Noriko Itoh, Heaveen Ahdi, Valerie Vessels, and Darian Nitin Mangu for assistance with animal care. We also thank Drs. Ryan Guglietta and Walter Babiec for technical advice. This work was supported by a grant from the Conrad N. Hilton Foundation (#20150232), the California Community Foundation (#BAPP-15-118094), and the Tom Sherak MS Hope Foundation to RRV. LGK was supported by the UCLA Laboratory of Neuroendocrinology (LNE) training grant (5T32HD007228) and by the National Institute on Aging of the National Institutes of Health (F31AG051381). Author contributions: L.G.K, W.W., S.A.J., R.R.V., and T.J.O. designed research; L.G.K., W.W., S.A.J., and T.J.O. performed research; L.G.K, W.W., S.A.J., and T.J.O. analyzed data; L.G.K., W.W., S.A.J., R.R.V., and T.J.O. wrote the paper.

CONFLICT OF INTEREST

The authors declare no competing financial interest.

REFERENCES

Acharjee S, Nayani N, Tsutsui M, Hill MN, Ousman SS, Pittman QJ (2013) Altered cognitive-emotional behavior in early experimental autoimmune encephalitis–cytokine and hormonal correlates. Brain Behav Immun 33:164–172.

Arima-Yoshida F, Watabe AM, Manabe T (2011) The mechanisms of the strong inhibitory modulation of long-term potentiation in the rat dentate gyrus. Eur J Neurosci 33:1637–1646.

Atack JR, Bayley PJ, Seabrook GR, Wafford KA, McKernan RM, Dawson GR (2006) L-655,708 enhances cognition in rats but is not proconvulsant at a dose selective for α5-containing $GABA_A$ receptors. Neuropharmacology 51:1023–1029.

Babiec WE, Jami SA, Guglietta R, Chen PB, O'Dell TJ (2017) Differential regulation of NMDA receptor-mediated transmission by SK channels underlies dorsal-ventral differences in dynamic of Schaffer collateral synaptic function. J Neurosci 37:1950–1964.

Bezaire MJ, Soltesz I (2013) Quantitative assessment of CA1 local circuits: knowledge base for interneuron-pyramidal cell connectivity. Hippocampus 23:751–785.

Bonin RP, Martin LJ, MacDonald JF, Orser BA (2007) α5$GABA_A$ receptors regulate the intrinsic excitability of mouse hippocampal pyramidal neurons. J Neurophysiol 98:2244–2254.

Caraiscos VB, Elliott EM, You-Ten KE, Cheng VY, Belelli D, Newell JG, Jackson MF, Lambert JJ, Rosahl TW, Wafford KA, MacDonald JF, Orser BA (2004) Tonic inhibition in mouse hippocampal CA1 pyramidal neurons is mediated by α5 subunit-containing gamma-aminobutyric acid type A receptors. Proc Natl Acad Sci USA 101:3662–3667.

Cembrowski MS, Wang L, Sugino K, Shields BC, Spruston N (2016) Hipposeq: a comprehensive RNA-seq database of gene expression in hippocampal principal neurons. Elife 5. https://doi.org/10.7554/eLife.14997 e14997.

Centonze D, Muzio L, Rossi S, Cavasinni F, De Chiara V, Bergami A, Musella A, D'Amelio M, Cavallucci V, Martorana A, Bergamaschi A, Cencioni MT, Diamantini A, Butti E, Comi G, Bernardi G, Cecconi F, Battistini L, Furlan R, Martino G (2009) Inflammation triggers synaptic alteration and degeneration in experimental autoimmune encephalomyelitis. J Neurosci 29:3442–3452.

Chadderton P, Margrie TW, Hausser M (2004) Integration of quanta in cerebellar granule cells during sensory processing. Nature 428:856–860.

Chai H, Diaz-Castro B, Shigetomi E, Monte E, Octeau JC, Yu X, Cohn W, Rajendran PS, Vondriska TM, Whitelegge JP, Coppola G, Khakh BS (2017) Neural circuit-specialized astrocytes: transcriptomic, proteomic, morphological, and functional evidence. Neuron 95:531–549.

Chiaravalloti ND, DeLuca J (2008) Cognitive impairment in multiple sclerosis. Lancet Neurol 7:1139–1151.

Clarkson AN, Huang BS, Macisaac SE, Mody I, Carmichael ST (2010) Reducing excessive GABA-mediated tonic inhibition promotes functional recovery after stroke. Nature 468:305–309.

Clements RJ, McDonough J, Freeman EJ (2008) Distribution of parvalbumin and calretinin immunoreactive interneurons in motor cortex from multiple sclerosis post-mortem tissue. Exp Brain Res 187:459–465.

Collinson N, Kuenzi FM, Jarolimek W, Maubach KA, Cothliff R, Sur C, Smith A, Otu FM, Howell O, Atack JR, McKernan RM, Seabrook GR, Dawson GR, Whiting PJ, Rosahl TW (2002) Enhanced learning and memory and altered GABAergic synaptic transmission in mice lacking the alpha 5 subunit of the $GABA_A$ receptor. J Neurosci 22:5572–5580.

Davies CH, Starkey SJ, Pozza MF, Collingridge GL (1991) GABA autoreceptors regulate the induction of LTP. Nature 349:609–611.

Denney DR, Sworowski LA, Lynch SG (2005) Cognitive impairment in three subtypes of multiple sclerosis. Arch Clin Neuropsychol 20:967–981.

Di Filippo M, Chiasserini D, Gardoni F, Viviani B, Tozzi A, Giampa C, Costa C, Tantucci M, Zianni E, Boraso M, Siliquini S, de Iure A, Ghiglieri V, Colcelli E, Baker D, Sarchielli P, Fusco FR, Di Luca M, Calabresi P (2013) Effects of central and peripheral inflammation on hippocampal synaptic plasticity. Neurobiol Dis 52:229–236.

Di Filippo M, de Iure A, Giampa C, Chiasserini D, Tozzi A, Orvietani PL, Ghiglieri V, Tantucci M, Durante V, Quiroga-Varela A, Mancini A, Costa C, Sarchielli P, Fusco FR, Calabresi P (2016) Persistent

activation of microglia and NADPH oxidase drive hippocampal dysfunction in experimental multiple sclerosis. Sci Reports 6:20926. https://doi.org/10.1038/srep20926.
Durkin MM, Smith KE, Borden LA, Weinshank RL, Branchek TA, Gustafson EL (1995) Localization of messenger RNAs encoding three GABA transporters in rat brain: an in situ hybridization study. Brain Res Mol Brain Res 33:7–21.
Dutta R, Chang A, Doud MK, Kidd GJ, Ribaudo MV, Young EA, Fox RJ, Staugaitis SM, Trapp BD (2011) Demyelination causes synaptic alterations in hippocampi from multiple sclerosis patients. Ann Neurol 69:445–454.
Etherington LA, Mihalik B, Pálvölgyi A, Ling I, Pallagi K, Kertész S, Varga P, Gunn BG, Brown AR, Livesey MR, Monteiro O, Belelli D, Barkóczy J, Spedding M, Gacsályi I, Antoni FA, Lambert JJ (2017) Selective inhibition of extra-synaptic α5-$GABA_A$ receptors by S44819, a new therapeutic agent. Neuropharmacology 125:353–364.
Evans JE, Frostholm A, Rotter A (1996) Embryonic and postnatal expression of four gamma-aminobutyric acid transporter mRNAs in the mouse brain and leptomeninges. J Comp Neurol 376:431–446.
Garcia-Oscos F, Salgado H, Hall S, Thomas F, Farmer GE, Bermeo J, Galindo LC, Ramirez RD, D'Mello S, Rose-John S, Atzori M (2012) The stress-induced cytokine interleukin-6 decreases the inhibition/excitation ratio in the rat temporal cortex via trans-signaling. Biol Psychiatry 71:574–582.
Glykys J, Mody I (2006) Hippocampal network hyperactivity after selective reduction of tonic inhibition in $GABA_A$ receptor α5 subunit-deficient mice. J Neurophysiol 95:2796–2807.
Grasselli G, Rossi S, Musella A, Gentile A, Loizzo S, Muzio L, Di Sanza C, Errico F, Musumeci G, Haji N, Fresegna D, Sepman H, De Chiara V, Furlan R, Martino G, Usiello A, Mandolesi G, Centonze D (2013) Abnormal NMDA receptor function exacerbates experimental autoimmune encephalomyelitis. Br J Pharmacol 168:502–517.
Groen MR, Paulsen O, Perez-Garci E, Nevian T, Wortel J, Dekker MP, Mansvelder HD, van Ooyen A, Meredith RM (2014) Development of dendritic tonic GABAergic inhibition regulates excitability and plasticity in CA1 pyramidal neurons. J Neurophysiol 112:287–299.
Guimaraes J, Sa MJ (2012) Cognitive dysfunction in multiple sclerosis. Front Neurol 3:74. https://doi.org/10.3389/fneur.2012.00074.
Gulyás AI, Megais M, Emri Z, Freund T (1999) Total number and ratio of excitatory and inhibitory synapses converging onto single interneurons of different types in the CA1 area of the rat hippocampus. J Neurosci 19:10082–10097.
Hamann M, Rossi DJ, Attwell D (2002) Tonic and spillover inhibition of granule cells control information flow through cerebellar cortex. Neuron 33:625–633.
Hu H, Gan J, Jonas P (2014) Fast-spiking, parvalbumin$^+$ GABAergic interneurons: from cellular design to microcircuit function. Science 345:1255263. https://doi.org/10.1126/science.
Itoh N, Itoh Y, Tassoni A, Ren E, Kaito M, Ohno A, Ao Y, Farkhondeh V, Johnsonbaugh H, Burda J, Sofroniew MV, Voskuhl RR (2018) Cell-specific and region-specific transcriptomics in the multiple sclerosis model: Focus on astrocytes. Proc Natl Acad Sci USA 115:E302–E309.
Jensen K, Chiu CS, Sokolova I, Lester HA, Mody I (2003) GABA transporter-1 (GAT1)-deficient mice: differential tonic activation of $GABA_A$ versus $GABA_B$ receptors in the hippocampus. J Neurophysiol 90:2690–2701.
Ju YH, Guzzo A, Chiu MW, Taylor P, Moran MF, Gurd JW, MacDonald JF, Orser BA (2009) Distinct properties of murine α5 gamma-aminobutyric acid type a receptors revealed by biochemical fractionation and mass spectroscopy. J Neurosci Res 87:1737–1747.
Kersante F, Rowley SC, Pavlov I, Gutierrez-Mecinas M, Semyanov A, Reul JM, Walker MC, Linthorst AC (2013) A functional role for both gamma-aminobutyric acid (GABA) transporter-1 and GABA transporter-3 in the modulation of extracellular GABA and GABAergic tonic conductances in the rat hippocampus. J Physiol 591:2429–2441.
Kim do Y, Hao J, Liu R, Turner G, Shi FD, Rho JM (2012) Inflammation-mediated memory dysfunction and effects of a ketogenic diet in a murine model of multiple sclerosis. PLoS One 7. https://doi.org/10.1371/journal.pone.0035476 e35476.
Litvan I, Grafman J, Vendrell P, Martinez JM (1988) Slowed information processing in multiple sclerosis. Arch Neurol 45:281–285.
Longoni G, Rocca MA, Pagani E, Riccitelli GC, Colombo B, Rodegher M, Falini A, Comi G, Filippi M (2015) Deficits in memory and visuospatial learning correlate with regional hippocampal atrophy in MS. Brain Struct Funct 220:435–444.
Mandolesi G, Grasselli G, Musella A, Gentile A, Musumeci G, Sepman H, Haji N, Fresegna D, Bernardi G, Centonze D (2012) GABAergic signaling and connectivity on Purkinje cells are impaired in experimental autoimmune encephalomyelitis. Neurobiol Dis 46:414–424.
Mandolesi G, Musella A, Gentile A, Grasselli G, Haji N, Sepman H, Fresegna D, Bullitta S, De Vito F, Musumeci G, Di Sanza C, Strata P, Centonze D (2013) Interleukin-1beta alters glutamate transmission at purkinje cell synapses in a mouse model of multiple sclerosis. J Neurosci 33:12105–12121.
Mandolesi G, Gentile A, Musella A, Fresegna D, De Vito F, Bullitta S, Sepman H, Marfia GA, Centonze D (2015) Synaptopathy connects inflammation and neurodegeneration in multiple sclerosis. Nat Rev Neurol 11:711–724.
Martin LJ, Zurek AA, MacDonald JF, Roder JC, Jackson MF, Orser BA (2010) α5$GABA_A$ receptor activity sets the threshold for long-term potentiation and constrains hippocampus-dependent memory. J Neurosci 30:5269–5282.
Mitchell SJ, Silver RA (2003) Shunting inhibition modulates neuronal gain during synaptic excitation. Neuron 38:433–445.
Nistico R, Mango D, Mandolesi G, Piccinin S, Berretta N, Pignatelli M, Feligioni M, Musella A, Gentile A, Mori F, Bernardi G, Nicoletti F, Mercuri NB, Centonze D (2013) Inflammation subverts hippocampal synaptic plasticity in experimental multiple sclerosis. PLoS One 8. https://doi.org/10.1371/journal.pone.0054666 e54666.
Novkovic T, Shchyglo O, Gold R, Manahan-Vaughan D (2015) Hippocampal function is compromised in an animal model of multiple sclerosis. Neuroscience 309:100–112.
Nusser Z, Mody I (2002) Selective modulation of tonic and phasic inhibitions in dentate gyrus granule cells. J Neurophysiol 87:2624–2628.
Pandit S, Jeong JA, Jo JY, Cho HS, Kim DW, Kim JM, Ryu PD, Lee SY, Kim HW, Jeon BH, Park JB (2013) Dual mechanisms diminishing tonic $GABA_A$ inhibition of dentate gyrus granule cells in Noda epileptic rats. J Neurophysiol 110:95–102.
Pavlov I, Savtchenko LP, Kullmann DM, Semyanov A, Walker MC (2009) Outwardly rectifying tonically active $GABA_A$ receptors in pyramidal cells modulate neuronal offset, not gain. J Neurosci 29:15341–15350.
Planche V, Panatier A, Hiba B, Ducourneau EG, Raffard G, Dubourdieu N, Maitre M, Leste-Lasserre T, Brochet B, Dousset V, Desmedt A, Oliet SH, Tourdias T (2016) Selective dentate gyrus disruption causes memory impairment at the early stage of experimental multiple sclerosis. Brain Behav Immun 60:240–254.
Prochnow N, Gold R, Haghikia A (2013) An electrophysiologic approach to quantify impaired synaptic transmission and plasticity in experimental autoimmune encephalomyelitis. J Neuroimmunol 264:48–53.
Quirk K, Blurton P, Fletcher S, Leeson P, Tang F, Mellilo D, Ragan CI, McKernan RM (1996) [3H]L-655,708, a novel ligand selective for the benzodiazepine site of $GABA_A$ receptors which contain the α5 subunit. Neuropharmacology 35:1331–1335.
Rao SM, Leo GJ, Ellington L, Nauertz T, Bernardin L, Unverzagt F (1991) Cognitive dysfunction in multiple sclerosis. II. Impact on employment and social functioning. Neurology 41:692–696.
Rossi S, Muzio L, De Chiara V, Grasselli G, Musella A, Musumeci G, Mandolesi G, De Ceglia R, Maida S, Biffi E, Pedrocchi A,

Menegon A, Bernardi G, Furlan R, Martino G, Centonze D (2011) Impaired striatal GABA transmission in experimental autoimmune encephalomyelitis. Brain Behav Immun 25:947–956.
Ruano L, Portaccio E, Goretti B, Niccolai C, Severo M, Patti F, Cilia S, Gallo P, Grossi P, Ghezzi A, Roscio M, Mattioli F, Stampatori C, Trojano M, Viterbo RG, Amato MP (2016) Age and disability drive cognitive impairment in multiple sclerosis across disease subtypes. Mult Scler J. https://doi.org/10.1177/1352458516674367.
Scimemi A, Semyanov A, Sperk G, Kullmann DM, Walker MC (2005) Multiple and plastic receptors mediate tonic GABAA receptor currents in the hippocampus. J Neurosci 25:10016–10024.
Semyanov A, Walker MC, Kullmann DM (2003) GABA uptake regulates cortical excitability via cell type-specific tonic inhibition. Nat Neurosci 6:484–490.
Semyanov A, Walker MC, Kullmann DM, Silver RA (2004) Tonically active $GABA_A$ receptors: modulating gain and maintaining the tone. Trends Neurosci 27:262–269.
Serantes R, Arnalich F, Figueroa M, Salinas M, Andres-Mateos E, Codoceo R, Renart J, Matute C, Cavada C, Cuadrado A, Montiel C (2006) Interleukin-1β enhances $GABA_A$ receptor cell-surface expression by a phosphatidylinositol 3-kinase/Akt pathway: relevance to sepsis-associated encephalopathy. J Biol Chem 281:14632–14643.
Sicotte NL, Kern KC, Giesser BS, Arshanapalli A, Schultz A, Montag M, Wang H, Bookheimer SY (2008) Regional hippocampal atrophy in multiple sclerosis. Brain 131:1134–1141.
Stellwagen D, Beattie EC, Seo JY, Malenka RC (2005) Differential regulation of AMPA receptor and GABA receptor trafficking by tumor necrosis factor-alpha. J Neurosci 25:3219–3228.
Wafford KA, van Niel MB, Ma QP, Horridge E, Herd MB, Peden DR, Belelli D, Lambert JJ (2009) Novel compounds selectively enhance δ subunit containing $GABA_A$ receptors and increase tonic currents in thalamus. Neuropharmacology 56:182–189.
Wang DS, Zurek AA, Lecker I, Yu J, Abramian AM, Avramescu S, Davies PA, Moss SJ, Lu WY, Orser BA (2012) Memory deficits induced by inflammation are regulated by α5-subunit-containing $GABA_A$ receptors. Cell Rep 2:488–496.
Whissell PD, Eng D, Lecker I, Martin LJ, Wang DS, Orser BA (2013) Acutely increasing $\delta GABA_A$ receptor activity impairs memory and inhibits synaptic plasticity in the hippocampus. Front Neural Circuits 7:146. https://doi.org/10.3389/fncir.2013.00146.
Wigstrom H, Gustafsson B (1983) Heterosynaptic modulation of homosynaptic long-lasting potentiation in the hippocampal slice. Acta Physiol Scand 119:455–458.
Wu Z, Guo Z, Gearing M, Chen G (2014) Tonic inhibition in dentate gyrus impairs long-term potentiation and memory in an Alzheimer's disease model. Nature Commun 5:4159.
Zarnowska ED, Rodgers FC, Oh I, Rau V, Lor C, Laha KT, Jurd R, Rudolph U, Eger 2nd EI, Pearce RA (2015) Etomidate blocks LTP and impairs learning but does not enhance tonic inhibition in mice carrying the N265M point mutation in the β3 subunit of the $GABA_A$ receptor. Neuropharmacology 93:171–178.
Ziehn MO, Avedisian AA, Tiwari-Woodruff S, Voskuhl RR (2010) Hippocampal CA1 atrophy and synaptic loss during experimental autoimmune encephalomyelitis, EAE. Lab Invest 90:774–786.
Ziehn MO, Avedisian AA, Dervin SM, Umeda EA, O'Dell TJ, Voskuhl RR (2012) Therapeutic testosterone administration preserves excitatory synaptic transmission in the hippocampus during autoimmune demyelinating disease. J Neurosci 32:12312–12324.

(Received 26 April 2017, Accepted 5 November 2018)
(Available online 14 November 2018)